

**THÈSE DE DOCTORAT
DE SORBONNE UNIVERSITÉ**

Spécialité : Physique

École doctorale n°564: Physique en Île-de-France

réalisée

au Laboratoire Kastler Brossel

sous la direction de Pierre-François Cohadon

présentée par

Pierre-Edouard Jacquet

pour obtenir le grade de :

DOCTEUR DE SORBONNE UNIVERSITÉ

Sujet de la thèse :

Progress towards cryogenic squeezed light optomechanics

soutenue le ????? 2025

devant le jury composé de :

M.	Mr.	Rapporteur
M.	Mr.	Rapporteur
M.	Mr.	Examinateur
Mme.	coucou	Examinateuse
Mme.	salut	Présidente du Jury
M.	aurevoir	Directeur de thèse



Remerciements

Merci bien

Contents

Introduction

Historical background

State of the art

Relevance of this work

Chapter I

Theory: Background

This chapter will cover the elementary concepts required to describe an membrane based optomechanical system in a quantum regime. We will first recall basics on optical field quantization as well describing coherent and squeezed light field, to then turn to the more specific frequency dependent squeezed light field. Secondly, we will cover the mathematical description of a mechanical resonator interacting with a generic coherent optical field, highlighting the differences with the seminal optomechanical system of a mirror on a spring. Finally, we will derive the equations of motions of a membrane based optomechanical system with frequency dependent squeezed optical fields [1].

Contents

I.1	Optics	7
I.1.1	Spatial Modes	7
I.1.2	Quantum Description	7
I.1.3	Coherent and Squeezed States	15
I.1.4	Classical Modulations	20
I.1.5	Quantum Sideband Diagram	21
I.2	Cavities	22
I.2.1	Cavity Geometries and Stability Conditions	22
I.2.2	Cavity Resonances	24
I.2.3	Mode-Matching	24
I.2.4	Simple Cavities	25
I.2.5	Non Linear Cavities	34
I.2.6	Optomechanical Cavities	40
I.3	Detection	47
I.3.1	Direct detection	47
I.3.2	Balanced Homodyne Detection	49

I.1 Optics

I.1.1 Spatial Modes

The spatial structure of an electromagnetic wave propagating along the z -axis can be described by a set of well-defined transverse modes, which are solutions of the paraxial Helmholtz equation. The most fundamental solution is the Gaussian mode, whose electric field amplitude reads

$$E(\mathbf{r}) = E_0 \frac{w_0}{w(z)} \exp\left(-\frac{x^2 + y^2}{w^2(z)}\right) \exp\left[-i\left(kz + \frac{k(x^2 + y^2)}{2R(z)} - \psi(z)\right)\right], \quad (\text{I.1})$$

where $\mathbf{r} = (x, y, z)$, E_0 is the field amplitude at the beam waist, $k = 2\pi/\lambda$ the wavenumber, and λ the optical wavelength. The various quantities introduced above are defined as

$$\begin{aligned} w(z) &\equiv w_0 \sqrt{1 + (z/z_R)^2}, & z_R &\equiv \pi w_0^2 / \lambda, \\ R(z) &\equiv z \left[1 + (z_R/z)^2\right], & \psi(z) &\equiv \arctan(z/z_R), \end{aligned}$$

with w_0 the waist, z_R the Rayleigh range, $R(z)$ the wavefront curvature, and $\psi(z)$ the Gouy phase. A compact expression of the Gaussian envelope is written as

$$E(\mathbf{r}) = E_0 \frac{iz_R}{q(z)} \exp\left(-\frac{ik(x^2 + y^2)}{2q(z)}\right) e^{ikz} \quad \text{with} \quad q(z) \equiv z + iz_R, \quad (\text{I.2})$$

where we defined the complex beam parameter $q(z)$. Beyond the fundamental Gaussian mode, more general solutions of the paraxial equation can be constructed. In Cartesian coordinates, these are the Hermite–Gaussian modes TEM_{mn} , given by

$$\begin{aligned} E_{mn}(\mathbf{r}) &= E_0 \frac{w_0}{w(z)} H_m\left(\frac{\sqrt{2}x}{w(z)}\right) H_n\left(\frac{\sqrt{2}y}{w(z)}\right) \exp\left(-\frac{x^2 + y^2}{w^2(z)}\right) \\ &\quad \times \exp\left[-i\left(kz + \frac{k(x^2 + y^2)}{2R(z)} - (m + n + 1)\psi(z)\right)\right], \quad (\text{I.3}) \end{aligned}$$

where H_m, H_n are Hermite polynomials.

I.1.2 Quantum Description

Quantised Electromagnetic Field

We will consider both cases of a finite quantisation volume V and an infinite volume: when dealing with cavity modes, we will use the finite volume description, while for propagating modes carrying sideband correlations we will use the infinite volume description, under the

two-photon formalism prescription. Both descriptions are linked through the input-output formalism introduced later on.

We first consider the quantised electromagnetic field in a volume V . The electric field operator can be written as

$$\hat{\mathbf{E}}(\mathbf{r}, t) = i \sum_{\ell} \mathcal{E}_{\ell} \left[\hat{a}_{\ell} \mathbf{f}_{\ell}(\mathbf{r}) e^{-i\omega_{\ell} t} - \hat{a}_{\ell}^{\dagger} \mathbf{f}_{\ell}^*(\mathbf{r}) e^{+i\omega_{\ell} t} \right], \quad (\text{I.4})$$

where $\mathcal{E}_{\ell} = \sqrt{\frac{\hbar\omega_{\ell}}{2\varepsilon_0 V}}$ is the field amplitude per photon in mode ℓ , \hbar is the reduced Planck constant, ω_{ℓ} is the angular frequency of mode ℓ , and ε_0 is the vacuum permittivity. The spatial mode functions $\mathbf{f}_{\ell}(\mathbf{r})$ form an orthonormal basis in V according to

$$\int_V d^3 r \mathbf{f}_{\ell}^*(\mathbf{r}) \cdot \mathbf{f}_{\ell'}(\mathbf{r}) = \delta_{\ell\ell'}, \quad \mathbf{f}_{\ell}(\mathbf{r}) \propto E_{mn}(\mathbf{r}) \boldsymbol{\epsilon}_x$$

where we assumed a linearly polarized field along the x -axis, with $\boldsymbol{\epsilon}_x$ the corresponding unit vector. The index $\ell = (m, n)$ then labels the different spatial modes, the Hermite–Gaussian modes in our case.

In the limit of an infinite quantisation volume $V \rightarrow \infty$, the discrete mode index ℓ becomes a continuous variable i.e. the mode spacing becomes infinitesimal. As detailed in the Appendix, we now need to consider a continuum of modes with annihilation operator $\hat{a}[\omega]$ labeled by their angular frequency ω . To come down to the two-photon formalism, we make the following assumptions :

- We consider frequencies $\omega = \omega_0 \pm \Omega$ centered around a carrier frequency ω_0 , with $\Omega \in [-B, +B] \ll \omega_0$ where B is the bandwidth. This is valid since the bandwidth B , generally up to tens of GHz, is small compared to ω_0 which is hundreds of THz for optical frequencies.
- We consider a single spatial mode, i.e. we drop the spatial dependence of the field and consider only one transverse mode function $\mathbf{f}(\mathbf{r})$, the fundamental Gaussian mode imposed by the laser source and/or spatial filtering elements. This is valid since the spatial envelope of the beam does not vary significantly over the considered bandwidth. The spatial mode function is then factored out of the integrals over frequency.
- We consider the electric field operator to only be dependent on time t , having projected the field onto the transverse mode function and integrated over the transverse plane, as well as setting the propagation coordinate $z = 0$ for simplicity.

Upon these assumptions, the electric field operator reduces to a time dependent operator (Heisenberg picture) expressed as

$$\hat{E}(t) = \mathcal{E}_0 \left[\cos\left(\omega_0 t - \frac{\pi}{2}\right) \int_{-\infty}^{\infty} \frac{d\Omega}{2\pi} (\hat{a}_+ + \hat{a}_-^\dagger) e^{-i\Omega t} + \sin\left(\omega_0 t - \frac{\pi}{2}\right) \int_{-\infty}^{\infty} \frac{d\Omega}{2\pi} i(\hat{a}_-^\dagger - \hat{a}_+) e^{-i\Omega t} \right] \quad (\text{I.5})$$

where we defined the sideband annihilation operators as $\hat{a}_+ \equiv \hat{a}[\omega_0 + \Omega]$ and $\hat{a}_- \equiv \hat{a}[\omega_0 - \Omega]$. The field amplitude per photon at the carrier frequency is given by $\mathcal{E}_0 = \sqrt{\hbar\omega_0/2\varepsilon_0 c A}$, where A is the effective cross-sectional area of the beam and c the speed of light in vacuum. The explicit relationship between the discrete mode operator \hat{a}_ℓ and the continuous mode operator $\hat{a}[\omega]$ (and thus their hermitian conjugate) is given in the Appendix.

Note: Although the electric field operator is written in the Heisenberg picture, the annihilation and creation operators $\hat{a}[\omega]$ and $\hat{a}[\omega]^\dagger$ are Schrodinger like operators, i.e. time independent operators. This is because we already factored out the time dependence $e^{-i\omega t}$ associated to each frequency mode when writing our annihilation/creation operators. As seen later on, the time dependence of the field operator defined through the Fourier transform arises from the superposition of many frequency modes, leading to beating at frequency Ω . This is the heart of the two-photon formalism, where a time dependent field Heisenberg like operator is built from the superposition of Schrodinger like annihilation/creation operators at different frequencies. In the litterature, the schrodinger like operators are sometimes written as \hat{a}_ω to draw a parallel between the discrete mode case \hat{a}_ℓ , but we will stick to the $\hat{a}[\omega]$ notation to avoid confusion with time dependent operators.

When writing annihilation operators, we will often drop the frequency dependence to lighten the notation, but it is implicit that they depend on frequency i.e. $\hat{a} \equiv \hat{a}[\omega]$, such that it applies to both sideband operators \hat{a}_+ and \hat{a}_- .

Commutation Relations

As demonstrated in the Appendix, the continuous annihilation and creation operators satisfy the following commutation relations:

$$[\hat{a}[\omega], \hat{a}^\dagger[\omega']] = 2\pi \delta(\omega - \omega'), \quad [\hat{a}[\omega], \hat{a}[\omega']] = 0, \quad [\hat{a}^\dagger[\omega], \hat{a}^\dagger[\omega']] = 0.$$

such that the sideband operators satisfy

$$[\hat{a}_\pm, \hat{a}_\pm^\dagger] = 2\pi \delta(\Omega - \Omega'), \quad [\hat{a}_\pm, \hat{a}_\mp] = 0, \quad [\hat{a}_\pm^\dagger, \hat{a}_\mp^\dagger] = 0.$$

Quadrature Operators

We describe the phase-space properties of a field mode using hermitian quadrature operators. These are linear combinations of the annihilation and creation operators that correspond to measurable observables in the electromagnetic field. Here again, we won't write explicitly the frequency dependence, but it is implicit in the following i.e. $\hat{\mathbf{u}} \equiv \hat{\mathbf{u}}[\Omega]$ and $\hat{\mathbf{a}} \equiv \hat{\mathbf{a}}[\Omega]$. The two most common quadratures are defined as follows:

$$\hat{\mathbf{u}} \equiv \begin{pmatrix} \hat{a}_1 \\ \hat{a}_2 \end{pmatrix} = \boldsymbol{\Gamma} \hat{\mathbf{a}} \quad \text{with} \quad \boldsymbol{\Gamma} \equiv \begin{pmatrix} 1 & 1 \\ -i & i \end{pmatrix} \quad \text{and} \quad \hat{\mathbf{a}} \equiv \begin{pmatrix} \hat{a}_+ \\ \hat{a}_-^\dagger \end{pmatrix} \quad (\text{I.6})$$

where we defined the field vector $\hat{\mathbf{a}}$ and the transfer matrix $\boldsymbol{\Gamma}$, later used to switch from *one-photon* to *two-photon* description of optical elements. The electric field operator can then be recasted as

$$\hat{E}(t) = \mathcal{E}_0 \left[\cos\left(\omega_0 t - \frac{\pi}{2}\right) \int_{-\infty}^{\infty} \frac{d\Omega}{2\pi} \hat{a}_1[\Omega] e^{-i\Omega t} + \sin\left(\omega_0 t - \frac{\pi}{2}\right) \int_{-\infty}^{\infty} \frac{d\Omega}{2\pi} \hat{a}_2[\Omega] e^{-i\Omega t} \right]. \quad (\text{I.7})$$

where it is now explicit that the electric field features two orthogonal components oscillating at the carrier frequency ω_0 , with amplitudes given by the quadrature operators \hat{a}_1 and \hat{a}_2 .

Fourier Transform

We now come to the aforementioned building of a time dependent field operator from the superposition of many frequency modes. This is done through the Fourier transform defined as

$$\begin{aligned} \hat{\mathbf{a}}(t) &= \int_{-\infty}^{+\infty} \frac{d\Omega}{2\pi} e^{-i\Omega t} \hat{\mathbf{a}}[\Omega] \\ \hat{\mathbf{a}}[\Omega] &= \int_{-\infty}^{+\infty} dt e^{i\Omega t} \hat{\mathbf{a}}(t) \end{aligned} \quad (\text{I.8})$$

In this definition, a notable property is that the hermitian conjugate in the time domain translates to a frequency inversion in the Fourier domain:

$$[\hat{a}(t)]^\dagger = \hat{a}^\dagger(t), \quad [\hat{a}_+]^\dagger = \hat{a}_-. \quad (\text{I.9})$$

It then follows that the quadrature operators in the time domain are effectively Hermitian operators, as expected for observables, while the frequency domain quadrature operators satisfy

$$\hat{a}_1^\dagger[\Omega] = \hat{a}_1[-\Omega], \quad \hat{a}_2^\dagger[\Omega] = \hat{a}_2[-\Omega]. \quad (\text{I.10})$$

Commutation Relations in vector form

The matrix form commutator in both time and frequency space reads

$$[\hat{\mathbf{a}}, \hat{\mathbf{a}}^\dagger] = \sigma_z \times \begin{cases} \delta(t - t') \\ 2\pi\delta(\Omega - \Omega'). \end{cases} \quad (\text{I.11})$$

with σ_z the Pauli Z matrix, and where it is implicit that we evaluate both at different frequencies or times respectively. An arbitrary rotated quadrature pair is obtained by

$$\hat{\mathbf{u}}_\phi \equiv \mathbf{R}(\phi) \hat{\mathbf{u}} = \mathbf{R}(\phi) \Gamma \hat{\mathbf{a}} \quad \text{with} \quad \mathbf{R}(\phi) \equiv \begin{pmatrix} \cos \phi & \sin \phi \\ -\sin \phi & \cos \phi \end{pmatrix}. \quad (\text{I.12})$$

and where we identify the useful identity

$$\mathbf{R}(\phi) \Gamma = \begin{pmatrix} e^{-i\phi} & e^{i\phi} \\ -ie^{-i\phi} & ie^{i\phi} \end{pmatrix}.$$

The commutators of the rotated quadrature operators read

$$[\hat{\mathbf{u}}_\phi, \hat{\mathbf{u}}_\phi^\dagger] = 2i \mathbf{J} \begin{cases} \delta(t - t') \\ 2\pi\delta(\Omega - \Omega'). \end{cases} \quad \text{with} \quad \mathbf{J} \equiv \begin{pmatrix} 0 & 1 \\ -1 & 0 \end{pmatrix}. \quad (\text{I.13})$$

This identity would not be true had we considered large sideband frequencies $\Omega \sim \omega_0$ i.e. it would feature corrections in all \mathbf{J} terms, including diagonal.

Linearization of the optical field

Let's now consider a quantum state living in this continuous mode space $|\psi\rangle$. We can always linearize the field operators around their mean value, which is particularly useful when dealing with intense fields featuring small quantum fluctuations around a large classical amplitude. This is the case for coherent and squeezed states, which are introduced right below. The annihilation operator is then decomposed as

$$\hat{a} = \bar{\alpha} + \delta\hat{a} \quad (\text{I.14})$$

where $\bar{\alpha} = \langle \psi | \hat{a} | \psi \rangle \in \mathbb{C}$ is the mean complex amplitude of the quantum state, and $\delta\hat{a}$ represents quantum fluctuations with $\langle \psi | \delta\hat{a} | \psi \rangle = 0$. Note this decomposition is valid for any quantum state, including coherent and squeezed states. We note $\bar{\alpha}$ to distinguish it from the complex amplitude α of a coherent state introduced below, which is a specific case of this

decomposition. The field vector is then expressed as

$$\hat{\mathbf{a}} = \begin{pmatrix} \bar{\alpha}_+ \\ \bar{\alpha}_-^* \end{pmatrix} + \begin{pmatrix} \delta\hat{a}_+ \\ \delta\hat{a}_-^\dagger \end{pmatrix} = \bar{\mathbf{a}} + \delta\hat{\mathbf{a}} \quad (\text{I.15})$$

and it then follows that the quadrature operators can also be expressed as

$$\hat{\mathbf{u}}_\phi = \mathbf{R}(\phi) \Gamma (\bar{\mathbf{a}} + \delta\hat{\mathbf{a}}) = \bar{\mathbf{u}}_\phi + \delta\hat{\mathbf{u}}_\phi. \quad (\text{I.16})$$

For the vacuum state $|0\rangle$, we have $\bar{\alpha}_\pm = 0$ and thus $\hat{\mathbf{a}} = \delta\hat{\mathbf{a}}$. Since we will always consider fluctuations around the mean value, we will systematically use the notation $\delta\hat{a}$ to refer to the annihilation operator, unless specified otherwise, as well as assuming the vacuum state as the reference when we write average values as $\langle \cdot \rangle \equiv \langle 0 | \cdot | 0 \rangle$. All the above definitions and properties thus apply to the fluctuation operators (commutation relations, Fourier transforms, etc.).

Amplitude and Phase Quadratures

Considering the mean field amplitude $\bar{\alpha} = |\bar{\alpha}|e^{i\bar{\varphi}}$, we will often refer to the amplitude and phase quadratures, defined respectively as the quadratures at angles $\phi = \bar{\varphi}$ and $\phi = \bar{\varphi} + \pi/2$. As the angle $\bar{\varphi}$ defines the mean field phase relative to a reference (e.g. a local oscillator), we will assume without loss of generality that $\bar{\varphi} = 0$, such that the amplitude and phase quadratures correspond to \hat{a}_1 and \hat{a}_2 respectively. We will then relabel them as

$$\delta\hat{p} \equiv \delta\hat{a}_{\phi=0} = \delta\hat{a}_1, \quad \delta\hat{q} \equiv \delta\hat{a}_{\phi=\pi/2} = \delta\hat{a}_2. \quad (\text{I.17})$$

Noise Spectral Density Matrix

A central concept in this thesis is the two-sided Noise Spectral Density matrix of the quadrature fluctuations, which characterizes the second-order statistical properties of the quantum state in the frequency domain. Namely, it describes the spectral distribution of the variances and covariances of the quadrature fluctuations. For a given quadrature angle ϕ , it is defined as

$$\begin{aligned} \mathbf{S}_\phi[\Omega] &= \frac{1}{2} \int \frac{\delta\Omega'}{2\pi} \langle \{\delta\hat{\mathbf{u}}_\phi, \delta\hat{\mathbf{u}}_\phi^\dagger\} \rangle \\ &= \frac{1}{2} \int \frac{\delta\Omega'}{2\pi} \mathbf{R}(\phi) \langle \{\delta\hat{\mathbf{u}}, \delta\hat{\mathbf{u}}^\dagger\} \rangle \mathbf{R}(-\phi) \\ &= \frac{1}{2} \int \frac{\delta\Omega'}{2\pi} \mathbf{R}(\phi) \begin{pmatrix} \langle \{\delta\hat{p}, \delta\hat{p}^\dagger\} \rangle & \langle \{\delta\hat{p}, \delta\hat{q}^\dagger\} \rangle \\ \langle \{\delta\hat{q}, \delta\hat{p}^\dagger\} \rangle & \langle \{\delta\hat{q}, \delta\hat{q}^\dagger\} \rangle \end{pmatrix} \mathbf{R}(-\phi) \end{aligned} \quad (\text{I.18})$$

where $\{\hat{A}, \hat{B}\} = \hat{A}\hat{B} + \hat{B}\hat{A}$ denotes the anticommutator, implicitly evaluated at frequencies Ω and Ω' , and integrated over Ω' . The diagonal elements of the noise spectral density matrix correspond to the power spectral densities of the quadrature fluctuations, while the off-diagonal elements represent the cross-spectral densities between different quadratures. The noise spectral density matrix is a Hermitian matrix, reflecting the physical properties of the quantum state. We will particularly focus on the amplitude and phase quadrature noise spectral density matrix, obtained by setting $\phi = 0$, and we will denote it as $\mathbf{S}[\Omega] \equiv \mathbf{S}_{\phi=0}[\Omega]$. The subscripts will then denote whether we refer to the transmitted or reflected fields of an optical cavity, the output spectrum of a squeezer, etc. For completeness we introduce the single-sided noise spectral density matrix, defined as

$$\bar{\mathbf{S}}_{\phi}[\Omega] = \frac{1}{2}(\mathbf{S}_{\phi}[\Omega] + \mathbf{S}_{\phi}[-\Omega]) \quad (\text{I.19})$$

such that the variance of a quadrature operator can be retrieved by integrating the single-sided noise spectral density over positive frequencies only (as one would with a real signal in a spectrum analyzer). A generalized version of the Heisenberg uncertainty relation can be expressed in terms of the noise spectral density matrix as

$$\det \mathbf{S}_{\phi}[\Omega] \geq 1 \quad (\text{I.20})$$

which sets a fundamental limit on the simultaneous knowledge of the quadrature fluctuations at a given frequency Ω .

Vacuum state

For the vacuum state $|0\rangle$, we derive the noise spectral density matrix using the commutation relations and the fact that $\langle \delta\hat{a} \rangle = 0$ (see Annexe). The calculation yields

$$\mathbf{S}_{\phi}^{\text{vac}}[\Omega] = \begin{pmatrix} 1 & 0 \\ 0 & 1 \end{pmatrix} \quad (\text{I.21})$$

for any angle ϕ and frequency Ω . This result indicates that the vacuum state has equal fluctuations in both quadratures, with no correlations between them, as expected for a minimum uncertainty state. The noise spectral density matrix of the vacuum state serves as a reference point for comparing other quantum states, such as coherent and squeezed states, which exhibit different fluctuation properties.

Linear Optical Systems

As we will develop further in the next section, the output fields of various optical systems can be expressed in a general linear form as

$$\delta\hat{\mathbf{u}}_{\text{out}} = \mathbf{T} \delta\hat{\mathbf{u}}_{\text{in}} + \mathbf{L} \delta\hat{\mathbf{u}}_{\text{vac}}. \quad (\text{I.22})$$

where \mathbf{T} and \mathbf{L} are 2×2 frequency dependent transfer matrices. The input and vacuum fields are assumed to be in the vacuum state, as well as being uncorrelated such that

$$\begin{aligned} \langle \delta\hat{\mathbf{u}}_{\text{in}} \delta\hat{\mathbf{u}}_{\text{in}}^\dagger \rangle &= 2\pi\delta(\Omega + \Omega')\mathbf{S}_{\text{in}}[\Omega] \\ \langle \delta\hat{\mathbf{u}}_{\text{vac}} \delta\hat{\mathbf{u}}_{\text{vac}}^\dagger \rangle &= 2\pi\delta(\Omega + \Omega')\mathbf{1} \\ \langle \delta\hat{\mathbf{u}}_{\text{in}} \delta\hat{\mathbf{u}}_{\text{vac}}^\dagger \rangle &= \mathbf{0} \end{aligned} \quad (\text{I.23})$$

Computing the noise spectra is then straightforward :

$$\mathbf{S}^{\text{out}}[\Omega] = \mathbf{T}\mathbf{S}^{\text{in}}\mathbf{T}^\dagger + \mathbf{L}\mathbf{L}^\dagger \quad (\text{I.24})$$

where $\mathbf{S}_{\text{vac}} = \mathbf{1}$ as seen above. For an arbitrary quadrature angle ϕ , we simply rotate the transfer matrices as

$$\mathbf{T}_\phi = \mathbf{R}(\phi) \mathbf{T} \mathbf{R}(-\phi), \quad \mathbf{L}_\phi = \mathbf{R}(\phi) \mathbf{L} \mathbf{R}(-\phi)$$

such that

$$\mathbf{S}_\phi^{\text{out}}[\Omega] = \mathbf{T}_\phi \mathbf{S}_\phi^{\text{in}} \mathbf{T}_\phi^\dagger + \mathbf{L}_\phi \mathbf{L}_\phi^\dagger \quad (\text{I.25})$$

Graphical Representation of Gaussian States

For Gaussian states, we can actually picture them in a 2D space, where the two axes correspond to the two quadratures \hat{a}_1 and \hat{a}_2 . In the case where the mean phase is zero, these quadratures correspond to the amplitude and phase quadratures \hat{p} and \hat{q} . The quantum state can then be represented as a 2D Gaussian distribution centered around the mean values of the quadratures, with the shape and orientation of the distribution characterized by the off diagonal elements of the noise spectral density matrix. The uncertainties in the quadratures are represented by the widths of the Gaussian distribution along each axis, while correlations between the quadratures are represented by the tilt of the distribution. This graphical representation provides an intuitive way to visualize and understand the properties of Gaussian quantum states, such as coherent and squeezed states, in terms of their quadrature fluctuations and correlations.

I.1.3 Coherent and Squeezed States

We now turn to standard optical quantum states, in particular gaussian states i.e. full positive in Wigner function representations such as coherent and squeezed states, that we will denote in braket notation as $|\alpha\rangle$ and $|\alpha, r, \theta\rangle$.

Coherent States:

The monochromatic coherent state $|\alpha\rangle$ is an eigenstate of the annihilation operator:

$$\hat{a}_+ |\alpha\rangle = \alpha \delta(\Omega) |\alpha\rangle \quad (\text{I.26})$$

where $\alpha = |\alpha| e^{i\bar{\varphi}}$ is a complex number representing the mean coherent amplitude. In this notation, the angle $\bar{\varphi}$ is the mean angle of the distribution, used to describe the relative phase to a reference (e.g. a local oscillator), as in Fig ???. The \hat{a} linear decomposition above (Eq ??) then yields $\alpha = \bar{\alpha}$ for a coherent state. A generic multimode coherent state is generated by the displacement operator $\hat{D}(\alpha)$ such that

$$|\alpha\rangle = \hat{D}(\alpha) |0\rangle \quad (\text{I.27})$$

where the general expression for the displacement operator acting on the vacuum state is given by

$$\hat{D}(\alpha) = \exp\left(\int \frac{d\Omega}{2\pi} [\alpha(\Omega) \hat{a}_-^\dagger - \alpha^*(\Omega) \hat{a}_+]\right) \quad (\text{I.28})$$

which collapses to

$$\hat{D}(\alpha) = \exp\left(\frac{1}{2\pi} [\alpha \hat{a}^\dagger[\omega_0] - \alpha^* \hat{a}[\omega_0]]\right) \quad (\text{I.29})$$

when defining a monochromatic coherent state $\alpha(\Omega) = \alpha \delta(\Omega)$, that is a coherent state at the carrier frequency only. Upon the action of this displacement operator, the sideband operator is transformed as

$$D^\dagger(\alpha) \hat{a}_+ D(\alpha) = \hat{a}_+ + \alpha \delta(\Omega) \quad (\text{I.30})$$

such that we can verify the eigenvalue equation (Eq ??) straightforwardly as

$$\begin{aligned} \hat{a}_+ |\alpha\rangle &= D(\alpha)(D^\dagger(\alpha) \hat{a}_+ D(\alpha)) |0\rangle \\ &= \hat{D}(\alpha)(\alpha \delta(\Omega) + \hat{a}_+) |0\rangle \\ &= \alpha \delta(\Omega) |\alpha\rangle \end{aligned}$$

Expectation values: Using the quadrature vector $\hat{\mathbf{u}}_\phi$ (Eq ??), and the $\mathbf{R}\Gamma$ identity, the

expectation values in a coherent state are

$$\langle \hat{D}^\dagger \hat{\mathbf{u}}_\phi \hat{D} \rangle = \mathbf{R}(\phi) \langle \hat{D}^\dagger \hat{\mathbf{u}} \hat{D} \rangle = 2\delta(\Omega) \begin{pmatrix} \text{Re}(|\alpha| e^{i(\bar{\varphi}-\phi)}) \\ \text{Im}(|\alpha| e^{i(\bar{\varphi}-\phi)}) \end{pmatrix} \quad (\text{I.31})$$

such that the components reduce to $2\text{Re}(\alpha)$ and $2\text{Im}(\alpha)$ if $\phi = 0$, and to $2|\alpha|$ and 0 if $\phi = \bar{\varphi}$, or equivalently if we set $\bar{\varphi} = \phi = 0$ as mentioned earlier (such that $\hat{\mathbf{u}}$ corresponds to the amplitude and phase quadratures). We also notice the delta function at $\Omega = 0$, indicating that the coherent state has a non-zero mean field only at the carrier frequency.

Spectrum: For a coherent state, the fluctuations are identical to that of the vacuum state, seen directly from equation (??). Since the fluctuation operators are unchanged by the displacement, the noise spectral density matrix remains that of the vacuum:

$$\mathbf{S}_\phi^{\text{coh}}[\Omega] = \begin{pmatrix} 1 & 0 \\ 0 & 1 \end{pmatrix} \quad (\text{I.32})$$

for any angle ϕ and frequency Ω . Relating to the linear optical systems introduced, this is equivalent to having identity transfer matrices $\mathbf{T} = \mathbf{1}$ and $\mathbf{L} = \mathbf{0}$, such that no additional noise is added to the input vacuum fluctuations. Coherent states only differ from vacuum by their non-zero mean field amplitudes at the carrier frequency $\Omega = 0$, symbolized by the delta function in the expectation values above.

Squeezed States:

Squeezed states $|\alpha, r, \theta\rangle$ are quantum gaussian states of light in which the noise (variance) of one quadrature is reduced below the vacuum level, at the expense of increased noise in the conjugate quadrature. A generic squeezed state is characterized by three parameters: the displacement amplitude α , the squeezing parameter r , and the squeezing angle θ . The so called 'bright' squeezed state is generated by applying both a displacement and a squeezing operation to the vacuum state:

$$|\alpha, r, \theta\rangle = \hat{S}(r, \theta) \hat{D}(\alpha) |0\rangle \quad (\text{I.33})$$

where the squeezing operator $\hat{S}(r, \theta)$ is defined as

$$\hat{S}(r, \theta) = \exp \left(r \int_{-\infty}^{\infty} \frac{d\Omega}{2\pi} \left[e^{-i2\theta(\Omega)} \hat{a}_+ \hat{a}_- - e^{i2\theta(\Omega)} \hat{a}_+^\dagger \hat{a}_-^\dagger \right] \right) \quad (\text{I.34})$$

where we assumed the squeezing parameter r to be frequency independent. This operator describes the process of parametric down-conversion, where pairs of photons are created

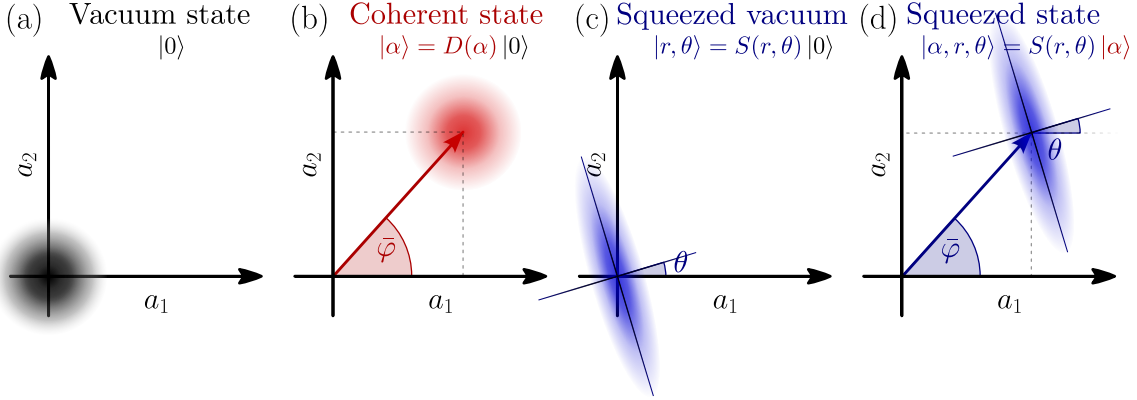


Fig. I.1 Phase-space representations of Gaussian quantum states. 2D cuts of the Wigner function in the quadrature plane ($a_1[\Omega]$, $a_2[\Omega]$) at a given frequency. (a) vacuum state: a circular Gaussian centered at the origin, featuring equal quantum fluctuations in both a_1 and a_2 quadratures. (b) coherent state: a displaced circular Gaussian, showing a shift in phase space along an angle φ with vacuum fluctuations. This corresponds to either the carrier ($\Omega = 0$), or a sideband frequency with a non zero modulation. (c) vacuum squeezed state: an elliptical Gaussian centered at the origin, with reduced noise along a rotated quadrature and increased noise in the orthogonal direction. (d) bright squeezed state: an ellipse shifted away from the origin, combining anisotropic fluctuations and a nonzero mean amplitude. The displacement angle φ and squeezing angle θ are independent.

or annihilated in the sideband modes \hat{a}_\pm with a phase relation determined by the squeezing angle $\theta(\Omega)$. We can then write the action of the squeezing operator on the sideband operators as

$$\hat{S}^\dagger \hat{a}_+ \hat{S} = \hat{a}_+ \cosh r - e^{i2\theta(\Omega)} \hat{a}_-^\dagger \sinh r \quad (\text{I.35})$$

and similarly for \hat{a}_- . This transformation shows how the squeezing operator mixes the annihilation and creation operators, leading to modified quadrature fluctuations in the squeezed state. Applying both transformations (displacement and squeezing) to the field vector, we have

$$\hat{D}^\dagger \hat{S}^\dagger \hat{a}_+ \hat{S} \hat{D} = \hat{a}_+ \cosh r - e^{i2\theta} \hat{a}_-^\dagger \sinh r + \gamma \delta(\Omega) \quad (\text{I.36})$$

with $\gamma = \alpha \cosh r - \alpha^* e^{i2\theta} \sinh r = |\gamma| e^{i\bar{\varphi}'}$ the displaced amplitude at the carrier frequency. We stress that the phase $\bar{\varphi}'$ generally differs from the displacement angle $\bar{\varphi}$ of the coherent amplitude α .

Expectation values: Similarly as in a coherent state, but this time from Eq (??), we can

derive the expectation values of the quadrature vector in a bright squeezed state as

$$\langle \hat{D}^\dagger \hat{S}^\dagger \hat{\mathbf{u}}_\phi \hat{S} \hat{D} \rangle = \mathbf{R}(\phi) \langle \hat{D}^\dagger \hat{S}^\dagger \hat{\mathbf{u}} \hat{S} \hat{D} \rangle = 2\delta(\Omega) \begin{pmatrix} \text{Re}(|\gamma| e^{i(\bar{\varphi}' - \phi)}) \\ \text{Im}(|\gamma| e^{i(\bar{\varphi}' - \phi)}) \end{pmatrix} \quad (\text{I.37})$$

indicating that the mean field is shifted by the displaced amplitude γ at the carrier frequency ω_0 .

Spectrum: We identify the field fluctuation transformation under the squeezing and displacement operators from ??:

$$\hat{D} \hat{S}^\dagger \delta \hat{\mathbf{a}} \hat{S} \hat{D} = \begin{pmatrix} \cosh r & -e^{i2\theta(\Omega)} \sinh r \\ -e^{-i2\theta(\Omega)} \sinh r & \cosh r \end{pmatrix} \delta \hat{\mathbf{a}} \quad (\text{I.38})$$

such that the quadrature fluctuations read

$$\hat{D}^\dagger \hat{S}^\dagger \delta \hat{\mathbf{u}} \hat{S} \hat{D} = \mathbf{T} \delta \hat{\mathbf{u}} \quad \text{with} \quad \mathbf{T} = \begin{pmatrix} \cosh r - \sinh r \cos 2\theta(\Omega) & -\sinh r \sin 2\theta(\Omega) \\ -\sinh r \sin 2\theta(\Omega) & \cosh r + \sinh r \cos 2\theta(\Omega) \end{pmatrix}. \quad (\text{I.39})$$

Using the linear optical system formalism introduced earlier, we identify the transfer matrices \mathbf{T} and $\mathbf{L} = \mathbf{0}$ (no additional noise). The noise spectral density matrix of a bright squeezed state is then computed as

$$\mathbf{S}^{\text{sqz}}[\Omega] = \mathbf{T} \mathbf{S}^{\text{vac}} \mathbf{T}^\dagger = \mathbf{T} \mathbf{T}^\dagger. \quad (\text{I.40})$$

Explicitly, this yields

$$\begin{aligned} \mathbf{S}^{\text{sqz}}[\Omega] &= \begin{pmatrix} \cosh 2r - \sinh 2r \cos 2\theta(\Omega) & -\sinh 2r \sin 2\theta(\Omega) \\ -\sinh 2r \sin 2\theta(\Omega) & \cosh 2r + \sinh 2r \cos 2\theta(\Omega) \end{pmatrix}. \\ &= \mathbf{R}(-\theta) \begin{pmatrix} e^{-2r} & 0 \\ 0 & e^{2r} \end{pmatrix} \mathbf{R}(\theta). \end{aligned} \quad (\text{I.41})$$

This result shows how the squeezing parameter r and squeezing angle θ influence the quadrature fluctuations in the squeezed state. The diagonal elements of the noise spectral density matrix represent the variances of the quadrature fluctuations, while the off-diagonal elements represent the correlations between the quadratures. At an arbitrary measurement angle ϕ ,

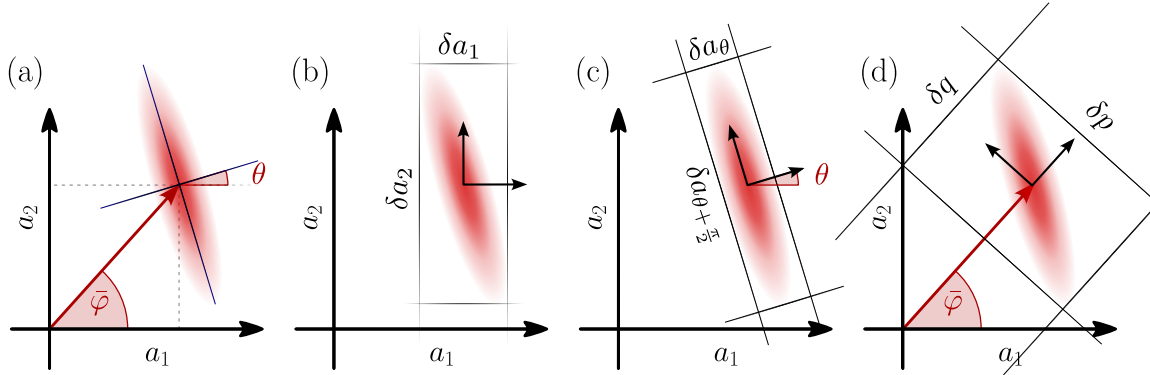


Fig. I.2 Phase-space representations of bright squeezed states with the different quadratures choices. (a) generic bright squeezed state. (b) projection of the quantum noise on the standard quadratures (a_1, a_2) . (c) projection of the quantum noise on the ellipse major axes quadratures $(a_\theta, a_{\theta+\pi/2})$, with θ the ellipse angle with respect to the standard quadratures. (d) projection of the quantum noise on the amplitude and phase quadratures (p, q) .

the noise spectral density matrix is given by

$$\begin{aligned} \mathbf{S}_\phi^{\text{sqz}}[\Omega] &= \mathbf{R}(\phi) \mathbf{S}^{\text{sqz}}[\Omega] \mathbf{R}(-\phi) \\ &= \mathbf{R}(\phi - \theta) \begin{pmatrix} e^{-2r} & 0 \\ 0 & e^{2r} \end{pmatrix} \mathbf{R}(\theta - \phi). \end{aligned} \quad (\text{I.42})$$

such that measuring along the squeezing angle $\phi = \theta(\Omega)$ yields the minimum variance in the first quadrature:

$$\mathbf{S}_{\phi=\theta}^{\text{sqz}}[\Omega] = \begin{pmatrix} e^{-2r} & 0 \\ 0 & e^{2r} \end{pmatrix}.$$

To obtain a full band reduction, one can then either use a frequency dependent squeezing angle $\theta(\Omega)$ and a fixed measurement quadrature ϕ , or inversely if the squeezing angle is fixed, one can rotate the measurement quadrature ϕ . These two techniques are known as frequency dependent squeezing [2] and variational readout [Vyatchanin1993, 2] respectively. Frequency dependent squeezing is the focus of our work here, and will be detailed in Chapter II.

Amplitude and Phase squeezed states: Considering a displaced squeezed state, two special cases are of interest: the amplitude squeezed state where $\theta = \bar{\varphi}$ and the phase squeezed state where $\theta = \bar{\varphi} + \pi/2$. In the first case, the amplitude quadrature \hat{p} is squeezed, while the phase quadrature \hat{q} is anti-squeezed. In the second case, the phase quadrature is squeezed, while the amplitude quadrature is anti-squeezed. The covariance matrices for

these states can be derived from Eq. (??) by setting $\psi = 0$ or $\psi = \pi/2$, respectively.

I.1.4 Classical Modulations

A key ingredient in our study is the concept of sidebands generated by classical modulations of a coherent field. These sidebands are frequency components that appear around the carrier frequency of the field due to the modulation process. We will consider two types of classical modulations: amplitude modulation (AM) and phase modulation (PM). These are instrumental in experimental physics, as they notably allow to extract usable error signals as to stabilize and lock various parameters of an optical setup, such as the length of a cavity or the phase of a local oscillator. Additionally, as we will see later, the optomechanical interaction itself is seen as a phase modulation of the intracavity field by the mechanical motion, generating sidebands and noises that carry information about the mechanical position.

Amplitude Modulation (AM) : Let the classical amplitude be modulated at Ω_{mod} in amplitude:

$$\alpha(t) = \bar{\alpha} (1 + \epsilon_a \cos(\Omega_{\text{mod}} t)) \quad (\text{I.43})$$

with $\epsilon_a \ll 1$, the field amplitude modulation depth. While the DC term lives at frequency ω_0 , the modulation introduces sidebands at frequencies $\omega_0 \pm \Omega_{\text{mod}}$, seen by expanding the cosine:

$$\alpha(t) = \bar{\alpha} \left(1 + \frac{\epsilon_a}{2} e^{i\Omega_{\text{mod}} t} + \frac{\epsilon_a}{2} e^{-i\Omega_{\text{mod}} t} \right) \quad (\text{I.44})$$

Phase Modulation (PM) : Now let the classical amplitude be modulated in phase at frequency Ω_{mod} :

$$\alpha(t) = \bar{\alpha} e^{i\epsilon_\phi \cos(\Omega_{\text{mod}} t)} \quad (\text{I.45})$$

with $\epsilon_\phi \ll 1$ the field phase modulation depth. Expanding to first order in ϵ_ϕ gives:

$$\alpha(t) \approx \bar{\alpha} \left(1 + \frac{i\epsilon_\phi}{2} e^{i\Omega_{\text{mod}} t} + \frac{i\epsilon_\phi}{2} e^{-i\Omega_{\text{mod}} t} \right) \quad (\text{I.46})$$

While the carrier term lives at frequency ω_0 , the modulation introduces sidebands at $\omega_0 \pm \Omega_{\text{mod}}$, both shifted in phase by $\pi/2$ relative to the carrier.

In both cases, amplitude or phase modulations, the field contains a carrier at frequency ω and two sidebands at $\omega \pm \Omega$. Amplitude modulation results in sidebands that are in phase with the carrier, while phase modulation produces sidebands with a $\pm\pi/2$ phase shift relative

to the carrier. We also note a general modulation process as :

$$\alpha(t) = \bar{\alpha}(1 + \varepsilon(t)) \quad (\text{I.47})$$

where $\varepsilon(t) \in \mathbb{C}$ is a modulation function that weakly modulates the complex amplitude in time, and that features information about the modulation frequency and depth. It then follows that the linearized amplitude-phase operators can be expressed as

$$\hat{\mathbf{u}}_{\bar{\alpha}}(t) = 2|\bar{\alpha}| \begin{pmatrix} 1 \\ 0 \end{pmatrix} + 2|\bar{\alpha}| \begin{pmatrix} \text{Re}(\varepsilon(t)) \\ \text{Im}(\varepsilon(t)) \end{pmatrix} + \begin{pmatrix} \delta\hat{p}(t) \\ \delta\hat{q}(t) \end{pmatrix} \quad (\text{I.48})$$

Computing the Fourier transform for amplitude and phase modulations yields

$$\begin{aligned} \varepsilon^{AM}(\Omega) &= \frac{\epsilon_a}{2} \left(\delta(\Omega - \Omega_{\text{mod}}) + \delta(\Omega + \Omega_{\text{mod}}) \right) \\ \varepsilon^{PM}(\Omega) &= \frac{i\epsilon_\phi}{2} \left(\delta(\Omega - \Omega_{\text{mod}}) + \delta(\Omega + \Omega_{\text{mod}}) \right) \end{aligned} \quad (\text{I.49})$$

And the quadrature operators of a modulated field can be expressed as

$$\hat{\mathbf{u}}_{\bar{\alpha}}[\Omega] = 2|\bar{\alpha}| \begin{pmatrix} 1 \\ 0 \end{pmatrix} \delta(\Omega) + 2|\bar{\alpha}| \begin{pmatrix} \text{Re}(\varepsilon[\Omega]) \\ \text{Im}(\varepsilon[\Omega]) \end{pmatrix} + \begin{pmatrix} \delta\hat{p}[\Omega] \\ \delta\hat{q}[\Omega] \end{pmatrix} \quad (\text{I.50})$$

We illustrate this by computing the spectra of a coherent field modulated in amplitude. The amplitude-phase quadrature fluctuation part reads

$$\delta\hat{\mathbf{u}}_{\bar{\alpha}}[\Omega] = |\bar{\alpha}|\epsilon_a \begin{pmatrix} \delta(\Omega - \Omega_{\text{mod}}) + \delta(\Omega + \Omega_{\text{mod}}) \\ 0 \end{pmatrix} + \begin{pmatrix} \delta\hat{p}[\Omega] \\ \delta\hat{q}[\Omega] \end{pmatrix} \quad (\text{I.51})$$

such that its covariance matrix reads

$$\mathbf{S}_{\bar{\alpha}}[\Omega] = 2|\bar{\alpha}|^2\epsilon_a^2 \left[\delta(\Omega - \Omega_{\text{mod}}) + \delta(\Omega + \Omega_{\text{mod}}) \right] \begin{pmatrix} 1 & 0 \\ 0 & 0 \end{pmatrix} + \mathbf{1} \quad (\text{I.52})$$

As seen in the above expression, the covariance matrix display a sum of dirac functions corresponding to a classical amplitude modulation of the field, as well as a flat vacuum noise across all frequencies.

I.1.5 Quantum Sideband Diagram

We now have all the tools to graphically represent the quantum states of light in the frequency domain. The so-called quantum sideband diagram is a useful representation to visualize the quantum states of light, especially when dealing with modulated fields and their sidebands. In this representation, we plot the carrier frequency ω_0 at the center, and the sidebands at

frequencies $\omega_0 \pm \Omega$ on either side.

Each sideband is represented by a vector in the quadrature plane, with its length and angle determined by the amplitude and phase of the sideband as seen above. The quantum noise associated with each sideband is represented by a gaussian distribution around the tip of the vector, with its shape and orientation determined by the noise spectral density matrix of the quantum state. The additional ingredient that the sideband diagram provides is the correlation between symmetrical sidebands, represented by markers connecting the two sidebands at $\omega_0 + \Omega$ and $\omega_0 - \Omega$. These correlations are crucial in understanding the properties of squeezed states, where the noise in one quadrature is reduced below the vacuum level, while the noise in the conjugate quadrature is increased. The sideband diagram allows us to visualize these correlations and their impact on the overall quantum state of light. This representation is particularly useful when analyzing the effects of optical cavities and other linear optical systems on quantum states, as they modify the amplitude and phase of the sidebands, hence the correlated/anticorrelated quadratures.

I.2 Cavities

Optical cavities are at the heart of this work, as they are used to coherently enhance the light-matter interaction in various systems, and also to filter and manipulate quantum states of light. In this section, we review the basic properties of optical cavities, their resonance conditions, and we derive the covariance matrices of their output fields.

I.2.1 Cavity Geometries and Stability Conditions

An optical cavity is a structure that *traps* photons by means of reflection between two or more mirrors. They can be either standing wave cavities, where the light bounces back and forth between two mirrors, or traveling wave cavities, where the light circulates in a loop. In both cases, the cavity supports discrete resonant modes determined by its geometry and the boundary conditions imposed by the mirrors. The stability criteria of a specific cavity configuration is derived considering the round trip ABCD matrix of the cavity describing how the complex beam parameter $q(z)$ introduced in (??) transforms after one round trip. The stability condition then simply reads as $-1 < (A + D)/2 < 1$. In the case of planar - travelling wave cavities, one needs to consider both the tangential and sagittal planes, as these cavities are astigmatic. The stricter condition, generally the sagittal plane one, then defines the stability range of the cavity.

Linear standing wave cavities: We first consider the two linear cavities used in this work, namely a concave-concave cavity (Fig ??.(a)) with two identical concave mirrors, and a plano-concave cavity with one flat mirror and one concave mirror (Fig ??.(b)). Using the

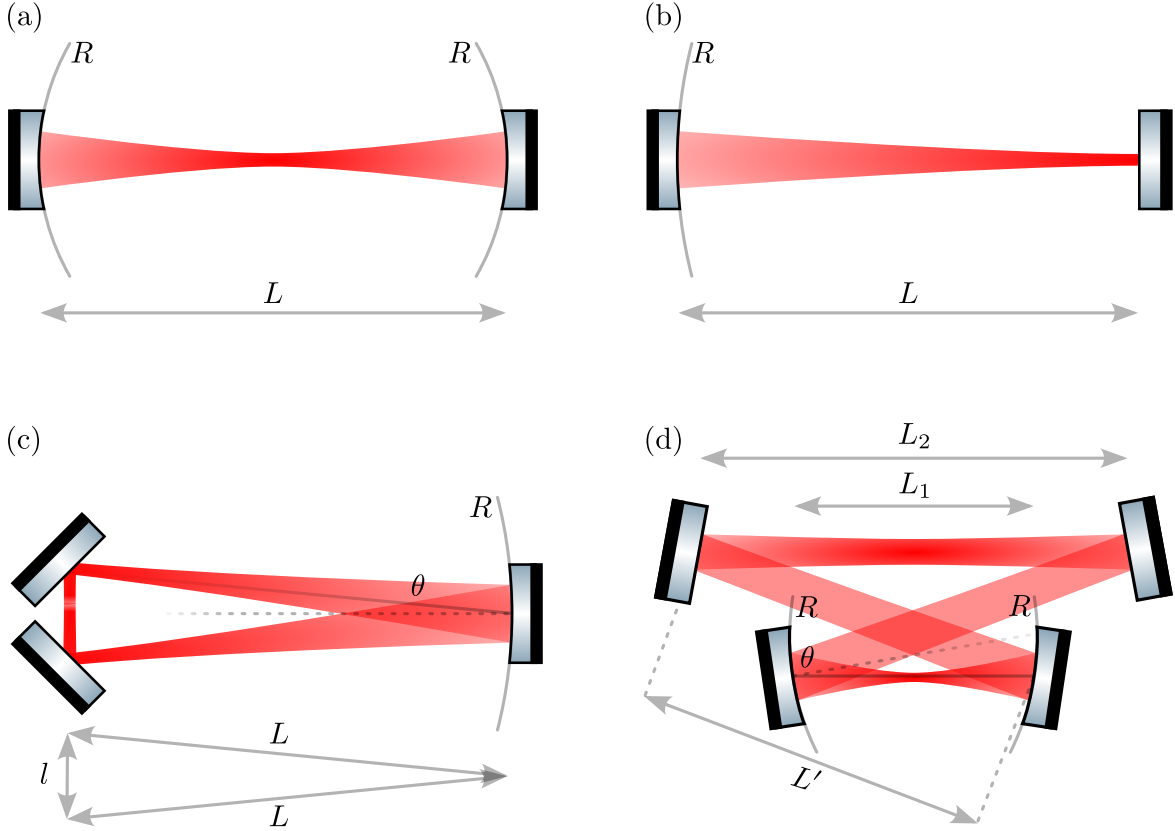


Fig. I.3 Geometries of various cavity types used in this work. (a) Linear concave-concave cavity (confocal in the $L \sim 2R$ case). (b) Linear plano-concave cavity. (a) and (b) are both standing wave cavities. (c) Planar triangular cavity. (d) Planar bow-tie cavity. (c) and (d) are both travelling wave cavities.

ABCD formalism for a confocal cavity of length L formed by two identical mirrors of radii of curvature R , the stability condition reads

$$0 < L < 2R \quad (\text{I.53})$$

For the plano-concave cavity, the stability condition reads

$$0 < L < R \quad (\text{I.54})$$

Planar traveling wave cavities: We now consider a triangular cavity formed by two concave mirrors of radius of curvature R and one flat mirror (Fig ??.(c)). The stability condition reads

$$0 < L_{rt} < 2R \cos(\theta) \quad (\text{I.55})$$

where $L_{rt} = 2L + l$ is the cavity round trip length, and θ is the angle of incidence of the

beam onto the curved mirror. This condition is the sagittal one, and is more stringent than the tangential one.

Considering now a bow-tie cavity formed by two concave mirrors of radius of curvature R and two flat mirrors (Figure ??.(d)), the full stability condition reads

$$0 < \left(1 - \frac{L_1 + 2L'}{R \cos \theta}\right) \left(1 - \frac{L_2}{R \cos \theta}\right) < 1 \quad (\text{I.56})$$

where L_1 is the distance between the two concave mirrors, L_2 the distance between the two flat mirrors, and L' the distance between a concave and a flat mirror (assuming a symmetric cavity). A simple design rule guaranteeing stability is then to set $L_1 + 2L' < R \cos \theta$ and $L_2 < R \cos \theta$.

I.2.2 Cavity Resonances

If the cavity is stable, it will then feature a discrete set of resonant modes everytime the cavity length is an integer multiple of half the wavelength $\lambda/2$ (standing wave cavity) or the wavelength λ (traveling wave cavity). In the frequency domain, modes are spaced by the free spectral range ω_{FSR} of the cavity, defined as

$$\omega_{\text{FSR}} = \frac{\pi c}{L} \quad (\text{linear cavity}), \quad \omega_{\text{FSR}} = \frac{2\pi c}{L_{rt}} \quad (\text{traveling wave cavity}) \quad (\text{I.57})$$

such that the resonant frequencies are given by

$$\omega_m = m \omega_{\text{FSR}}, \quad m \in \mathbb{N} \quad (\text{I.58})$$

and the cavity is on resonance when the input laser frequency ω_0 matches one of the resonant frequencies ω_m i.e. $\omega_0 = \omega_m$. To achieve this, one can either tune the laser frequency or the cavity length. In our experiments, we use the second option by mounting one of the cavity mirrors on a piezoelectric actuator. Changing the cavity length L by δL shifts the resonant frequencies by

$$\delta\omega_m = -m \frac{\pi c}{L^2} \delta L = -\frac{\omega_m}{L} \delta L \quad (\text{I.59})$$

I.2.3 Mode-Matching

A cavity also supports TEM_{mn} transverse modes, each with a specific spatial profile and resonant frequency. The resonant frequencies of these transverse modes are shifted relative to the fundamental mode by an amount that depends on the cavity geometry and the mode indices (m, n) . Coupling an incoming beam into a stable optical cavity requires that the

spatial mode of the beam matches that of the cavity. This means that the mode function of the incoming beam, assumed to be a TEM₀₀ Gaussian mode $f_0(\mathbf{r})$, must overlap with the cavity's fundamental mode $f'_0(\mathbf{r})$. If the basis functions are not perfectly aligned, the incoming field can be expanded in the orthonormal basis of cavity modes as

$$f_0(\mathbf{r}) = c_0 f'_0(\mathbf{r}) + \sum_{m>0} c_m f'_m(\mathbf{r}), \quad (\text{I.60})$$

where the coefficients c_m quantify the projection of the incident field onto the cavity eigenmodes. Only the component $c_0 f'_0$ couples efficiently to the fundamental cavity mode due the mirror geometry, while any mismatch excites higher-order transverse modes f'_m . The mode-matching procedure therefore consists in maximizing the overlap integral

$$\eta = \left| \int d^3\mathbf{r} f_0^*(\mathbf{r}) f'_0(\mathbf{r}) \right|^2, \quad (\text{I.61})$$

which ensures that essentially all the incoming photons populate the desired cavity mode, while suppressing excitation of spurious modes.

I.2.4 Simple Cavities

We consider a single field cavity mode described by the annihilation operator \hat{a} , interacting with several independent noise inputs. The system is governed by a Hamiltonian

$$\hat{H} = -\hbar\Delta\hat{a}^\dagger\hat{a} \quad (\text{I.62})$$

with $\Delta \equiv \omega_0 - \omega_c$ the cavity detuning to the laser frequency, and each input introduces dissipation characterized by a decay rate $\kappa_i = T_i/\tau$, with T_i the power transmittivity of the mirror and $\tau = 2L/c$ the roundtrip time of the cavity. This is we consider an input coupler (mirror) with decay rate κ_1 and an output coupler (mirror) with decay rate κ_2 . The laser field is shone onto the cavity by the input coupler.

In the frame rotating at the laser frequency, the dynamics of \hat{a} is given by the Quantum Langevin Equation (QLE):

$$\begin{aligned} \frac{d}{dt}\hat{a}(t) &= -\frac{i}{\hbar}[\hat{a}, \hat{H}] - \frac{\kappa}{2}\hat{a}(t) + \sqrt{\kappa_1}\hat{a}_{\text{in}}(t) + \sqrt{\kappa_2}\delta\hat{a}_{\text{vac}}(t) + \sqrt{\kappa_0}\delta\hat{a}_l(t) \\ &= -\left(\frac{\kappa}{2} - i\Delta\right)\hat{a}(t) + \sqrt{\kappa_1}\hat{a}_{\text{in}}(t) + \sqrt{\kappa_2}\delta\hat{a}_{\text{vac}}(t) + \sqrt{\kappa_0}\delta\hat{a}_l(t) \end{aligned} \quad (\text{I.63})$$

where $\kappa = \kappa_0 + \kappa_1 + \kappa_2$ is the total decay rate, with $\kappa_0 = \gamma/\tau$ and $\delta\hat{a}_l(t)$ the rate and fluctuation operator of additional losses. Here losses γ have ppm units. Another key element

to deriving both steady state behaviour as well as quadrature spectra is the input-output formula given by:

$$\hat{a}_{\text{ref}} = \sqrt{\kappa_1} \hat{a} - \hat{a}_{\text{in}}, \quad \hat{a}_{\text{trans}} = \sqrt{\kappa_2} \hat{a} - \delta \hat{a}_{\text{vac}} \quad (\text{I.64})$$

for both the reflected and transmitted field. In the input-output formula, the \hat{a}_{in} refers to the field incoming on the coupler considered, which are simple vacuum fluctuations on the output coupler since we don't shine the laser by this port.

As introduced in the previous subsection, one can split the annihilation operator in a mean field part α and a fluctuation part $\delta \hat{\mathbf{a}}(t)$ (vector form) such that this equation turns into two i.e. a scalar differential equation, and an operator differentail equation, that is:

$$\begin{cases} 0 = -\left(\frac{\kappa}{2} - i\Delta\right) \bar{\alpha} + \sqrt{\kappa_1} \bar{\alpha}_{\text{in}} \\ \dot{\delta \hat{\mathbf{a}}}(t) = -\begin{pmatrix} \kappa/2 - i\Delta & 0 \\ 0 & \kappa/2 + i\Delta \end{pmatrix} \delta \hat{\mathbf{a}}(t) + \sqrt{\kappa_1} \delta \hat{\mathbf{a}}_{\text{in}}(t) + \sqrt{\kappa_2} \delta \hat{\mathbf{a}}_{\text{vac}}(t) + \sqrt{\kappa_0} \delta \hat{\mathbf{a}}_{\text{l}}(t) \end{cases} \quad (\text{II.62})$$

Mean field solution (Static case): Taking the first scalar equation and expressing the mean intracavity field gives

$$\bar{\alpha} = \frac{\sqrt{\kappa_1}}{\kappa/2 - i\Delta} \bar{\alpha}_{\text{in}} \quad (\text{I.65})$$

Patching it up with the input-output formula this gives

$$\bar{\alpha}_{\text{ref}} = \left(\frac{\kappa_1}{\kappa/2 - i\Delta} - 1 \right) \bar{\alpha}_{\text{in}} \quad \bar{\alpha}_{\text{trans}} = \frac{\sqrt{\kappa_1 \kappa_2}}{\left(\kappa/2 - i\Delta \right)} \bar{\alpha}_{\text{in}}. \quad (\text{I.66})$$

The reflection and transmission coefficients are then

$$R(\Delta) = \left| \frac{\bar{\alpha}_{\text{ref}}}{\bar{\alpha}_{\text{in}}} \right|^2 = \frac{(\kappa_1 - \kappa/2)^2 + \Delta^2}{(\kappa/2)^2 + \Delta^2} \quad T(\Delta) = \left| \frac{\bar{\alpha}_{\text{trans}}}{\bar{\alpha}_{\text{in}}} \right|^2 = \frac{\kappa_1 \kappa_2}{(\kappa/2)^2 + \Delta^2}. \quad (\text{I.67})$$

The cavity linewidth (FWHM) is then given by κ , as illustrated In Fig ??.(b). Plugging back the expression of $\kappa_i = T_i/\tau$ in the reflection coefficient, we have

$$R(\pm\infty) = 1 \quad R(0) = \left(\frac{T_1 - T_2 - \gamma}{T_1 + T_2 + \gamma} \right)^2 \quad (\text{I.68})$$

such that the relative depth of the resonance dip gives us information about the cavity losses and couplings. In particular, the resonance dip vanishes when $T_1 = T_2 + \gamma$, which is the so called *impedance matching* condition: no light is reflected at resonance and all of it is transmitted or lost.

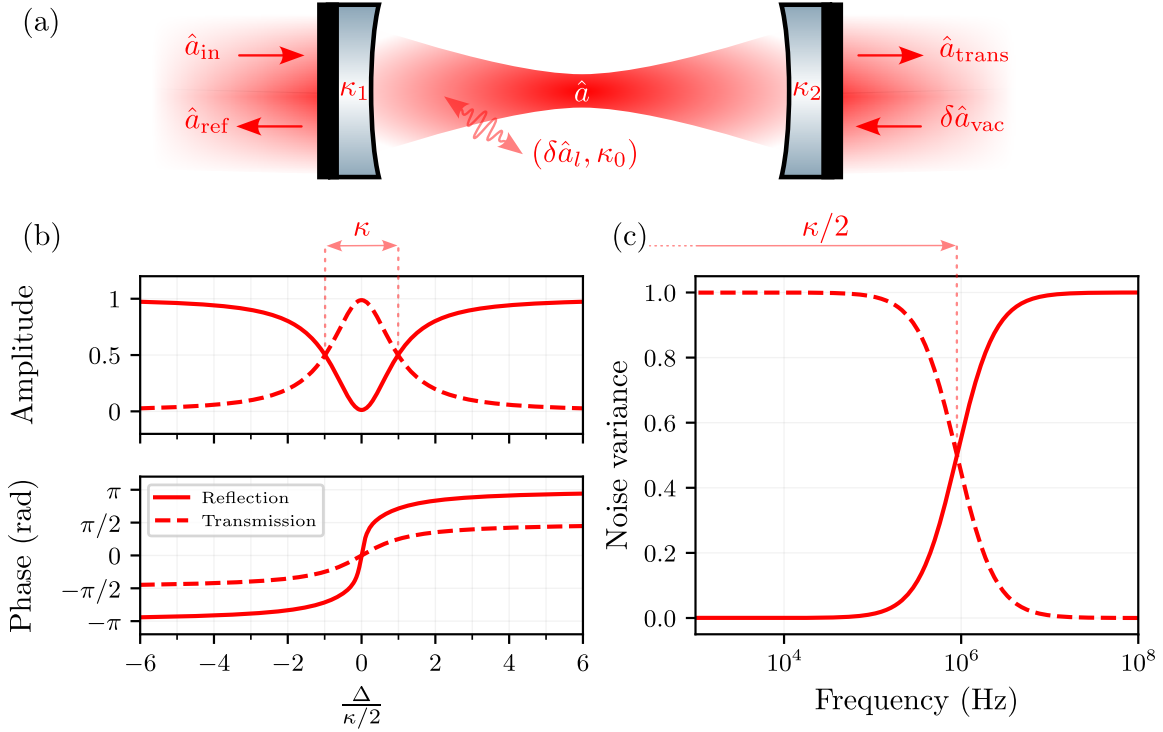


Fig. I.4 Filtering properties of optical cavities. (a) Cavity diagram and definitions. \hat{a} 's are the various fields at play. κ 's are the various couplings involved i.e. input and output mirrors, as well as intrinsic cavity cavity losses, with $\delta\hat{a}$'s the associated fluctuations. (b) Amplitude and phase response of an optical cavity as a function of the laser detuning (in cavity linewidth unit). In this case, both mirrors are identical ($\kappa_1 = \kappa_2$) and cavity losses are negligible ($\kappa_0 \ll \kappa_1$). (c) Transfer functions of the input classical noises as in (??)

We also define the cavity finesse \mathcal{F} , which is a measure of the sharpness of the resonance peaks relative to its FSR, as

$$\mathcal{F} = \frac{\omega_{\text{FSR}}}{\kappa} = \frac{\pi c}{L\kappa} = \frac{2\pi}{T_1 + T_2 + \gamma} \quad (\text{I.69})$$

which also gives the average number of round trips a photon makes before escaping the cavity i.e. $\langle n_{rt} \rangle = \mathcal{F}/\pi$. For a given cavity length (so same FSR), the higher the finesse, the longer the photon lifetime in the cavity κ^{-1} .

Mean field solution (Dynamical case):

We now let the detuning vary linearly in time, and express it in units of cavity bandwidth as $\Delta(t) = \Delta_0 + v \frac{\kappa^2}{2} t$ where we defined v as the sweep speed in units of cavity bandwidth per

κ^{-1} . The intracavity field yields the standard differential equation

$$\dot{\bar{\alpha}}(t) = -\left(\frac{\kappa}{2} - i\left(\Delta_0 + \frac{v\kappa^2}{2}t\right)\right)\bar{\alpha}(t) + \sqrt{\kappa_1}\bar{\alpha}_{\text{in}} \quad (\text{I.70})$$

This is solved by the means of integration factor method, such that we find

$$\begin{aligned} \alpha(t) &= \exp\left[\left(-\frac{\kappa}{2} + i\Delta_0\right)t + i\frac{v\kappa^2}{4}t^2\right] \\ &\times \left[\alpha(0) + \sqrt{\kappa_1}\bar{\alpha}_{\text{in}} \int_0^t \exp\left(\left(\frac{\kappa}{2} - i\Delta_0\right)s - i\frac{v\kappa^2}{4}s^2\right) ds\right]. \end{aligned} \quad (\text{I.71})$$

This expression describes the transient response of the intracavity field as the detuning is swept through resonance. When scanning over the cavity resonance at a rate exceeding the cavity bandwidth, photons at various detuning start to build up in the cavity without reaching the steady state value. This results in a characteristic asymmetric lineshape, where these different *colored* photons start beating against each other, leading to oscillations in the transmitted and reflected intensities. This is illustrated in Fig ??.(c) for different sweep speeds. The above does feature an analytical formula involving error functions erf, such that can either fit the data by performing a numerical integration or the analytical formula. However if the data array feature too few points numerical integration becomes numerically costly. [figure to do](#)

Fluctuations solution: To derive the covariance matrix we go to Fourier space such that

$$\mathbf{M}_\Delta \delta \hat{\mathbf{a}}[\Omega] = \sqrt{\kappa_1} \delta \hat{\mathbf{a}}_{\text{in}}[\Omega] + \sqrt{\kappa_2} \delta \hat{\mathbf{a}}_{\text{vac}}[\Omega] + \sqrt{\kappa_0} \delta \hat{\mathbf{a}}_{\text{l}}[\Omega] \quad (\text{I.72})$$

with

$$\mathbf{M}_\Delta = \begin{pmatrix} \kappa/2 - i(\Delta + \Omega) & 0 \\ 0 & \kappa/2 + i(\Delta - \Omega) \end{pmatrix}$$

For notational convenience, we will drop the explicit dependence on Ω in the following. Inverting the above relation and plugging it in the input-output relations gives the reflected and transmitted fields as

$$\begin{aligned} \delta \hat{\mathbf{a}}_{\text{ref}} &= (\kappa_1 \mathbf{M}_\Delta^{-1} - \mathbf{1}) \delta \hat{\mathbf{a}}_{\text{in}} + \sqrt{\kappa_1} \mathbf{M}_\Delta^{-1} (\sqrt{\kappa_2} \delta \hat{\mathbf{a}}_{\text{vac}} + \sqrt{\kappa_0} \delta \hat{\mathbf{a}}_{\text{l}}) \\ \delta \hat{\mathbf{a}}_{\text{trans}} &= \sqrt{\kappa_2} \mathbf{M}_\Delta^{-1} (\sqrt{\kappa_1} \delta \hat{\mathbf{a}}_{\text{in}} + \sqrt{\kappa_0} \delta \hat{\mathbf{a}}_{\text{l}}) + (\kappa_2 \mathbf{M}_\Delta^{-1} - \mathbf{1}) \delta \hat{\mathbf{a}}_{\text{vac}} \end{aligned} \quad (\text{I.73})$$

Using $\delta\hat{\mathbf{a}} = \boldsymbol{\Gamma}^{-1}\delta\hat{\mathbf{u}}$ the reflected and transmitted quadratures read

$$\begin{aligned}\delta\hat{\mathbf{u}}_{\text{ref}} &= (\kappa_1 \boldsymbol{\Gamma} \mathbf{M}_{\Delta}^{-1} \boldsymbol{\Gamma}^{-1} - \mathbf{1}) \delta\hat{\mathbf{u}}_{\text{in}} + \sqrt{\kappa_1} \boldsymbol{\Gamma} \mathbf{M}_{\Delta}^{-1} \boldsymbol{\Gamma}^{-1} (\sqrt{\kappa_2} \delta\hat{\mathbf{u}}_{\text{vac}} + \sqrt{\kappa_0} \delta\hat{\mathbf{u}}_{\text{l}}) \\ \delta\hat{\mathbf{u}}_{\text{trans}} &= \sqrt{\kappa_2} \boldsymbol{\Gamma} \mathbf{M}_{\Delta}^{-1} \boldsymbol{\Gamma}^{-1} (\sqrt{\kappa_1} \delta\hat{\mathbf{u}}_{\text{in}} + \sqrt{\kappa_0} \delta\hat{\mathbf{u}}_{\text{l}}) + (\kappa_2 \boldsymbol{\Gamma} \mathbf{M}_{\Delta}^{-1} \boldsymbol{\Gamma}^{-1} - \mathbf{1}) \delta\hat{\mathbf{u}}_{\text{vac}}\end{aligned}\quad (\text{I.74})$$

where the matrix product above reads

$$\boldsymbol{\Gamma} \mathbf{M}_{\Delta}^{-1} \boldsymbol{\Gamma}^{-1} = \frac{1}{(\kappa/2 - i\Omega)^2 + \Delta^2} \begin{pmatrix} \kappa/2 - i\Omega & -\Delta \\ \Delta & \kappa/2 - i\Omega \end{pmatrix}.$$

The structure above is the engine behind frequency-dependent squeezing. On resonance, we have

$$\mathbf{M}_0^{-1} = \frac{1}{\kappa/2 - i\Omega} \mathbf{I} \implies \boldsymbol{\Gamma} \mathbf{M}_0^{-1} \boldsymbol{\Gamma}^{-1} = \frac{1}{\kappa/2 - i\Omega} \mathbf{I}$$

causing symmetric sidebands around the carrier to be filtered identically both in amplitude and phase — so the quadrature along which these sidebands are correlated (if considering squeezed correlations) remains the same at all frequencies. The moment the cavity is detuned, the $\boldsymbol{\Gamma} \mathbf{M}_{\Delta}^{-1} \boldsymbol{\Gamma}^{-1}$ off-diagonal terms asymmetrically mix the upper and lower sidebands; in the two-photon picture this is a frequency-dependent rotation and scaling of the (p, q) basis. The amplitude (Lorentzian) part sets how strongly each sideband passes, while the phase accrued inside the cavity sets the rotation angle that now varies with Ω . A broadband field with a single squeezing angle at the input is therefore converted into an output whose squeezing angle “twists” with frequency: near one band it can align with the phase quadrature, and at another it can align with the amplitude quadrature. This is exactly the mechanism exploited by filter cavities in precision interferometry: by choosing bandwidth, detuning, and coupling, one tailors the rotation profile to the target noise crossover. Practically, the attainable rotation and the preserved squeezing are limited by optical loss and mode mismatch, which inject uncorrelated vacuum and partially unwind the correlations the detuned cavity imprints on sidebands.

Note: On resonance ($\Delta = 0$), the output quadratures can then be written as

$$\begin{aligned}\delta\hat{\mathbf{u}}_{\text{ref}} &= \frac{\kappa_1 - \kappa/2 + i\Omega}{\kappa/2 - i\Omega} \delta\hat{\mathbf{u}}_{\text{in}} + \frac{\sqrt{\kappa_1 \kappa_2}}{\kappa/2 - i\Omega} \delta\hat{\mathbf{u}}_{\text{vac}} + \frac{\sqrt{\kappa_1 \kappa_0}}{\kappa/2 - i\Omega} \delta\hat{\mathbf{u}}_{\text{l}} \\ \delta\hat{\mathbf{u}}_{\text{trans}} &= \frac{\sqrt{\kappa_1 \kappa_2}}{\kappa/2 - i\Omega} \delta\hat{\mathbf{u}}_{\text{in}} + \frac{\kappa_2 - \kappa/2 + i\Omega}{\kappa/2 - i\Omega} \delta\hat{\mathbf{u}}_{\text{vac}} + \frac{\sqrt{\kappa_2 \kappa_0}}{\kappa/2 - i\Omega} \delta\hat{\mathbf{u}}_{\text{l}}\end{aligned}\quad (\text{I.75})$$

and their noise spectra are

$$\begin{aligned}\mathbf{S}_{\text{ref}}[\Omega] &= \frac{(\kappa_1 - \kappa/2)^2 + \Omega^2}{(\kappa/2)^2 + \Omega^2} \mathbf{S}_{\text{in}}[\Omega] + \frac{\kappa_1}{(\kappa/2)^2 + \Omega^2} (\kappa_0 \mathbf{1} + \kappa_2 \mathbf{1}) \\ \mathbf{S}_{\text{trans}}[\Omega] &= \frac{(\kappa_2 - \kappa/2)^2 + \Omega^2}{(\kappa/2)^2 + \Omega^2} \mathbf{1} + \frac{\kappa_2}{(\kappa/2)^2 + \Omega^2} (\kappa_0 \mathbf{1} + \kappa_1 \mathbf{S}_{\text{in}})\end{aligned}\quad (\text{I.76})$$

where the vacuum and loss covariance matrices are equal to $\mathbf{1}$. As these two vacua sum up linearly, it is equivalent to consider a single vacuum with an effective decay rate $\kappa_2 + \kappa_0 \rightarrow \kappa_2$ to lighten the notation. We then absorb intrinsic losses into the output coupler, and consider only two ports: the input coupler with decay rate κ_1 and the output coupler with decay rate κ_2 . We stress that this substitution is only valid when considering the **reflected** quadratures. When focusing on the transmitted quadratures, one can perform a similar redefinition with κ_1 i.e. $\kappa_1 + \kappa_0 \rightarrow \kappa_1$.

Transfer matrices and Spectra: Expressing the reflected and transmitted quadratures in matrix form yields

$$\begin{aligned}\delta \hat{\mathbf{u}}_{\text{ref}} &= \mathbf{T}_{\text{ref}} \delta \hat{\mathbf{u}}_{\text{in}} + \mathbf{L}_{\text{ref}} \delta \hat{\mathbf{u}}_{\text{vac}} \\ \delta \hat{\mathbf{u}}_{\text{trans}} &= \mathbf{T}_{\text{trans}} \delta \hat{\mathbf{u}}_{\text{in}} + \mathbf{L}_{\text{trans}} \delta \hat{\mathbf{u}}_{\text{vac}}\end{aligned}\quad (\text{I.77})$$

where the transfer matrices for the input and loss ports given by

$$\begin{aligned}\mathbf{T}_{\text{ref}} &= \kappa_1 \mathbf{\Gamma} \mathbf{M}_{\Delta}^{-1} \mathbf{\Gamma}^{-1} - \mathbf{1}, \quad \mathbf{L}_{\text{ref}} = \sqrt{\kappa_1 \kappa_2} \mathbf{\Gamma} \mathbf{M}_{\Delta}^{-1} \mathbf{\Gamma}^{-1} \\ \mathbf{T}_{\text{trans}} &= \sqrt{\kappa_1 \kappa_2} \mathbf{\Gamma} \mathbf{M}_{\Delta}^{-1} \mathbf{\Gamma}^{-1}, \quad \mathbf{L}_{\text{trans}} = \kappa_2 \mathbf{\Gamma} \mathbf{M}_{\Delta}^{-1} \mathbf{\Gamma}^{-1} - \mathbf{1}\end{aligned}$$

Conveniently, we introduce the complex reflectivities and transmissivities experienced by the sideband fields as

$$\begin{aligned}r_{\Delta}[\Omega] &= \frac{\kappa_1}{\kappa/2 - i(\Delta + \Omega)} - 1 \\ r'_{\Delta}[\Omega] &= \frac{\kappa_2}{\kappa/2 - i(\Delta + \Omega)} - 1 \\ t_{\Delta}[\Omega] &= \frac{\sqrt{\kappa_1 \kappa_2}}{\kappa/2 - i(\Delta + \Omega)}\end{aligned}\quad (\text{I.78})$$

Here we introduced two different reflection coefficients: $r_{\Delta}[\Omega]$ for the input coupler, and $r'_{\Delta}[\Omega]$ for the output coupler describing the reflection of the incoming field fluctuations on each port. The transmission coefficient $t_{\Delta}[\Omega]$ is the same for both ports since it describes the field fluctuations transmitted from one port to the other, no matter what the direction of propagation is. We can now define the modulus and phase of the positive and negative

sideband reflectivities and transmissivities as

$$\begin{aligned} r_+ e^{i\phi_+} &= r_\Delta[\Omega] \quad , \quad r_- e^{-i\phi_-} = r_\Delta^*[-\Omega] \\ r'_+ e^{i\phi'_+} &= r'_\Delta[\Omega] \quad , \quad r'_- e^{-i\phi'_-} = r'^*_\Delta[-\Omega] \\ t_+ e^{i\theta_+} &= t_\Delta[\Omega] \quad , \quad t_- e^{-i\theta_-} = t_\Delta^*[-\Omega] \end{aligned} \quad (\text{I.79})$$

describing the amplitude filtering and dephasing underwent by a sideband at Ω and its two-photon conjugate in both reflection and transmission. The output quadrature transfer matrices can then be expressed as

$$\mathbf{T}_{\text{ref}} = \Gamma \begin{pmatrix} r_+ e^{i\phi_+} & 0 \\ 0 & r_- e^{-i\phi_-} \end{pmatrix} \Gamma^{-1} \quad \text{and} \quad \mathbf{L}_{\text{ref}} = \Gamma \begin{pmatrix} t_+ e^{i\theta_+} & 0 \\ 0 & t_- e^{-i\theta_-} \end{pmatrix} \Gamma^{-1}$$

and in transmission as

$$\mathbf{T}_{\text{trans}} = \Gamma \begin{pmatrix} t_+ e^{i\theta_+} & 0 \\ 0 & t_- e^{-i\theta_-} \end{pmatrix} \Gamma^{-1} \quad \text{and} \quad \mathbf{L}_{\text{trans}} = \Gamma \begin{pmatrix} r'_+ e^{i\phi'_+} & 0 \\ 0 & r'_- e^{-i\phi'_-} \end{pmatrix} \Gamma^{-1}$$

We use the usual transformation for the positive and negative sideband reflectivities as

$$\begin{aligned} \bar{r} &= \frac{r_+ + r_-}{2} \quad , \quad \delta r = \frac{r_+ - r_-}{2} \\ \bar{\phi} &= \frac{\phi_+ + \phi_-}{2} \quad , \quad \delta\phi = \frac{\phi_+ - \phi_-}{2} \end{aligned} \quad (\text{I.80})$$

to finally write the reflected quadrature transfer matrices as

$$\mathbf{T}_{\text{ref}} = e^{i\delta\phi} \mathbf{R}(-\bar{\phi}) \left(\bar{r} \mathbf{1} + i \delta r \mathbf{R}(\pi/2) \right) \quad \text{and} \quad \mathbf{L}_{\text{ref}} = e^{i\delta\theta} \mathbf{R}(-\bar{\theta}) \left(\bar{t} \mathbf{1} + i \delta t \mathbf{R}(\frac{\pi}{2}) \right) \quad (\text{I.81})$$

as well as the transmitted quadrature transfer matrices

$$\mathbf{T}_{\text{trans}} = e^{i\delta\theta} \mathbf{R}(-\bar{\theta}) \left(\bar{t} \mathbf{1} + i \delta t \mathbf{R}(\frac{\pi}{2}) \right) \quad \text{and} \quad \mathbf{L}_{\text{trans}} = e^{i\delta\phi} \mathbf{R}(-\bar{\phi}) \left(\bar{r}' \mathbf{1} + i \delta r' \mathbf{R}(\frac{\pi}{2}) \right) \quad (\text{I.82})$$

such that the covariance matrices for the reflected and transmitted quadratures of a detuned cavity are given by

$$\begin{aligned} \mathbf{S}_{\text{ref}}[\Omega] &= \mathbf{T}_{\text{ref}} \mathbf{S}_{\text{in}} \mathbf{T}_{\text{ref}}^\dagger + \mathbf{L}_{\text{ref}} \mathbf{L}_{\text{ref}}^\dagger \\ \mathbf{S}_{\text{trans}}[\Omega] &= \mathbf{T}_{\text{trans}} \mathbf{S}_{\text{in}} \mathbf{T}_{\text{trans}}^\dagger + \mathbf{L}_{\text{trans}} \mathbf{L}_{\text{trans}}^\dagger \end{aligned} \quad (\text{I.83})$$

$$\mathbf{T}_r[\Omega] = \Gamma \mathbf{r}_\Delta[\Omega] \Gamma^{-1} = \frac{1}{2} \begin{pmatrix} r_+ e^{i\phi_+} + r_- e^{-i\phi_-} & i(r_+ e^{i\phi_+} - r_- e^{-i\phi_-}) \\ -i(r_+ e^{i\phi_+} - r_- e^{-i\phi_-}) & r_+ e^{i\phi_+} + r_- e^{-i\phi_-} \end{pmatrix} \quad (\text{I.84})$$

and similarly for the one photon transmission matrix

$$\mathbf{t}_\Delta[\Omega] = \sqrt{\kappa_1 \kappa_2} \mathbf{M}_\Delta^{-1} = \begin{pmatrix} t_\Delta[\Omega] & 0 \\ 0 & t_\Delta^*[-\Omega] \end{pmatrix} \quad \text{with} \quad t_\Delta[\Omega] = \frac{\sqrt{\kappa_1 \kappa_2}}{\kappa/2 - i(\Delta + \Omega)} \quad (\text{I.85})$$

such that

$$\mathbf{T}_t[\Omega] = \boldsymbol{\Gamma} \mathbf{t}_\Delta[\Omega] \boldsymbol{\Gamma}^{-1} = \frac{1}{2} \begin{pmatrix} t_\Delta[\Omega] + t_\Delta^*[-\Omega] & i(t_\Delta[\Omega] - t_\Delta^*[-\Omega]) \\ -i(t_\Delta[\Omega] - t_\Delta^*[-\Omega]) & t_\Delta[\Omega] + t_\Delta^*[-\Omega] \end{pmatrix} \quad (\text{I.86})$$

Example 1: Mode Cleaner

Let us consider a configuration such that $\kappa_1 = \kappa_2 \approx \kappa/2$ where we assume negligible losses $\kappa_0 \ll \kappa_{1,2}$. It represents a cavity where the input and output mirror transmittivities are equal, and we set the laser resonant to the cavity ($\Delta = 0$), such that the transmitted quadratures are written

$$\delta \hat{\mathbf{u}}_t[\Omega] = \frac{\kappa/2}{\kappa/2 - i\Omega} \delta \hat{\mathbf{u}}_{\text{in}}[\Omega] + \frac{i\Omega}{\kappa/2 - i\Omega} \delta \hat{\mathbf{u}}_{\text{vac}}[\Omega]. \quad (\text{I.87})$$

The resulting transmitted quadrature covariance matrix is given by:

$$\mathbf{S}_t[\Omega] = \frac{(\kappa/2)^2}{(\kappa/2)^2 + \Omega^2} \mathbf{S}_{\text{In}}[\Omega] + \frac{\Omega^2}{(\kappa/2)^2 + \Omega^2} \mathbf{1} \quad (\text{I.88})$$

Now consider that the input fluctuations are above those of vacuum i.e. the input field features classical noise. We would then have $S_{pp}^{\text{in}} > S_{pp}^{\text{vac}} = 1$ and $S_{qq}^{\text{in}} > S_{qq}^{\text{vac}} = 1$. One can notice that the prefactor to the input noises is a Lorentzian function - a low pass filter. Hence, the noises of the input fields are low pass filtered by the cavity, while the vacuum fluctuations are high pass filtered at precisely the same cutoff $\kappa/2$. The mean field of the *bright* coherent input is fully transmitted, but its super-vacuum fluctuations, potentially classically modulated, are filtered by the cavity. Taking a high finesse cavity such that the cutoff frequency is low, the transmitted field now features vacuum sidebands: it has been *cleaned* from classical noise. This is the principle of a *mode cleaner* cavity, which is used in many precision experiments to provide a spectrally pure laser field, as well as a spatially filtered beam such that the transmitted beam is a pure TEM₀₀.

Example 2: Detuned single port cavity

We now consider a lossless single port cavity with $\kappa_2 = 0$ and $\kappa_1 = \kappa$. the transfer matrix for the reflected **field** then reads

$$\kappa \mathbf{M}_\Delta^{-1} - \mathbf{1} = \begin{pmatrix} \kappa/2 + i(\Delta + \Omega) & 0 \\ \kappa/2 - i(\Delta + \Omega) & \kappa/2 - i(\Delta - \Omega) \\ 0 & \kappa/2 + i(\Delta - \Omega) \end{pmatrix}$$

where we see that the upper and lower sidebands are reflected with different amplitude ρ_+ and ρ_- and phase shifts ϕ_+ and ϕ_- when the cavity is detuned ($\Delta \neq 0$). We then have :

$$\rho_+ = \left| \frac{\kappa/2 + i(\Delta + \Omega)}{\kappa/2 - i(\Delta + \Omega)} \right| = 1, \quad \rho_- = \left| \frac{\kappa/2 - i(\Delta - \Omega)}{\kappa/2 + i(\Delta - \Omega)} \right| = 1 \quad (\text{I.89})$$

$$\phi_+[\Omega] = 2 \arctan \left(\frac{\Delta + \Omega}{\kappa/2} \right), \quad \phi_-[\Omega] = 2 \arctan \left(\frac{\Delta - \Omega}{\kappa/2} \right) \quad (\text{I.90})$$

such that we can define the overall and differential phase shifts as

$$\bar{\phi}[\Omega] = \phi_+[\Omega] + \phi_-[\Omega] = \arctan \frac{4\Omega\kappa}{(\frac{\kappa}{2})^2 + \Delta^2 - \Omega^2} \quad \Delta\phi[\Omega] = \phi_+[\Omega] - \phi_-[\Omega] = \arctan \frac{4\Delta\kappa}{(\frac{\kappa}{2})^2 - \Delta^2 + \Omega^2} \quad (\text{I.91})$$

In the two-photon formalism, this asymmetric phase shift translates into a frequency-dependent rotation of the quadratures.

The transfer matrix is expressed as

$$\mathbf{T}_r[\Omega] = \frac{1}{(\kappa/2 - i\Omega)^2 + \Delta^2} \begin{pmatrix} (\kappa/2)^2 - \Delta^2 + \Omega^2 & -\kappa\Delta \\ +\kappa\Delta & (\kappa/2)^2 - \Delta^2 + \Omega^2 \end{pmatrix} \quad (\text{I.92})$$

$$\kappa \mathbf{\Gamma} \mathbf{M}_\Delta^{-1} \mathbf{\Gamma}^{-1} - \mathbf{1} = \frac{1}{(\kappa/2 - i\Omega)^2 + \Delta^2} \begin{pmatrix} (\kappa/2)^2 - \Delta^2 + \Omega^2 & -\kappa\Delta \\ +\kappa\Delta & (\kappa/2)^2 - \Delta^2 + \Omega^2 \end{pmatrix}$$

such that the covariance matrix is given by

$$\mathbf{S}_r[\Omega] = \begin{pmatrix} S_{pp}^r[\Omega] & S_{pq}^r[\Omega] \\ S_{qp}^r[\Omega] & S_{qq}^r[\Omega] \end{pmatrix} \quad (\text{I.93})$$

where we won't write the full expressions of the matrix elements for brevity. The key point is that the off-diagonal terms are non zero, meaning that the reflected quadratures are correlated. This is the frequency-dependent rotation mechanism described above.

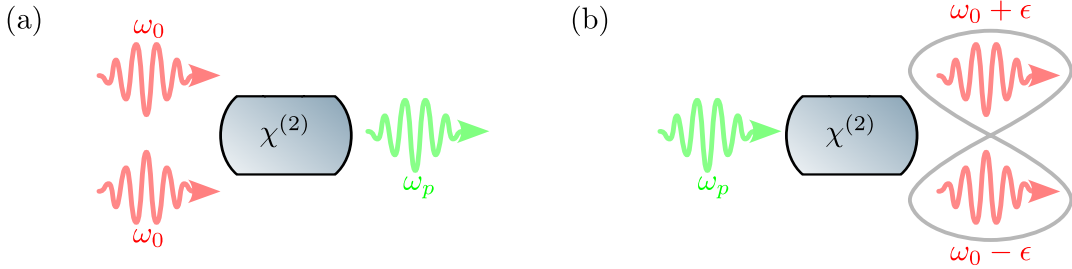


Fig. I.5 *Diagrams of $\chi^{(2)}$ non linear processes. (a) Second Harmonic Generation ($2\omega_0 = \omega_p$). (b) Parametric Down Conversion. The outgoing photons are entangled.*

This configuration is used in our experiment to measure the squeezing spectrum of the OPO, as the

I.2.5 Non Linear Cavities

We now turn to the description of optical cavities in which a $\chi^{(2)}$ medium is embedded within. This non linear medium can be used both for sum frequency generation, or difference frequency generation. The generic Hamiltonian describing a degenerate $\chi^{(2)}$ parametric process is

$$H = \hbar\omega_p \hat{b}^\dagger \hat{b} + \hbar\omega_0 \hat{a}^\dagger \hat{a} + \frac{i\hbar\epsilon}{2} (\hat{b} \hat{a}^{\dagger 2} - \hat{b}^\dagger \hat{a}^2) \quad (\text{I.94})$$

where we assumed perfect phase matching for simplicity, that is $\epsilon \in \mathbb{R}$. In our experiment with squeezed light, we do use both as to first generate a pump field using a Second Harmonic Generation (SHG) scheme, then use the generated field to *pump* a degenerate Optical Parametric Oscillator (OPO). The equations of motion of both fields are very similar in their structure, yet different in their phenomenology. Here we outline the main results and predictions for both.

Second Harmonic Generation

The SHG scheme consists in shining a laser field at frequency ω_0 onto the cavity, and the non linear medium generates a field at frequency $\omega_p = 2\omega_0$, that is, two photons at ω_0 described by operator \hat{a} , are converted into a single photon at ω_p described by operator \hat{b} . The input field is thus \hat{a}_{in} at ω_0 , while the input fields at ω_p are vacua $\hat{b}_{\text{in}} = \delta b_l = \delta \hat{b}_{\text{vac}}$. We restrain the theoretical description to our experiment, where the end mirror reflectivity is ~ 1 for our generated green beam, as seen in the figure below $\kappa_{2,b} = 0$. We will not derive the noise spectra for this scheme as they are not of interest in this work, displaying standard vacuum type fluctuations in both the pump and second harmonic field.

We rather focus on the mean field solution. The scalar part of the QLE on resonance for

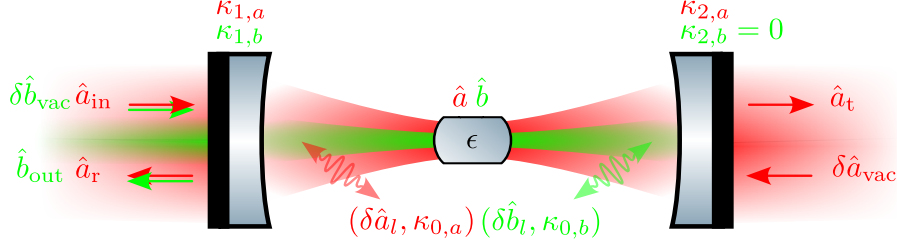


Fig. I.6 Cavity diagram for the Second Harmonic Generation. \hat{a} 's are the various fields at play, κ 's are the various couplings involved, with $\delta\hat{a}$'s the associated fluctuations, similar as in Fig I.4, now considering both the infrared pump, and the generated green beam.

both fields are given by

$$\begin{aligned} 0 &= -\frac{\kappa_a}{2} \bar{\alpha} + \epsilon \bar{\alpha}^* \bar{\beta} + \sqrt{\kappa_{1,a}} \bar{\alpha}_{in}, \\ 0 &= -\frac{\kappa_b}{2} \bar{\beta} + \frac{\epsilon}{2} \bar{\alpha}^2. \end{aligned} \quad (I.95)$$

where subscript a and b refer to the ω_0 and ω_p fields respectively. Solving for the $\bar{\beta}$ field and computing the output field $\bar{\beta}_{out}$ from the input mirror using the input-output relations, yields an output intensity of

$$\begin{aligned} |\bar{\beta}_{out}|^2 &= \frac{\kappa_a^2 \kappa_{1,b}^2}{4 \varepsilon^2} \left[\left(1 + \frac{108 \varepsilon^2 \kappa_{1,a}}{\kappa_a^3 \kappa_b} |\bar{\alpha}_{in}|^2 \left(1 + \sqrt{1 + \frac{\kappa_a^3 \kappa_b}{54 \varepsilon^2 \kappa_{1,a} |\bar{\alpha}_{in}|^2}} \right) \right)^{1/6} \right. \\ &\quad \left. - \left(1 + \frac{108 \varepsilon^2 \kappa_{1,a}}{\kappa_a^3 \kappa_b} |\bar{\alpha}_{in}|^2 \left(1 + \sqrt{1 + \frac{\kappa_a^3 \kappa_b}{54 \varepsilon^2 \kappa_{1,a} |\bar{\alpha}_{in}|^2}} \right) \right)^{-1/6} \right]^4. \end{aligned} \quad (I.96)$$

This cumbersome expression can be simplified in two limits. In the low input power limit, the output power scales quadratically with the input power, whereas at high powers it scales as $|\alpha_{in}|^{4/3}$.

Pseudo linear behaviour: For intermediate powers, the output power scales almost linearly with the input power, which is precisely the regime in which we will operate. The crossover between these regimes is set by the non linear gain ϵ and the cavity decay rates $\kappa_{a,b}$.

Optical Parametric Oscillation & Amplification

For this scheme, we consider a pump field with frequency $\omega_p = 2\omega_0$. A first key difference from the SHG scheme can be highlighted by the fact that we are now pumping at $2\omega_0$, such that pairs of entangled photons are generated at $\omega_0 + \epsilon$ and $\omega_0 - \epsilon$, with ϵ a sideband frequency allowed by the cavity bandwidth, hence conserving energy.

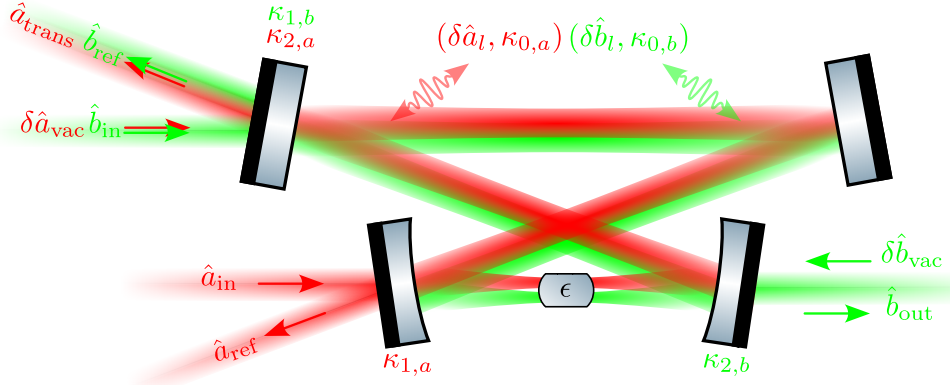


Fig. I.7 Cavity diagram for the Optical Parametric Oscillator. \hat{a} 's are the various fields at play, κ 's are the various couplings involved, with $\delta\hat{a}$'s the associated fluctuations, similar as in Fig I.4, now considering both the green pump, and the generated infrared squeezed beam. The beams are shifted for illustrative purposes but share the same optical axis in the experiment.

We further consider the pump is not *depleted*, such that we can change \hat{b} to its mean field value $|\bar{\beta}|e^{i\bar{\varphi}_b}$, and we disregard the \hat{b} fluctuations in the equations of motion for simplicity. A careful and complete derivations could also be carried out by keeping all terms in the equations of motion, but it is not serving our purpose here so we will these assumptions to lighten the notation. The total non linear gain is defined as $g = \epsilon|\bar{\beta}|$, and the QLEs for the steady state and fluctuation parts of the \hat{a} field yields:

$$\begin{cases} 0 = -\left(\frac{\kappa}{2} - i\Delta\right)\bar{a} + ge^{i\bar{\varphi}_b}\bar{a}^* + \sqrt{\kappa_1}\bar{a}_{in} \\ \delta\dot{\bar{a}}(t) = -\begin{pmatrix} \kappa/2 - i\Delta & -ge^{i\bar{\varphi}_b} \\ -ge^{-i\bar{\varphi}_b} & \kappa/2 + i\Delta \end{pmatrix}\delta\hat{a}(t) + \sqrt{\kappa_1}\delta\hat{a}_{in}(t) + \sqrt{\kappa_2}\delta\hat{a}_{vac}(t) \end{cases} \quad (I.97)$$

Mean field solution (Static case): Assuming a real input field $\bar{a}_{in} = |\bar{a}_{in}|$, the transmitted field is given by:

$$\bar{a}_t = \frac{\sqrt{\kappa_1\kappa_2}}{\kappa/2} \frac{1 + i\frac{\Delta}{\kappa/2} + xe^{i\bar{\varphi}_b}}{1 + \left(\frac{\Delta}{\kappa/2}\right)^2 - |x|^2} |\bar{a}_{in}| \quad (I.98)$$

where we define the normalised pump parameter $x = 2g/\kappa \in \mathbb{R}$. This normalised pump parameter also equals the ratio of the pump field amplitude by the pump field threshold often written B/B_{thr} . For a resonant cavity, the expression reduces to the well known parametric amplification/deamplification scheme

$$\bar{\alpha}_t = \frac{\sqrt{\kappa_1 \kappa_2}}{\kappa/2} \frac{1 + xe^{i\bar{\varphi}_b}}{1 - |x|^2} |\bar{\alpha}_{\text{in}}| \quad (\text{I.99})$$

in which the amplification or deamplification processes are set by the phase of the pump $\bar{\varphi}_b$. In the absence of a non linear medium $x = 0$ we recover the standard cavity results shown above. The threshold is defined at $x = 1$, where the rate of generation of entangled pairs exceeds the rate at which they leak from the cavity. In other words, x is unity when the round trip gain equals the round trip losses. That's precisely the point where the no depletion approximation breaks down, as illustrated by the divergence seen in transmitted field at this very value (how could one obtain a diverging field from a pump field with a finite number of photons). We also notice two special cases, when $\bar{\varphi}_b = \{0, \pi\}$, coinciding with the amplification and the deamplification processes respectively.

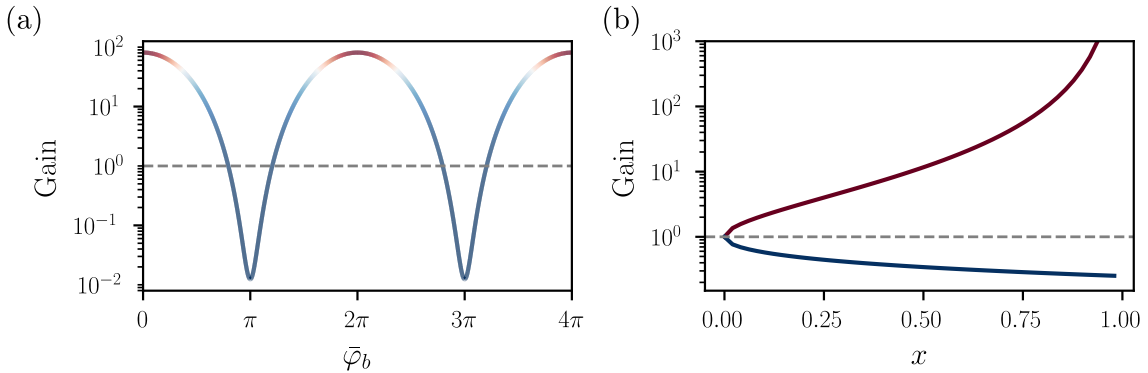


Fig. I.8 *add pump phase colorbar* Classical amplification-deamplification of an infrared seed in an Optical Parametric Oscillator below threshold. (a) Gain of the infrared seed as a function of the green pump phase. The color variations correspond to the pump phase. (b) Amplification-Deamplification of an infrared seed as a function of the normalized pump parameter $x (< 1)$. The colors correspond to the ones on figure (a) (its extrema).

Fluctuations solution: The general expression of the QLE in Fourier space is given by

$$\tilde{\mathbf{M}}_\Delta \delta \hat{\mathbf{a}}[\Omega] = \sqrt{\kappa_1} \delta \hat{\mathbf{a}}_{\text{in}}[\Omega] + \sqrt{\kappa_2} \delta \hat{\mathbf{a}}_{\text{vac}}[\Omega] \quad (\text{I.100})$$

with

$$\tilde{\mathbf{M}}_\Delta = \begin{pmatrix} \kappa/2 - i(\Delta + \Omega) & -ge^{i\bar{\varphi}_b} \\ -ge^{-i\bar{\varphi}_b} & \kappa/2 + i(\Delta - \Omega) \end{pmatrix}$$

where we defined $\tilde{\mathbf{M}}_\Delta$ to not be confused with the matrix \mathbf{M}_Δ defined earlier for a simple cavity. Note that a genuine *frequency dependent* squeezing angle could be obtained by detuning the OPO cavity, but the frequency range over which the squeezing angle varies is limited by the cavity bandwidth, which is typically small compared to the frequency range of interest in our experiment. This phenomenon was realised experimentally few years ago [Vahlbruch2006], but is not the focus of our work.

In the context of our work, we will assume :

- the pump phase is locked to $\bar{\varphi}_b = \{0, \pi\}$ i.e. amplification or deamplification regime,
- the cavity is resonant $\Delta = 0$,

We further normalise all frequencies to the cavity bandwidth $\kappa/2$ such that $\Omega \rightarrow \Omega/(\kappa/2)$ and $g \rightarrow g/(\kappa/2) = x$, such that the off diagonal terms below can simply be written $\mp x$ factoring out the cavity bandwidth. We carry out the derivation for $\bar{\varphi}_b = 0$ (amplification) for simplicity, and the $\bar{\varphi}_b = \pi$ (deamplification) case is obtained by changing x to $-x$ in the final expressions. The matrix QLE in Fourier space is written as

$$\tilde{\mathbf{M}}_0 \delta \hat{\mathbf{a}}[\Omega] = \sqrt{\kappa_1} \delta \hat{\mathbf{a}}_{\text{in}}[\Omega] + \sqrt{\kappa_2} \delta \hat{\mathbf{a}}_{\text{vac}}[\Omega] \quad (\text{I.101})$$

with

$$\tilde{\mathbf{M}}_0 = \frac{\kappa}{2} \begin{pmatrix} 1 - i \frac{\Omega}{\kappa/2} & -x \\ -x & 1 - i \frac{\Omega}{\kappa/2} \end{pmatrix}$$

Transfer matrices and Spectra: As before with a simple cavity, the transmitted quadratures at resonance are then

$$\delta \hat{\mathbf{u}}_{\text{OPO}}[\Omega] = \mathbf{T}_{\text{OPO}}[\Omega] \delta \hat{\mathbf{u}}_{\text{in}}[\Omega] + \mathbf{L}_{\text{OPO}}[\Omega] \delta \hat{\mathbf{u}}_{\text{vac}}[\Omega] \quad (\text{I.102})$$

where we defined the transfer matrices for the input and loss ports as

$$\mathbf{T}_{\text{OPO}}[\Omega] = \sqrt{\kappa_1 \kappa_2} \mathbf{\Gamma} \tilde{\mathbf{M}}_0^{-1} \mathbf{\Gamma}^{-1}, \quad \mathbf{L}_{\text{OPO}}[\Omega] = \kappa_2 \mathbf{\Gamma} \tilde{\mathbf{M}}_0^{-1} \mathbf{\Gamma}^{-1} - \mathbf{1}....$$

After a bit of algebra, the covariance matrix of the transmitted field at $\bar{\varphi}_b = 0$ is then

computed as

$$\mathbf{S}_{\text{OPO}}^0[\Omega] = \begin{pmatrix} 1 + \frac{\kappa_2}{\kappa} \frac{4x}{(1-x)^2 + \left(\frac{\Omega}{\kappa/2}\right)^2} & 0 \\ 0 & 1 - \frac{\kappa_2}{\kappa} \frac{4x}{(1+x)^2 + \left(\frac{\Omega}{\kappa/2}\right)^2} \end{pmatrix} \quad (\text{I.103})$$

On a side note, when deriving the noise spectra for the intracavity field, the maximum amount of squeezing is limited to 3dB, while the transmitted field can feature arbitrarily high squeezing levels. This is interpreted as additional correlations between vacuum fluctuations being reflected at the output port of the OPO and the squeezed field leaking from this very same output port, allowing for strong squeezing.

The perfect squeezer: Starting from (??), in the idealized limit of perfect escape efficiency ($\eta_{\text{esc}} = 1$) and for analysis frequencies much smaller than the cavity bandwidth ($\Omega/\kappa \rightarrow 0$), the expression simplifies to

$$\mathbf{S}_{\text{OPO}}^0[\Omega] = \begin{pmatrix} \frac{(1+x)^2}{(1-x)^2} & 0 \\ 0 & \frac{(1-x)^2}{(1+x)^2} \end{pmatrix} \quad (\text{I.104})$$

Introducing the standard squeezing parameter r through the relation $x = \tanh \frac{r}{2}$, one can rewrite the numerator and denominator as

$$1 + \tanh \frac{r}{2} = \frac{e^{+\frac{r}{2}}}{\cosh \frac{r}{2}}, \quad 1 - \tanh \frac{r}{2} = \frac{e^{-\frac{r}{2}}}{\cosh \frac{r}{2}},$$

such that

$$\frac{(1 \pm \tanh \frac{r}{2})^2}{(1 \mp \tanh \frac{r}{2})^2} = \left(\frac{e^{\pm \frac{r}{2}}}{e^{\mp \frac{r}{2}}} \right)^2 = e^{\pm 2r}.$$

Thus when $\bar{\varphi}_b = \{0, \pi\}$, in the lossless, low-frequency limit the transmitted noise levels reduce to the well-known parametric result

$$\mathbf{S}_{\text{OPO}}^0[\Omega] = \begin{pmatrix} e^{+2r} & 0 \\ 0 & e^{-2r} \end{pmatrix} \quad \text{and} \quad \mathbf{S}_{\text{OPO}}^\pi[\Omega] = \begin{pmatrix} e^{-2r} & 0 \\ 0 & e^{+2r} \end{pmatrix} \quad (\text{I.105})$$

where we can now establish that an amplified field ($\bar{\varphi}_b = 0$) corresponds to a squeezed phase quadrature and an anti-squeezed amplitude quadrature, while a deamplified field ($\bar{\varphi}_b = \pi$) corresponds to a squeezed amplitude quadrature and an anti-squeezed phase quadrature. Later on, we will use this idealized expression to describe how squeezed light interacts with

a mechanical resonator whose frequency is much smaller than the OPO bandwidth.

Losses: Squeezing is very sensitive to optical losses, which couple uncorrelated vacuum fluctuations into the squeezed field and degrade the squeezing level. The escape efficiency $\eta_{\text{esc}} = \kappa_2/\kappa$ of the OPO cavity is one such loss mechanism, but there are many others in a real experiment: propagation losses, mode-mismatch, non-unity quantum efficiency of the photodetectors, etc. One can then distinguish between *intracavity* losses, which are accounted for in the escape efficiency, and *extracavity* losses, which we denote by η_{ext} and lump all other loss mechanisms into a single effective loss. The effect of these losses can be modeled as a beam-splitter mixing the squeezed field with vacuum fluctuations, such that the lossy covariance matrix is given by

$$\mathbf{S}_{\text{det}}[\Omega] = (1 - \eta) \mathbf{S}_{\text{OPO}}^{\bar{\varphi}_b}[\Omega] + \eta \mathbf{1} \quad (\text{I.106})$$

This expression is actually true for any Gaussian state suffering from losses.

Frequency dependence: Similarly to what was seen earlier considering general quantum states, squeezing at an arbitrary angle θ can be obtained by rotating the covariance matrix. However, one can now make the squeezing angle frequency dependent above as

$$\mathbf{S}_{\text{OPO}}^\theta[\Omega] = \mathbf{R}(\theta[\Omega]) \mathbf{S}_{\text{OPO}}^0[\Omega] \mathbf{R}^\dagger(\theta[\Omega]). \quad (\text{I.107})$$

where $\theta[]$ The $\mathbf{S}[\Omega]$ can either be the full cavity one, or the idealized one. As already mentionned, the mechanical frequencies of interest will be deep in the OPO bandwidth such that we will use the ideal squeezer expression (??) in addition with extrinsic losses (??). The explicit of the covariance matrix at a frequency dependent angle is then

$$\mathbf{S}_{\text{OPO}}^\theta[\Omega] = \begin{pmatrix} \cosh 2r + \sinh 2r \cos 2\theta[\Omega] & -\sinh 2r \sin 2\theta[\Omega] \\ -\sinh 2r \sin 2\theta[\Omega] & \cosh 2r - \sinh 2r \cos 2\theta[\Omega] \end{pmatrix} \quad (\text{I.108})$$

I.2.6 Optomechanical Cavities

We now turn to standard optomechanical cavities. As in the simple FP case, we consider a cavity mode, in which we now allow one of the the coupler (traditionnaly the output coupler), to be itself a *mechanical* harmonic oscillator with annihilation operator \hat{c} , effective mass m , angular frequency Ω_m and damping rate Γ_m . In canonical optomechanical systems the mechanics operators are usually denoted as \hat{b} but in our case it would be redundant with the operators describing the pump field in non linear systems. The position can be expressed in terms of our bosonic operators as $\hat{x} = x_0(\hat{c} + \hat{c}^\dagger)$ with $x_0 = \sqrt{\hbar/(2m\Omega_m)}$ the resonator's

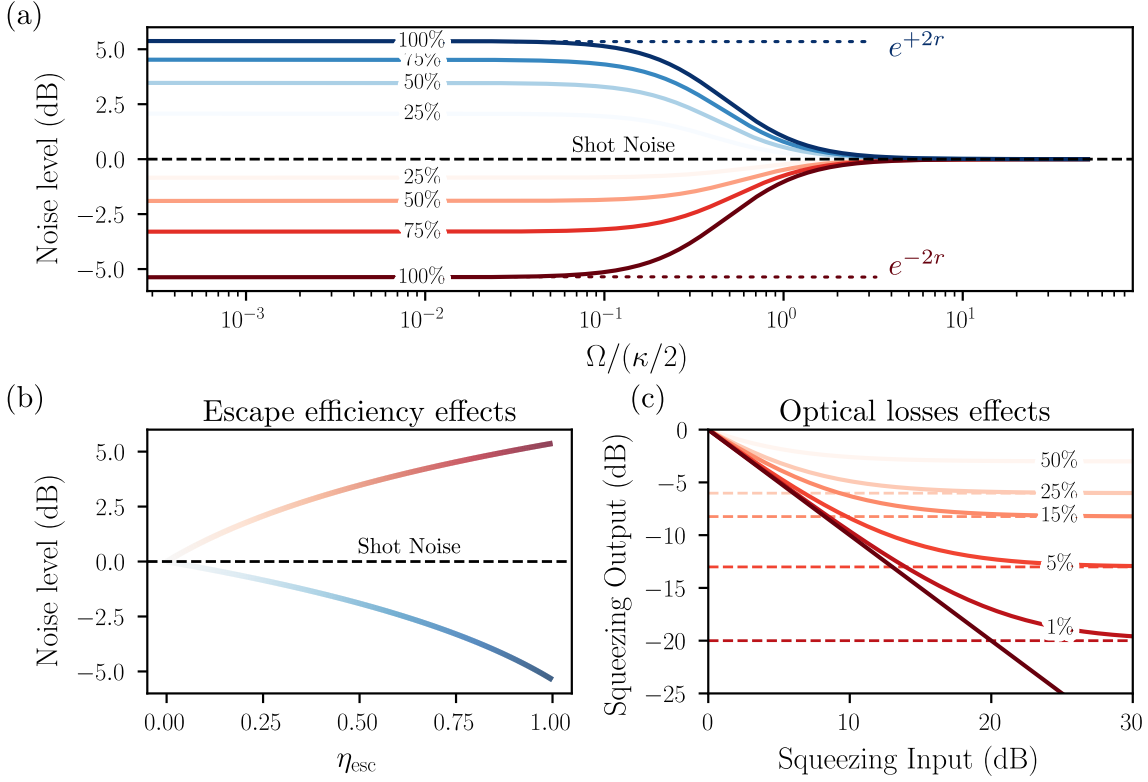


Fig. I.9 Squeezing degradation properties of a non perfect OPO. (a) Squeezing-Antisqueezing levels obtained as a function of frequency (in cavity linewidth unit). The squeezing-antisqueezing levels are maximised at 100% escape efficiency and inside the cavity linewidth (see dark red and dark blue curves). (b) Squeezing-antisqueezing levels as a function of the escape efficiency. (c) Output Squeezing level as a function of the Input Squeezing level (right at the OPO output) considering various optical loss values (extrinsic losses).

zero point fluctuations.

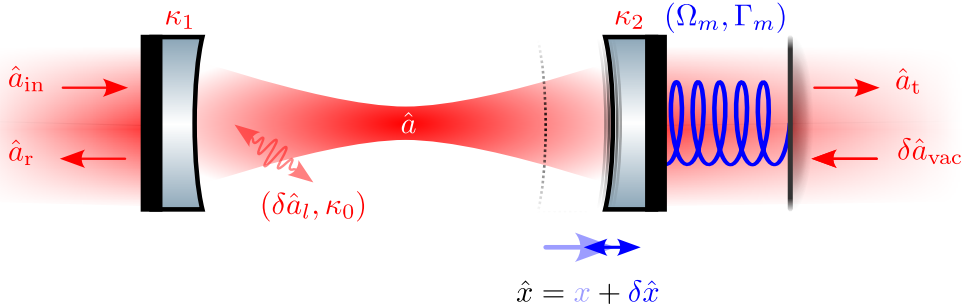


Fig. I.10 Diagram generic optomechanical system. \hat{a} 's are the various fields at play, κ 's are the various couplings involved, with $\delta\hat{a}$'s the associated fluctuations. \hat{x} is the quantum position operator of the mechanical resonator which linearly shifts the cavity resonance frequency.

Mechanics & Radiation Pressure Force

The equation of motion of such an oscillator are given by

$$m \ddot{x} = -m \Omega_m^2 \hat{x} - m \Gamma_m \dot{\hat{x}} + \hat{F} \quad (\text{I.109})$$

where \hat{F} is the total force acting on the oscillator. In Fourier space, we recover the standard linear response form

$$\hat{x}[\Omega] = \chi[\Omega] \hat{F}[\Omega] \quad \text{with} \quad \chi[\Omega] = \frac{1}{m(\Omega_m^2 - \Omega^2 - i\Gamma_m \Omega)} \quad (\text{I.110})$$

where $\chi[\Omega]$ is the susceptibility linearly relating the position $\hat{x}[\Omega]$ to the external force $\hat{F}[\Omega]$. This susceptibility can also be written as

$$\chi[\Omega] = |\chi[\Omega]| e^{i\phi_m[\Omega]} \quad (\text{I.111})$$

with

$$\text{with } \phi_m[\Omega] = \arctan\left(\frac{\Gamma_m \Omega}{\Omega_m^2 - \Omega^2}\right) \quad \text{and} \quad |\chi[\Omega]| = \frac{1}{m \sqrt{(\Omega_m^2 - \Omega^2)^2 + (\Gamma_m \Omega)^2}}.$$

Similarly to the simple Fabry-Perot cavity (being a driven damped harmonic oscillator too), we can define the analog of the Finesse, namely the quality factor, defined as

$$Q = \frac{\Omega_m}{\Gamma_m} \quad (\text{I.112})$$

which is the number of oscillations before the resonator's energy is damped by a factor $1/e$. On resonance, the susceptibility is purely imaginary and reads $\chi[\Omega_m] = -iQ/(m\Omega_m^2)$.

As before, the position is also linearized considering small quantum fluctuations compared to its mean value, such that we write $\hat{x} = x + \delta\hat{x}$. Importantly, the total position fluctuation $\delta\hat{x} = \sum \delta\hat{x}_i$ is the sum of individual fluctuations that can arise from various sources, such as a the zero point fluctuations, thermal fluctuations or radiation pressure induced fluctuations. In the following we will only consider a radiation pressure induced fluctuations $\delta\hat{x}_{\text{RPN}}$, such that $\delta\hat{x} = \delta\hat{x}_{\text{RPN}}$.

Due to the continuous yet discrete photon *hits* at a rate exceeding the resonator frequency, the resonator *feels* an effective force. This radiation pressure force is expressed as

$$\hat{F} = 2 \frac{\hbar k_L}{\tau_c} \hat{a}^\dagger \hat{a} = 2 \frac{\hbar k_L}{\tau_c} |\bar{\alpha}|^2 + 2 \frac{\hbar k_L}{\tau_c} |\bar{\alpha}| \delta\hat{p} + \mathcal{O}(\delta\hat{a}^\dagger \delta\hat{a}) \quad (\text{I.113})$$

where $k_L = 2\pi/\lambda$ is the laser wavevector, and $\tau_c = 2L/c$ is the cavity round-trip time, and we neglect second order terms. This force then features a static component shifting

the resonator away from its equilibrium position, that be the x component, as well as a fluctuating component $\delta\hat{F} \propto \delta\hat{p}$ jittering the resonator around its mean displacement, that's $\delta\hat{x}_{\text{RPN}}$. The position mean value and its fluctuations under radiation pressure can therefore be expressed to first order as

$$x = \frac{2\hbar k_L |\bar{\alpha}|^2}{\tau_c} \chi[0], \quad \delta\hat{x}_{\text{RPN}}[\Omega] = \frac{2\hbar k_L |\bar{\alpha}|}{\tau_c} \chi[\Omega] \delta\hat{p}[\Omega]. \quad (\text{I.114})$$

Optomechanical QLE

Considering an optomechanical cavity of length L at rest, such that the mean resonator position is initially 0, the bare cavity free spectral range is given by $\omega_{\text{FSR}} = \pi c/L$ and the cavity frequency $\omega_c = N\omega_{\text{FSR}}$. Injecting light inside this cavity then shifts the mechanical resonator position as seen above, which in turn changes the cavity length $L \rightarrow L+x$, thus its frequency. Writing the Hamiltonian, we simply Taylor expand to first order in \hat{x} the cavity frequency $\omega_c(\hat{x}) = \omega_c + \hat{x} \partial\omega_c/\partial x$ such that we have:

$$\hat{H} = -\hbar\Delta\hat{a}^\dagger\hat{a} + \hbar G\hat{x}\hat{a}^\dagger\hat{a} + \hbar\Omega_m\hat{c}^\dagger\hat{c} \quad (\text{I.115})$$

where $G = \partial\omega_c/\partial x = -\omega_c/L$. One can also identify a useful identity by considering the radiation pressure force (??) and the Hamiltonian above, such that

$$\hat{F}_{\text{rad}} = -\frac{\partial\hat{H}}{\partial\hat{x}} = -\hbar G\hat{a}^\dagger\hat{a} \quad \Rightarrow \quad G = -2\frac{k_L}{\tau_c} \quad (\text{I.116})$$

consistent with our previous expression of G such that we rewrite the position fluctuation as $\delta\hat{x}_{\text{tot}}[\Omega] = -\hbar G|\bar{\alpha}|\chi[\Omega]\delta\hat{p}[\Omega]$. Plugging in the QLE and ignoring vacuum and loss fluctuations for notational simplicity, the field's equation are written as

$$\begin{cases} 0 = -\left(\frac{\kappa}{2} - i\bar{\Delta}\right)\bar{\alpha} + \sqrt{\kappa_1}|\bar{\alpha}_{\text{in}}| \\ \delta\dot{\hat{\mathbf{a}}}(t) = -\begin{pmatrix} \kappa/2 - i\bar{\Delta} & 0 \\ 0 & \kappa/2 + i\bar{\Delta} \end{pmatrix} \delta\hat{\mathbf{a}}(t) + iG\bar{\alpha}\delta\hat{x} \begin{pmatrix} +1 \\ -1 \end{pmatrix} + \sqrt{\kappa_1}\delta\hat{\mathbf{a}}_{\text{in}}(t) + \sqrt{\kappa_2}\delta\hat{\mathbf{a}}_{\text{vac}}(t) \end{cases} \quad (\text{I.117})$$

where we introduced the radiation pressure induced detuning $\bar{\Delta} = \Delta - Gx$ - that is, the mean resonator displacement shifts the cavity frequency, hence the detuning - and where we assume the input field to be real.

This so called *dispersive* coupling, where the cavity frequency $\omega_c(x)$ depends linearly on the resonator's position to firs order, is the hallmark of the optomechanical interaction. In the canonical model, the cavity linewidth κ do not depend on the resonator's position.

Mean field solution & Bistability: Writing the mean intracavity amplitude by keeping

the *unperturbed* detuning Δ for clarity and substituting for the static displacement x , we get

$$\bar{\alpha} = \frac{\sqrt{\kappa_1}}{\kappa/2 - i\left(\Delta - \frac{\hbar G^2 |\bar{\alpha}|^2}{m_{\text{eff}} \Omega_m^2}\right)} |\bar{\alpha}_{\text{in}}| \quad (\text{I.118})$$

where the $|\bar{\alpha}|^2$ dependence in disguise in the mean mechanical displacement is the root of the bistable behaviour of optomechanical cavities. We show the induced hysteresis in figure ...

For moderate injected powers, this is the standard intracavity field formula where we simply relabel $\Delta - Gx \rightarrow \Delta$ to lighten the notation. When resonant, the intracavity field does not pick up any phase and is real i.e. $\bar{\alpha} = |\bar{\alpha}| = 2\sqrt{\kappa_1}/\kappa |\bar{\alpha}_{\text{in}}|$.

Optomechanical cavities do display optical ringdowns too, as detailed in the cavity sub-part above, but this is a purely optical phenomenon: the mechanics plays no role in the optical ringdown (to first order?).

Fluctuations solution: As previously, going to Fourier space now yields

$$\mathbf{M}_{\bar{\Delta}} \delta \hat{\mathbf{a}}[\Omega] = i G \bar{\alpha} \delta \hat{x}[\Omega] \begin{pmatrix} +1 \\ -1 \end{pmatrix} + \sqrt{\kappa_1} \delta \hat{\mathbf{a}}_{\text{in}}[\Omega] + \sqrt{\kappa_2} \delta \hat{\mathbf{a}}_{\text{vac}}[\Omega] \quad (\text{I.119})$$

where we injected the mean field solution (??) in our equations assuming moderate input power to ignore bistable behaviour. We focus on the resonant case to derive our noise spectra, such that $\mathbf{M}_0 = (\kappa/2 - i\Omega)\mathbf{I}$ and the intracavity quadratures are

$$\delta \hat{\mathbf{u}}[\Omega] = \frac{2G|\bar{\alpha}|}{\kappa/2 - i\Omega} \delta \hat{x}[\Omega] \begin{pmatrix} 0 \\ 1 \end{pmatrix} + \frac{\sqrt{\kappa_1}}{\kappa/2 - i\Omega} \delta \hat{\mathbf{u}}_{\text{in}}[\Omega] + \frac{\sqrt{\kappa_2}}{\kappa/2 - i\Omega} \delta \hat{\mathbf{u}}_{\text{vac}}[\Omega] \quad (\text{I.120})$$

Writing explicitly our amplitude-phase quadratures then gives

$$\begin{aligned} \delta \hat{p}[\Omega] &= \frac{\sqrt{\kappa_1}}{\kappa/2 - i\Omega} \delta \hat{p}_{\text{in}}[\Omega] + \frac{\sqrt{\kappa_2}}{\kappa/2 - i\Omega} \delta \hat{p}_{\text{vac}}[\Omega] \\ \delta \hat{q}[\Omega] &= \frac{2G|\bar{\alpha}|}{\kappa/2 - i\Omega} \delta \hat{x}[\Omega] + \frac{\sqrt{\kappa_1}}{\kappa/2 - i\Omega} \delta \hat{q}_{\text{in}}[\Omega] + \frac{\sqrt{\kappa_2}}{\kappa/2 - i\Omega} \delta \hat{q}_{\text{vac}}[\Omega] \end{aligned} \quad (\text{I.121})$$

This expression highlights the fact that only the phase is affected by the resonator position fluctuations. Physically, this can be understood by considering first that a fluctuating field amplitude leads to a fluctuating radiation pressure force, which in turn *shakes* the mechanical resonator, which changes the phase of the field reflected. The reciprocal process does not happen: a fluctuating phase does not lead to a fluctuating radiation pressure force, hence the output amplitude fluctuations are unaffected by the mechanics.

Importantly, considering the field reflected off the cavity, we define the displacement to phase fluctuation transduction $\mathcal{C}[\Omega]$ such that

$$\delta\hat{q}_r[\Omega] = \mathcal{C}[\Omega] \delta\hat{x}[\Omega] \quad \text{with} \quad \mathcal{C}[\Omega] = \frac{2\sqrt{\kappa_1}G|\bar{\alpha}|}{\kappa/2 - i\Omega} = \frac{\kappa_1}{\kappa} \frac{16\mathcal{F}\sqrt{\bar{I}_{\text{in}}}}{\lambda(1 - i2\Omega/\kappa)} \quad (\text{I.122})$$

where we plugged in useful experimental parameters \mathcal{F} , λ and \bar{I}_{in} . The prefactor κ_1/κ is the analog of the escape efficiency for optomechanical cavities, and is unity for single port cavities. We stress that the total phase fluctuations are the sum of various contributions, including the input phase fluctuations, the vacuum fluctuations entering from the loss port, and the position induced phase fluctuations, whether they arise from radiation pressure or other sources. This transduction factor will be used later to express the displacement sensitivity/spectra in terms of experimental parameters.

Plugging in the position fluctuations derived earlier ((??) and (??)) in the intracavity phase fluctuations we get

$$\begin{aligned} \delta\hat{q}[\Omega] &= \frac{\mathcal{C}^2[\Omega]}{2\kappa_1} \hbar\chi[\Omega] \left(\sqrt{\kappa_1} \delta\hat{p}_{\text{in}}[\Omega] + \sqrt{\kappa_2} \delta\hat{p}_{\text{vac}}[\Omega] \right) \\ &\quad + \frac{1}{\kappa/2 - i\Omega} \left(\sqrt{\kappa_1} \delta\hat{q}_{\text{in}}[\Omega] + \sqrt{\kappa_2} \delta\hat{q}_{\text{vac}}[\Omega] \right) \end{aligned} \quad (\text{I.123})$$

such that we can readily express the intracavity quadratures in matrix form as

$$\delta\hat{\mathbf{u}}[\Omega] = \begin{pmatrix} \frac{1}{\kappa/2 - i\Omega} & 0 \\ \frac{\mathcal{K}[\Omega]}{\kappa_1} & \frac{1}{\kappa/2 - i\Omega} \end{pmatrix} \left(\sqrt{\kappa_1} \delta\hat{\mathbf{u}}_{\text{in}}[\Omega] + \sqrt{\kappa_2} \delta\hat{\mathbf{u}}_{\text{vac}}[\Omega] \right). \quad (\text{I.124})$$

with

$$\mathcal{K}[\Omega] = \frac{\mathcal{C}^2[\Omega]}{2} \hbar\chi[\Omega] = \left(\frac{\kappa_1}{\kappa} \right)^2 \frac{128\hbar\mathcal{F}^2\bar{I}_{\text{in}}}{\lambda^2(1 - i2\Omega/\kappa)^2} \chi[\Omega]$$

We then obtain the reflected and transmitted quadrature fluctuations

$$\begin{aligned} \delta\hat{\mathbf{u}}_r[\Omega] &= \mathbf{T}_r[\Omega] \delta\hat{\mathbf{u}}_{\text{in}}[\Omega] + \mathbf{L}_r[\Omega] \delta\hat{\mathbf{u}}_{\text{vac}}[\Omega] \\ \delta\hat{\mathbf{u}}_t[\Omega] &= \mathbf{T}_t[\Omega] \delta\hat{\mathbf{u}}_{\text{in}}[\Omega] + \mathbf{L}_t[\Omega] \delta\hat{\mathbf{u}}_{\text{vac}}[\Omega]. \end{aligned} \quad (\text{I.125})$$

where we defined the transfer matrices

$$\mathbf{T}_r[\Omega] = \begin{pmatrix} \frac{\kappa_1}{\kappa/2 - i\Omega} - 1 & 0 \\ \mathcal{K}[\Omega] & \frac{\kappa_1}{\kappa/2 - i\Omega} - 1 \end{pmatrix} \quad \mathbf{L}_r[\Omega] = \begin{pmatrix} \frac{\sqrt{\kappa_1\kappa_2}}{\kappa/2 - i\Omega} & 0 \\ \sqrt{\frac{\kappa_2}{\kappa_1}} \mathcal{K}[\Omega] & \frac{\sqrt{\kappa_1\kappa_2}}{\kappa/2 - i\Omega} \end{pmatrix}$$

$$\mathbf{T}_t[\Omega] = \begin{pmatrix} \frac{\sqrt{\kappa_1\kappa_2}}{\kappa/2 - i\Omega} & 0 \\ \sqrt{\frac{\kappa_2}{\kappa_1}} \mathcal{K}[\Omega] & \frac{\sqrt{\kappa_1\kappa_2}}{\kappa/2 - i\Omega} \end{pmatrix} \quad \mathbf{L}_t[\Omega] = \begin{pmatrix} \frac{\kappa_2}{\kappa/2 - i\Omega} - 1 & 0 \\ \frac{\kappa_2}{\kappa_1} \mathcal{K}[\Omega] & \frac{\kappa_2}{\kappa/2 - i\Omega} - 1 \end{pmatrix}$$

Convergence to VIRGO/LIGO notation: To sanity check this expression, we need to make sure we recover the standard expressions used in the LIGO/VIRGO community. This is we will assume the mechanical resonator is free, that is $\Omega_m \rightarrow 0$ and $\Gamma_m \rightarrow 0$. The susceptibility then reduces to $\chi[\Omega] = 1/M\Omega^2$, and we will consider sideband frequencies $\Omega \ll \kappa/2$ such that all terms in $\Omega/(\kappa/2)$ can be neglected. We also consider a single port cavity such that $\kappa_1 = \kappa$ and $\kappa_2 = 0$. The reflected quadrature fluctuations then read

$$\delta \hat{\mathbf{u}}_r[\Omega] = \begin{pmatrix} 1 & 0 \\ \frac{32\omega_0 P_{\text{in}}}{ML^2\kappa^2\Omega^2} & 1 \end{pmatrix} \delta \hat{\mathbf{u}}_{\text{in}}[\Omega]. \quad (\text{I.126})$$

In GW papers, the pre factor will often be 8 (and not 32) as they use the cavity half width at half maximum rather than κ . We indeed recover the standard expression used in the GW community, which is a good sanity check of our derivation. We do stress however that this expression is only valid for a free mass, and that the full expression including the mechanical resonance is required to describe optomechanical cavities in general.

Reflected spectra: We can now compute the covariance matrix of the reflected quadratures, assuming vacuum fluctuations both at the input and at the loss port. We additionally consider a quasi single port cavity for simplicity $\kappa_1 \gg \kappa_2$, such that $\kappa_1 \sim \kappa$, as well as the bad cavity limit $\Omega \ll \kappa/2$. The reflected covariance matrix is then given by

$$\mathbf{S}_r[\Omega] = \mathbf{T}_r[\Omega] \mathbf{S}_{\text{in}}[\Omega] \mathbf{T}_r^\dagger[\Omega] = \begin{pmatrix} 1 & \mathcal{K}[\Omega] \\ \mathcal{K}^*[\Omega] & 1 + |\mathcal{K}[\Omega]|^2 \end{pmatrix} \quad (\text{I.127})$$

where the off-diagonal entries are complex conjugates of each other, ensuring the covariance matrix is Hermitian as required. The diagonal terms are the amplitude and phase noise spectra respectively, while the off-diagonal terms quantify correlations between amplitude and phase. The presence of these correlations is the hallmark of optomechanical/ponderomotive squeezing i.e. using the non linear response of the resonator to squeeze light. This effect is

not seen nor sought in our experiment, but is a very active field of research in the optomechanics community.

One now sees two essential components in the reflected phase spectrum. The first is the direct phase fluctuations, which is simply shot noise seen as 1. The second is the back-action term $\propto |\mathcal{K}[\Omega]|^2$, which is the phase fluctuations induced by the resonator motion driven by radiation pressure fluctuations.

I.3 Detection

Having layed out the theoretical framework to describe the optical fields interacting with our various cavities, we now turn to the detection schemes used to probe these fields. To detect the optical field reflected or transmitted from these optical systems, we will use two main techniques: direct detection and balanced homodyne detection.

I.3.1 Direct detection

Direct detection consists in measuring the intensity of the optical field impinging on a photodiode. We will detail three cases: the single field case, where only the signal field is incident on the photodiode, the case where a local oscillator (LO) field is added to the signal field, and finally the case where two beams at different slightly different wavelengths are incident on the photodiode.

Single field: The photocurrent operator, originating from the photoelectric effect is given by

$$\hat{I} = e \hat{a}^\dagger \hat{a} \quad (\text{I.128})$$

with e the electron charge. We introduce the quantum efficiency of the photodiode η_d to account for non unity detection efficiency, such that the detected field operator is written as

$$\hat{a} \rightarrow \sqrt{\eta_d} \hat{a} + \sqrt{1 - \eta_d} \hat{a}_{\text{vac}}$$

where \hat{a}_{vac} are vacuum fluctuations entering due to non unity detection efficiency. Assuming a real mean field $\bar{\alpha}$, photocurrent operator then reads

$$\hat{I} = \eta_d e \left(|\bar{\alpha}|^2 + \bar{\alpha} \delta p + \sqrt{\eta_d(1 - \eta_d)} \bar{\alpha} \delta p_{\text{vac}} \right) \quad (\text{I.129})$$

where we neglected second order terms. The photocurrent fluctuations in Fourier space are

then given by

$$\delta\hat{I}[\Omega] = \eta_d e \bar{\alpha} \left(\delta p[\Omega] + \sqrt{\frac{1 - \eta_d}{\eta_d}} \delta p_{\text{vac}}[\Omega] \right) \quad (\text{I.130})$$

such that the photocurrent noise spectrum is

$$S_{II}[\Omega] = \eta_d^2 e^2 |\bar{\alpha}|^2 \left(S_{pp}[\Omega] + \frac{1 - \eta_d}{\eta_d} \right) \quad (\text{I.131})$$

where $S_{pp}[\Omega]$ is the amplitude quadrature noise spectrum of the incident field. This expression highlights that direct detection is only sensitive to amplitude quadrature fluctuations.

Two fields: Let's now consider an auxiliary field at the same frequency \hat{a}_{LO} , called the local oscillator (LO), which is a coherent field dephased from our real signal field \hat{a} by a phase ϕ_{LO} such that the total field impinging on the photodiode is $\hat{a}_{\text{tot}} = \hat{a} + \hat{a}_{\text{LO}}$. So far, we do not consider the LO to be consequently stronger than the signal field, as we will do in the homodyne detection. This coherent addition can be performed using a beam-splitter or a polarizing beam-splitter, depending on the experimental implementation. The mean field of the total field is then given by $\bar{a}_{\text{tot}} = \bar{a} + |\bar{a}_{\text{LO}}|e^{i\phi_{\text{LO}}}$, and its fluctuations are $\delta\hat{a}_{\text{tot}} = \delta\hat{a} + \delta\hat{a}_{\text{LO}}$. For simplicity we will assume a quantum efficiency of 1 in the following. The photocurrent operator mean values is then given by

$$\bar{I} = e \left(|\bar{a}|^2 + |\bar{a}_{\text{LO}}|^2 + 2|\bar{a}||\bar{a}_{\text{LO}}| \cos \phi_{\text{LO}} \right) \quad (\text{I.132})$$

where we see the interference term between the signal and the LO: scanning the LO phase ϕ_{LO} (with a piezoelectric actuator) will lead to interference fringes on the mean photocurrent, which can be used to lock the LO phase. We won't developp the full expression of the photocurrent fluctuation spectrum here (see Annexe B), as they feature a cumbersome linear combination of the amplitude and phase quadrature noise spectra of both the signal and the LO fields, as well as cross correlation terms between the two fields (if any), which is not very interesting experimentally. However, we can already sense that adding a LO field allows to access phase quadrature fluctuations of the signal field, which was not possible with direct detection alone.

Let's consider 'slow' (hence low frequency) classical fluctuations of the LO phase $\delta\phi_{\text{LO}}(t)$ around a mean value $\bar{\phi}_{\text{LO}}$, such that $\phi_{\text{LO}}(t) = \bar{\phi}_{\text{LO}} + \delta\phi_{\text{LO}}(t)$ with $\delta\phi_{\text{LO}}(t) \ll 1$. Developing the photocurrent to first order in these classical fluctuations, the mean photocurrent fluctuations then reads

$$\delta\bar{I}(t) \propto \delta\phi_{\text{LO}}(t) \quad (\text{I.133})$$

such that slow phase fluctuations of the LO are directly transduced into photocurrent fluc-

tuations. The classical phase noise of the LO can therefore pollute the photocurrent noise spectrum at low frequency, as well as limit the lock stability of the LO phase. Let's now consider the case where the LO is phase modulated at a frequency Ω_{mod} as seen previously

$$\alpha_{\text{LO}}(t) \approx \bar{\alpha}_{\text{LO}} \left(1 + i\epsilon_\phi \cos(\Omega_{\text{mod}} t) \right)$$

such that the mean photocurrent fluctuations are now given by

$$\delta \bar{I}(t) \propto \cos(\Omega_{\text{mod}} t) \delta\phi_{\text{LO}}(t) \quad (\text{I.134})$$

so that the LO phase noise is spectrally only transduced around the modulation frequency Ω_{mod} . Demodulating the photocurrent at Ω_{mod} then yields an error signal proportional to the LO phase fluctuations, which can be used to lock the LO phase to a desired value $\bar{\phi}_{\text{LO}}$, while rejecting low frequency phase noise of the LO.

Two fields at different frequencies: Finally, let's consider the case where the signal and LO fields are at slightly different wavelengths/frequencies, such that \hat{a} is at frequency ω_0 and \hat{a}_{LO} at frequency $\omega_0 + \Delta\omega$. The total field impinging on the photodiode is then written as $\hat{a}_{\text{tot}} = \hat{a} + \hat{a}_{\text{LO}} e^{-i\Delta\omega t}$ since our operators are defined in a frame rotating at ω_0 . The mean photocurrent is then given by

$$\bar{I} = e \left(|\bar{\alpha}|^2 + |\bar{\alpha}_{\text{LO}}|^2 + 2|\bar{\alpha}||\bar{\alpha}_{\text{LO}}| \cos(\Delta\omega t + \phi_{\text{LO}}) \right) \quad (\text{I.135})$$

where we see that the interference term now oscillates at the beat frequency $\Delta\omega$. Demodulating the photocurrent at a frequency $\Delta\tilde{\omega} \sim \Delta\omega$, phase $\tilde{\phi}$, and low pass filtering the photocurrent then gives

$$\bar{I}_{\text{demod}} \propto \cos((\Delta\omega - \Delta\tilde{\omega})t + \phi - \tilde{\phi}). \quad (\text{I.136})$$

This very signal can then be used to lock the frequency of an auxiliary laser to the desired frequency offset $\Delta\tilde{\omega}$ from the main laser. However, this signal featuring many zero crossings, one needs to tune the auxiliary laser frequency close enough to the desired offset so that it ensures the feedback loop locks to the correct zero crossing. This is generally done manually by scanning the auxiliary laser frequency until the right zero crossing is found, confirmed by monitoring the beatnote on a spectrum analyzer.

I.3.2 Balanced Homodyne Detection

Balanced homodyne detection (HD) is a common technique to measure arbitrary quadratures of an optical field with high sensitivity. It consists in mixing the signal field \hat{a} with a strong

local oscillator (LO) field \hat{a}_{LO} on a 50:50 beam-splitter, and detecting the two output ports with identical photodiodes. The beamsplitter operation reads

$$\begin{cases} \hat{a}_{\text{out},1} = \frac{1}{\sqrt{2}}(\hat{a} + \hat{a}_{\text{LO}}) \\ \hat{a}_{\text{out},2} = \frac{1}{\sqrt{2}}(\hat{a} - \hat{a}_{\text{LO}}) \end{cases} \quad (\text{I.137})$$

The two photodiodes then measure the photocurrents $\hat{I}_1 = e \hat{a}_{\text{out},1}^\dagger \hat{a}_{\text{out},1}$ and $\hat{I}_2 = e \hat{a}_{\text{out},2}^\dagger \hat{a}_{\text{out},2}$. The BHD photocurrent is then defined as the difference between the two photocurrents $\hat{I}_{\text{BHD}} = \hat{I}_1 - \hat{I}_2$, which reads

$$\hat{I}_{\text{HD}} = e (\hat{a}_{\text{LO}}^\dagger \hat{a} + \hat{a}^\dagger \hat{a}_{\text{LO}}) \quad (\text{I.138})$$

Assuming a real mean field for the signal $\bar{\alpha}$ and a phase shifted LO mean field $\bar{\alpha}_{\text{LO}} = |\bar{\alpha}_{\text{LO}}| e^{i\phi_{\text{LO}}}$, we can linearize the HD photocurrent to first order in the fluctuations as

$$\hat{I}_{\text{HD}} = 2e |\bar{\alpha}_{\text{LO}}| |\bar{\alpha}| \cos \phi_{\text{LO}} + e |\bar{\alpha}_{\text{LO}}| (\cos \phi_{\text{LO}} \delta \hat{p} + \sin \phi_{\text{LO}} \delta \hat{q}) \quad (\text{I.139})$$

where we recognise the mean photocurrent term in $2e |\bar{\alpha}_{\text{LO}}| |\bar{\alpha}| \cos \phi_{\text{LO}}$ as in the two fields direct detection case. This slowly varying mean photocurrent can be used to lock the LO phase ϕ_{LO} to a desired value, as previously described, with a piezoelectric actuator and phase modulation/demodulation scheme if needed. The HD photocurrent fluctuations in Fourier space are then given by

$$\delta \hat{I}_{\text{HD}}[\Omega] = e |\bar{\alpha}_{\text{LO}}| (\cos \phi_{\text{LO}} \delta \hat{p}[\Omega] + \sin \phi_{\text{LO}} \delta \hat{q}[\Omega]) \quad (\text{I.140})$$

such that the HD photocurrent noise spectrum reads

$$S_{II}^{\text{HD}}[\Omega] = e^2 |\bar{\alpha}_{\text{LO}}|^2 (\cos^2 \phi_{\text{LO}} S_{pp}[\Omega] + \sin^2 \phi_{\text{LO}} S_{qq}[\Omega] + 2 \sin \phi_{\text{LO}} \cos \phi_{\text{LO}} S_{pq}[\Omega]) \quad (\text{I.141})$$

where $S_{pp}[\Omega]$, $S_{qq}[\Omega]$ and $S_{pq}[\Omega]$ are respectively the amplitude, phase and cross correlation noise spectra of the signal field. By tuning the LO phase ϕ_{LO} , one can therefore measure arbitrary quadratures of the signal field with high sensitivity thanks to the strong LO field amplifying the signal fluctuations. This is the main advantage of HD over direct detection, where only amplitude quadrature fluctuations can be measured. To calibrate the HD detection efficiency, one can block the signal field, such that the LO now probes vacuum fluctuations only. This reference is then used to evaluate the squeezing level of the signal field when unblocked.

The practical implementation of these detection schemes and the associated locks are detailed in chapter 3.

Chapter II

Theory: Squeezed Light & Optomechanics

This chapter will cover the elementary concepts required to describe an membrane based optomechanical system in a quantum regime. We will first recall basics on optical field quantization as well describing coherent and squeezed light field, to then turn to the more specific frequency dependent squeezed light field. Secondly, we will cover the mathematical description of a mechanical resonator interacting with a generic coherent optical field, highlighting the differences with the seminal optomechanical system of a mirror on a spring. Finally, we will derive the equations of motions of a membrane based optomechanical system with frequency dependent squeezed optical fields.

Contents

II.1	Squeezed Light and Optomechanics	53
II.1.1	Standard Quantum Limit	53
II.1.2	Frequency Independent Squeezing in Optomechanical Cavities	56
II.1.3	Frequency Dependent Squeezing in Optomechanical Cavities	59
II.1.4	Filter Cavities for Frequency Dependent Squeezing	60
II.2	Cavity Optomechanics with Membrane based systems	61
II.2.1	Classical Description	61
II.2.2	Quantum Langevin Equations	64
II.2.3	Mechanical Resonators	71
II.2.4	Noise spectra	71

II.1 Squeezed Light and Optomechanics

We will now introduce the concept of Standard Quantum Limit (SQL) in the context of optomechanical measurements, and show how frequency dependent squeezed light can be used to surpass this limit.

For the rest of this section we will assume the following

- A cavity on resonance: $\Delta = 0$.
- A single port optomechanical cavity: $\kappa_1 \sim \kappa$.
- The unresolved sideband regime: $(\Omega, \Omega_m) \ll \kappa/2$.

II.1.1 Standard Quantum Limit

The question of interest is now:

what is the best displacement sensitivity one can achieve?

We start by recalling the reflected phase fluctuation of an optomechanical cavity from section I.2.5 under the aforementioned assumptions:

$$\delta\hat{q}_r[\Omega] = \delta\hat{q}_{\text{in}}[\Omega] + \mathcal{K}[\Omega] \delta\hat{p}_{\text{in}}[\Omega] \quad \text{with} \quad \mathcal{K}[\Omega] = \frac{\mathcal{C}^2}{2} \hbar\chi[\Omega] = \frac{128\mathcal{F}^2\bar{I}_{\text{in}}}{\lambda^2} \hbar\chi[\Omega]$$

where \mathcal{C} is now positive and frequency independent. The resulting reflected phase spectrum reads

$$S_{qq}^r[\Omega] = S_{qq}^{\text{in}}[\Omega] + |\mathcal{K}[\Omega]|^2 S_{pp}^{\text{in}}[\Omega] + 2 \operatorname{Re} [\mathcal{K}[\Omega] S_{pq}^{\text{in}}[\Omega]]$$

The phase to displacement transduction relation with an optomechanical escape efficiency of 1:

$$\delta\hat{q}_x = \mathcal{C}\delta\hat{x}[\Omega] = \frac{16\mathcal{F}\sqrt{\bar{I}_{\text{in}}}}{\lambda} \delta\hat{x}[\Omega]$$

Using these two relations, we can then express displacement fluctuations in terms of input amplitude and phase fluctuations, assuming the reflected field is a perfect probe of the mechanical resonator position fluctuations i.e. $\delta\hat{q}_r[\Omega] = \delta\hat{q}_x[\Omega]$. This treatment is formally equivalent to considering the output phase as a statistical estimator of the position fluctuations being a stationary random process as done in quantum measurement theory [3]. We then write

$$\delta\hat{x}[\Omega] = \mathcal{C}^{-1} \delta\hat{q}_{\text{in}}[\Omega] + \frac{\mathcal{C}}{2} \hbar\chi[\Omega] \delta\hat{p}_{\text{in}}[\Omega] \tag{II.1}$$

such that the associated displacement spectrum reads

$$S_{xx}[\Omega] = \mathcal{C}^{-2} S_{qq}^{\text{in}}[\Omega] + \left(\frac{\mathcal{C}}{2} \hbar |\chi[\Omega]| \right)^2 S_{pp}^{\text{in}}[\Omega] + \hbar |\chi[\Omega]| \operatorname{Re} \left[e^{i\phi_m[\Omega]} S_{pq}^{\text{in}}[\Omega] \right] \quad (\text{II.2})$$

We then identify three contributions to the displacement spectrum:

- The first term is the laser shot noise (or imprecision noise) scaling inversely with the input power \bar{I}_{in} , arising from the input phase fluctuations $S_{qq}^{\text{in}}[\Omega]$ and given by

$$S_{xx}^{\text{SN}}[\Omega] = \frac{\lambda^2}{256\mathcal{F}^2 \bar{I}_{\text{in}}} S_{qq}^{\text{in}}[\Omega] \quad (\text{II.3})$$

- The second term is the radiation pressure noise (or backaction noise) scaling linearly with the input power \bar{I}_{in} , arising from the input amplitude fluctuations $S_{pp}^{\text{in}}[\Omega]$ driving the mechanical resonator via radiation pressure given by

$$S_{xx}^{\text{RPN}}[\Omega] = \frac{64\mathcal{F}^2 \bar{I}_{\text{in}}}{\lambda^2} \hbar^2 |\chi[\Omega]|^2 S_{pp}^{\text{in}}[\Omega] \quad (\text{II.4})$$

- The third term is a correlation term between amplitude and phase fluctuations $S_{pq}^{\text{in}}[\Omega]$, which can be non-zero for arbitrary squeezed states as seen in the previous section and given by

$$S_{xx}^{\text{cor}}[\Omega] = \hbar |\chi[\Omega]| \operatorname{Re} \left[e^{i\phi_m[\Omega]} S_{pq}^{\text{in}}[\Omega] \right] \quad (\text{II.5})$$

And we write the total displacement spectrum as the sum of these three contributions

$$S_{xx}[\Omega] = S_{xx}^{\text{SN}}[\Omega] + S_{xx}^{\text{RPN}}[\Omega] + S_{xx}^{\text{cor}}[\Omega] \quad (\text{II.6})$$

We now consider vacuum/coherent fluctuations such that $S_{qq}^{\text{in}}[\Omega] = S_{pp}^{\text{in}}[\Omega] = 1$ and $S_{pq}^{\text{in}}[\Omega] = 0$, so that the displacement spectrum simplifies to

$$S_{xx}[\Omega] = \mathcal{C}^{-2} + \left(\frac{\mathcal{C}}{2} \hbar |\chi[\Omega]| \right)^2 \quad (\text{II.7})$$

and we look at what noise dominates the displacement spectrum around the mechanical resonance $\Omega \sim \Omega_m$. In this frequency range, there are two frequencies at which the displacement noise contributions are equal, given by the condition $S_{xx}^{\text{SN}}[\Omega] = S_{xx}^{\text{RPN}}[\Omega]$, leading to the frequency Ω_{SQL} defined as

$$\Omega_{\text{SQL}}^{\pm} = \sqrt{\Omega_m^2 - \frac{\Gamma_m^2}{2}} \pm \frac{1}{2} \sqrt{\Gamma_m^4 - 4\Gamma_m^2 \Omega_m^2 + \left(\frac{\hbar \mathcal{C}^2}{m} \right)^2} \quad (\text{II.8})$$

and consistent with the LIGO/Virgo notation [[harry_advanced_2010](#), [aasi_enhanced_2013](#)]. Over the frequency range of interest $\Omega \in [\Omega_m - \Omega_{SQL}, \Omega_m + \Omega_{SQL}]$, the displacement noise is dominated by the radiation pressure noise, while outside this range, the noise is dominated by the shot noise. However, for every sideband frequency, there exists an optimal input power $\bar{I}_{in}^{SQL}[\Omega]$ at which both contributions are equal, minimizing the total displacement noise. This limit is called the Standard Quantum Limit (SQL) and is a direct consequence of Heisenberg's uncertainty principle applied to continuous position measurements [[braginsky_quantum_1992](#), [3](#)]. This SQL intensity is given by

$$S_{xx}^{SN}[\Omega] = S_{xx}^{RPN}[\Omega] \implies \bar{I}_{in}^{SQL}[\Omega] = \frac{\lambda^2}{128\mathcal{F}^2\hbar|\chi[\Omega]|} \quad (\text{II.9})$$

such that plugging back in this SQL intensity in (??) gives the SQL displacement spectrum as

$$S_{xx}^{SQL}[\Omega] = \hbar|\chi[\Omega]| \implies S_{xx}^{SN}[\Omega] + S_{xx}^{RPN}[\Omega] \geq \hbar|\chi[\Omega]| \quad (\text{II.10})$$

which is the fundamental limit to continuous position measurements with coherent light. We also note that for high Q resonators, $\Omega_{SQL} \gg \Gamma_m$, so approximating the susceptibility by its real part holds over a relatively large frequency range but fails at resonance where the susceptibility is purely imaginary.

Thermal Noise

Thermal noise is a major limitation in optomechanical experiments, as it can mask the quantum effects one aims to observe. The mechanical resonator is indeed coupled to a thermal bath at temperature T , which drives the resonator into a thermal state with mean phonon occupation number $\bar{n}_{th} = k_B T / (\hbar\Omega_m)$ in the high temperature limit $k_B T \gg \hbar\Omega_m$. The position fluctuations induced by this thermal force is given by

$$S_{xx}^{th}[\Omega] = \frac{2\hbar}{1 - e^{-\hbar\Omega/k_B T}} \text{Im } \chi[\Omega] \simeq 2m\Gamma_m k_B T |\chi[\Omega]|^2 \quad \text{if } k_B T \gg \hbar\Omega \quad (\text{II.11})$$

where we used the identity $\text{Im } \chi[\Omega] = m\Gamma_m \Omega |\chi[\Omega]|^2$. At $T = 0K$, this reduces to the zero point fluctuations spectrum $S_{xx}^{ZPF}[\Omega] = m\Gamma_m \hbar\Omega_m |\chi[\Omega]|^2 < S_{xx}^{SQL}[\Omega]$, such that is often neglected in the total displacement spectrum. However, at finite temperature, the thermal noise can be much larger than the SQL. Therefore, the total displacement spectrum now reads

$$S_{xx}[\Omega] = S_{xx}^{SN}[\Omega] + S_{xx}^{RPN}[\Omega] + S_{xx}^{cor}[\Omega] + S_{xx}^{th}[\Omega] \quad (\text{II.12})$$

In order to experimentally probe these quantum limits without being limited by various technical noises, one would then need:

- A high finesse cavity, such that the shot noise $S_{xx}^{\text{SN}} \propto \mathcal{F}^{-2}$ level is low, and the radiation pressure noise $S_{xx}^{\text{RPN}} \propto \mathcal{F}^2$ is high. One should however ensure the cavity bandwidth κ is still much larger than the mechanical frequency Ω_m . This can be ensured by tuning the cavity length L and mirror transmissions.
- A low mass, low frequency, high quality factor mechanical resonator, such that the susceptibility modulus at resonance $|\chi[\Omega_m]| = Q/m\Omega_m^2$ is high, and it comes out of the shot noise level significantly.
- A low temperature environment, such that the thermal noise $S_{xx}^{\text{th}} \propto T$ is low and does not mask the quantum effects. This can be ensured by cryogenic cooling of the mechanical resonator, as well as using high quality factor resonators to reduce the mechanical linewidth Γ_m .

We now want to derive the displacement spectrum of an optomechanical system driven by a squeezed light field, whether frequency independent or dependent.

II.1.2 Frequency Independent Squeezing in Optomechanical Cavities

We first recall the (idealized) covariance matrices for both a phase squeezed field and an amplitude squeezed field

$$\mathbf{S}_{\text{OPO}}^0[\Omega] = \begin{pmatrix} e^{+2r} & 0 \\ 0 & e^{-2r} \end{pmatrix}, \quad \mathbf{S}_{\text{OPO}}^\pi[\Omega] = \begin{pmatrix} e^{-2r} & 0 \\ 0 & e^{+2r} \end{pmatrix}$$

For a phase squeezed field, the displacement spectrum reads

$$S_{xx}^0[\Omega] = \mathcal{C}^{-2}e^{-2r} + \left(\frac{\mathcal{C}}{2}\hbar|\chi[\Omega]|\right)^2 e^{+2r} \quad (\text{II.13})$$

while for an amplitude squeezed field, the displacement spectrum reads

$$S_{xx}^\pi[\Omega] = \mathcal{C}^{-2}e^{+2r} + \left(\frac{\mathcal{C}}{2}\hbar|\chi[\Omega]|\right)^2 e^{-2r} \quad (\text{II.14})$$

We then see that phase squeezing reduces the shot noise contribution but increases the radiation pressure noise contribution, while amplitude squeezing reduces the radiation pressure noise contribution but increases the shot noise contribution. The input cross correlations being zero, this is completely equivalent to the coherent state with a rescaled input intensity $e^{\pm 2r}\bar{I}_{\text{in}}$ (hidden in \mathcal{C}) for phase/amplitude squeezing respectively. However, neither of these two configurations can reduce both contributions simultaneously, and therefore cannot improve the SQL limit. This is illustrated in figure ??.

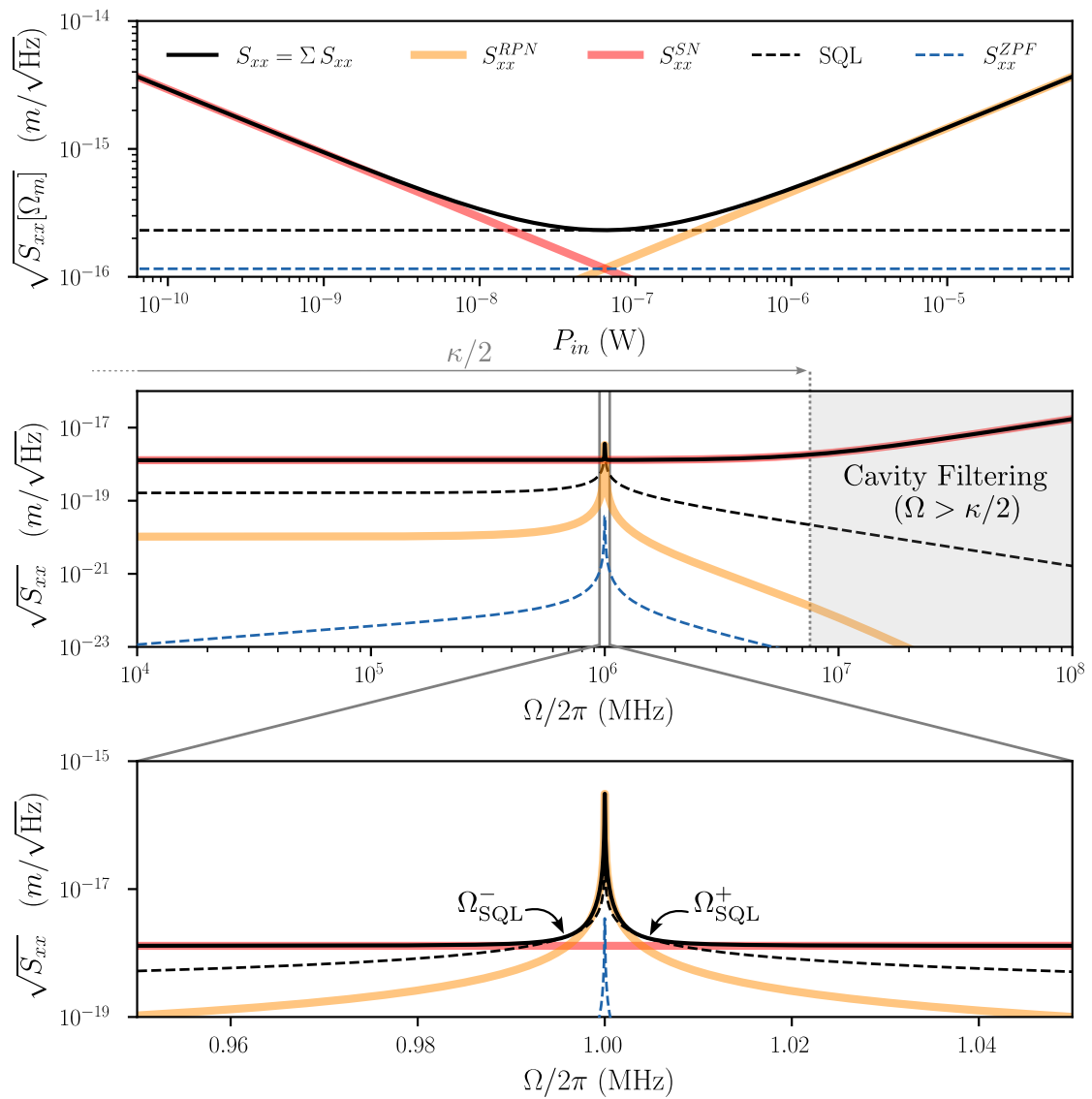


Fig. II.1 DYes

Now consider an input squeezed state with a frequency independent squeezing angle $\theta = \pi/4$ with covariance matrix

$$\mathbf{S}_{\text{OPO}}^{\pi/4}[\Omega] = \begin{pmatrix} \cosh 2r & -\sinh 2r \\ -\sinh 2r & \cosh 2r \end{pmatrix}.$$

The resulting displacement spectrum then reads

$$S_{xx}^{\pi/4}[\Omega] = \left(C^{-2} + \left(\frac{C}{2} \hbar |\chi[\Omega]| \right)^2 \right) \cosh 2r - \hbar |\chi[\Omega]| \sinh 2r \cos \phi_m[\Omega] \quad (\text{II.15})$$

and we seek the frequency range where the displacement spectrum is below the SQL, i.e. $S_{xx}^{\pi/4}[\Omega] < S_{xx}^{\text{SQL}}[\Omega]$. This condition is satisfied when

$$\tanh r < \cos \phi_m[\Omega] < 1 \quad (\text{II.16})$$

Because $\tanh r$ tends to 1 as r increases, the frequency range where the displacement spectrum is below the SQL decreases with increasing squeezing factor r . Furthermore, due to the interplay between quadrature correlations and the projection of the $\pi/4$ ellipse onto the output quadrature axis, acting as an effective increase of the shot noise floor with effective intensity $\bar{I}_{\text{in}} \cosh^{-1} r$, there is an effective range of r above which the displacement spectrum is always above the SQL (for a fixed input intensity). This is illustrated in figure ??.

Additionally, and as seen in Fig ..., the optimal angle to maximally reduce the displacement spectrum varies with frequency, being 0 at frequencies outside the resonator's bandwidth, $\pi/2$ at the mechanical resonance frequency Ω_m , and about $\pm\pi/4$ at $\Omega_m \pm \Omega_{\text{SQL}}$.

This motivates the use of frequency dependent squeezed states to reduce the displacement spectrum below the SQL over a broad frequency range, where every sideband frequency needs to be rotated by a different angle to minimize the displacement spectrum. More specifically, sideband noises contributing to both shot noise and radiation pressure noise need to be correlated in a frequency dependent manner to optimally cancel the total displacement noise in the vicinity of the mechanical resonance.

II.1.3 Frequency Dependent Squeezing in Optomechanical Cavities

We now consider a squeezed state with a frequency dependent angle whose covariance matrix is given by

$$\mathbf{S}_{\text{OPO}}^{\theta}[\Omega] = \begin{pmatrix} \cosh 2r + \sinh 2r \cos 2\theta[\Omega] & -\sinh 2r \sin 2\theta[\Omega] \\ -\sinh 2r \sin 2\theta[\Omega] & \cosh 2r - \sinh 2r \cos 2\theta[\Omega] \end{pmatrix}$$

The resulting displacement spectrum then reads

$$\begin{aligned} S_{xx}[\Omega] = & \mathcal{C}^{-2}(\cosh 2r - \sinh 2r \cos 2\theta[\Omega]) \\ & + \left(\frac{\mathcal{C}}{2}\hbar|\chi[\Omega]|\right)^2 (\cosh 2r + \sinh 2r \cos 2\theta[\Omega]) \\ & - \hbar|\chi[\Omega]| \sinh 2r \sin 2\theta[\Omega] \cos \phi_m[\Omega] \end{aligned} \quad (\text{II.17})$$

As shown in the annex, picking the squeezing angle as

$$2\theta[\Omega] = \arctan \left[\frac{2|\mathcal{K}[\Omega]| \cos \phi_m[\Omega]}{1 - |\mathcal{K}[\Omega]|^2} \right] \quad (\text{II.18})$$

minimizes the displacement spectrum at every sideband frequency, leading to

$$\begin{aligned} S_{xx}[\Omega] = & \cosh 2r \left(\mathcal{C}^{-2} + \left(\frac{\mathcal{C}}{2}\hbar|\chi[\Omega]|\right)^2 \right) \\ & - \sinh 2r \sqrt{\left(\mathcal{C}^{-2} - \left(\frac{\mathcal{C}}{2}\hbar|\chi[\Omega]|\right)^2 \right)^2 + \left(\hbar|\chi[\Omega]| \cos \phi_m[\Omega] \right)^2}. \end{aligned} \quad (\text{II.19})$$

This broadband reduction of the displacement spectrum below the SQL is illustrated in figure ???. However, for a resonant optomechanical cavity i.e. $\Delta = 0$, it is impossible to beat the SQL at the mechanical resonance, where the susceptibility is purely imaginary $\phi_m[\Omega_m] = \pi/2$.

Convergence to VIRGO/LIGO notation: We once again show that this general treatment converges to the one used in the context of gravitational wave detectors. In the free mass regime, $\mathcal{K}[\Omega]$ is real, such that $\phi_m[\Omega] = 0$. One can then rewrite the optimal squeezing angle as

$$2\theta[\Omega] = \arctan \left[\frac{2\mathcal{K}[\Omega]}{1 - \mathcal{K}^2[\Omega]} \right] = 2 \arctan \mathcal{K}[\Omega] \quad (\text{II.20})$$

where we used the identity $\arctan 2x/(1 - x^2) = 2 \arctan x \pmod{\pi}$, such that this comes down to the expression used in the context of gravitational wave detectors [harry_advanced_2010,

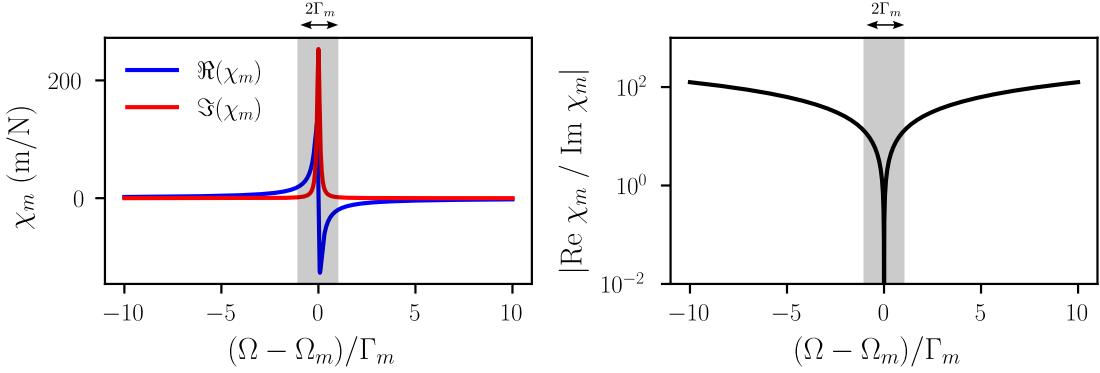


Fig. II.2 DYes

aasi_enhanced_2013]. Furthermore, the mechanical frequency and damping rate will be significantly smaller than the $\hbar\mathcal{C}^2/m$ term such that using the free-mass susceptibility $\chi[\Omega] = -1/m\Omega^2$ boils down the the SQL frequency to the known expression

$$\Omega_{\text{SQL}} = \sqrt{\frac{\hbar\mathcal{C}^2}{2m}} \implies \kappa[\Omega] = \left(\frac{\Omega_{\text{SQL}}}{\Omega}\right)^2 \quad (\text{II.21})$$

The displacement spectrum then reduces to the common expression

$$S_{xx}[\Omega] = \mathcal{C}^{-2} \left(1 + \left(\frac{\Omega_{\text{SQL}}}{\Omega}\right)^2\right) e^{-2r} \quad (\text{II.22})$$

which is the free-mass approximation result used in the GW community.

II.1.4 Filter Cavities for Frequency Dependent Squeezing

To generate frequency dependent squeezed states, one can use a detuned optical cavity called a filter cavity [4]. The principle is to reflect a frequency independent squeezed state off a single sided detuned cavity, such that only the sidebands resonant with the cavity will undergo a phase shift, effectively rotating the squeezing ellipse by a frequency dependent angle. The transfer matrix for a single sideband from a detuned single port cavity was given by

$$\kappa M_{\Delta}^{-1}[\Omega] - \mathbf{1} = \begin{pmatrix} \kappa/2 + i(\Delta + \Omega) & 0 \\ \kappa/2 - i(\Delta + \Omega) & 0 \\ 0 & \frac{\kappa/2 - i(\Delta - \Omega)}{\kappa/2 + i(\Delta - \Omega)} \end{pmatrix}$$

We recall from section II.1.4 that the reflected quadratures from a detuned cavity are

given by

$$\mathbf{T}_r[\Omega] = \frac{1}{(\kappa/2 - i\Omega)^2 + \Delta^2} \begin{pmatrix} (\kappa/2)^2 - \Delta^2 + \Omega^2 & -\kappa\Delta \\ +\kappa\Delta & (\kappa/2)^2 - \Delta^2 + \Omega^2 \end{pmatrix}$$

such that the phase picked up by sidebands at frequency Ω is given by

$$\phi_{fc}[\Omega] = \arctan\left(\frac{2\Delta\kappa}{\kappa^2/4 - \Delta^2 + \Omega^2}\right) \quad (\text{II.23})$$

II.2 Cavity Optomechanics with Membrane based systems

II.2.1 Classical Description

To gain intuition and derive elementary parameters used in the next section, we first describe the classical fields propagating in a three mirror cavity where a membrane with complex amplitude reflection and transmission coefficients $r_m = |r_m|e^{i\phi_r}$ and $t_m = |t_m|e^{i\phi_t}$ is placed between two high reflectivity mirrors of amplitude reflection coefficients ~ -1 . The membrane splits the cavity in two sub-cavities of lengths L_1 and L_2 , with $L = L_1 + L_2$ the total cavity length. The membrane is initially at mean position $x = 0$, and is modelled as a thin dielectric slab of thickness d and refractive index n , with amplitude reflection and transmission coefficients r_m and t_m given by [thompson_strong_2008]

$$r_m = \frac{(n^2 - 1) \sin knd}{2in \cos knd + (n^2 + 1) \sin knd}, \quad t_m = \frac{2n}{2in \cos knd + (n^2 + 1) \sin knd}. \quad (\text{II.24})$$

In the lossless case, we will assume the index of refraction n is real, such that $|r_m|^2 + |t_m|^2 = 1$. The right-moving mean field amplitudes in the left and right sub-cavities are denoted $\bar{\alpha}_L$ and $\bar{\alpha}_R$, while the left-moving mean field amplitudes are denoted $\bar{\alpha}'_L$ and $\bar{\alpha}'_R$. The cavity fields are then related by

$$\begin{aligned} \bar{\alpha}_R &= t_m \bar{\alpha}_L + r_m \bar{\alpha}'_R \\ \bar{\alpha}'_L &= t_m \bar{\alpha}'_R + r_m \bar{\alpha}_L. \end{aligned} \quad (\text{II.25})$$

In this case, energy conservation i.e. $|\bar{\alpha}_L|^2 + |\bar{\alpha}'_R|^2 = |\bar{\alpha}'_L|^2 + |\bar{\alpha}_R|^2$ imposes that $2(\phi_t - \phi_r) = \pi$ such that we can chose $r_m = |r_m|$ and $t_m = i|t_m|$. We rewrite the the cavity fields by injecting the identities $\bar{\alpha}_L = -\bar{\alpha}'_L e^{2ikL_1}$ and $\bar{\alpha}'_R = -\bar{\alpha}_R e^{2ikL_2}$ such that we get the useful system

$$\begin{aligned} (1 + |r_m|e^{2ikL_2})\bar{\alpha}_R &= -i|t_m|e^{2ikL_1}\bar{\alpha}'_L \\ (1 + |r_m|e^{2ikL_1})\bar{\alpha}'_L &= -i|t_m|e^{2ikL_2}\bar{\alpha}_R. \end{aligned} \quad (\text{II.26})$$

Resonance Frequencies

By eliminating the right and left fields in the above system, we arrive at the transcendental equation [5]

$$-\cos kL = |r_m| \cos(k\Delta L), \quad \text{with} \quad \Delta L = L_2 - L_1. \quad (\text{II.27})$$

Following the method in Sankey et al. [6], we now proceed to derive the cavity resonance frequencies as a function of the membrane position x around its mean position $x = 0$. We will also always consider a long cavity such that $L \gg \lambda, x$. The cavity sublengths considering a non zero mean membrane position are then $L_1 \rightarrow L_1 + x$ and $L_2 \rightarrow L_2 - x$. It follows that $\Delta L \rightarrow \Delta L - 2x$. We will consider the effect of this displacement on the cavity wavenumbers/frequencies as a perturbation $k(x) = k_N + \delta k(x)$ with $k_N = N\pi/L$, that is the membrane displacement does not change the longitudinal mode index N but modulates it by at most π/L (or equivalently by one empty cavity FSR in the frequency domain). We will omit the x dependency in both k and δk for ease of notation. It then follows that terms in kL and kx can be expanded as

$$\cos(kL) = (-1)^N \cos(\delta k L) \quad \text{and} \quad \cos(kx) \sim \cos(k_N x)$$

where we assumed that $\delta k x \sim 0$. The transcendental equation becomes

$$(-1)^{N+1} \cos(\delta k L) = |r_m| \cos(k_N \Delta L) \left[\cos(\delta k \Delta L) \cos(2k_N x) + \sin(\delta k \Delta L) \sin(2k_N x) \right] \quad (\text{II.28})$$

and where we simplified the sines terms already equal to zero. We will now consider the Membrane At The Edge (MATE) model where $L_1 \sim L \gg L_2 \rightarrow \Delta L \sim L$. Solving for δk reinjecting in the dispersion relation $\omega_c(x) = ck(x)$ leads to

$$\omega_c(x) \simeq \omega_{FSR} \left(N + \frac{1}{\pi} \arctan \left(-\frac{1 + |r_m| \cos 2k_N x}{|r_m| \sin 2k_N x} \right) \right) \quad (\text{II.29})$$

where $\omega_{FSR} = \pi c/L$ is the empty cavity free spectral range. When the laser is resonant with the cavity, we then substitute $N\omega_{FSR}$ and k_N by ω_0 and k the laser angular frequency and wavenumber. Taking the derivatives of these resonance frequencies with respect to the membrane position x gives the linear and quadratic dispersive optomechanical couplings $G^{(1)}(x) = \partial\omega_c/\partial x$ and $G^{(2)}(x) = \partial^2\omega_c/\partial x^2$ as

$$\begin{aligned} G^{(1)}(x) &= \frac{2|r_m|k_N\omega_{FSR}}{\pi} \frac{|r_m| + \cos(2k_N x)}{1 + |r_m|^2 - 2|r_m| \cos(2k_N x)} \\ G^{(2)}(x) &= -\frac{4|r_m|k_N^2\omega_{FSR}}{\pi} \frac{|r_m|(1 - |r_m|^2) \sin(2k_N x)}{(1 + |r_m|^2 - 2|r_m| \cos(2k_N x))^2} \end{aligned} \quad (\text{II.30})$$

Cavity transmission and reflection

From the system in (??), and having derived just above the resonant cavity wavevectors k , we can compute the power ratio of the two sub-cavity fields as a function of x when the MATE system is on resonance. This is

$$\frac{|\bar{\alpha}_R|^2}{|\bar{\alpha}'_L|^2} = \frac{P_R}{P_L} = \frac{1 + 2|r_m| \cos(2kL_1 + 2kx) + |r_m|^2}{1 - |r_m|}. \quad (\text{II.31})$$

with $P_{L,R} \propto |\bar{\alpha}_{L,R}|^2$. It then follows that the the power fraction leaking from the left and right mirrors, i.e. the resonant reflection and transmission coefficients $R(\Delta = 0, x)$ and $T(\Delta = 0, x)$ are given by

$$\begin{aligned} R(\Delta = 0, x) &= \frac{|t_1|^2 P_L}{|t_1|^2 P_L + |t_2|^2 P_R} \\ &= \frac{|t_1|^2 (1 - |r_m|^2)}{|t_1|^2 (1 - |r_m|^2) + |t_2|^2 (1 + |r_m|^2 + 2|r_m| \cos 2kx)} \\ T(\Delta = 0, x) &= \frac{|t_2|^2 P_R}{|t_1|^2 P_L + |t_2|^2 P_R} \\ &= \frac{|t_2|^2 (1 + |r_m|^2 + 2|r_m| \cos 2kx)}{|t_1|^2 (1 - |r_m|^2) + |t_2|^2 (1 + |r_m|^2 + 2|r_m| \cos 2kx)} \end{aligned} \quad (\text{II.32})$$

and we get the expected relation $R(\Delta = 0, x) + T(\Delta = 0, x) = 1$.

Cavity Linewidth and Finesse

To derive the position dependent cavity linewidth $\kappa(x)$ and finesse $\mathcal{F}(x)$, we once again resort to the Sankey et al. method [6]. The total energy stored in the cavity is given by

$$E = \frac{2(L_1 + x)}{c} P_L + \frac{2(L_2 - x)}{c} P_R \quad (\text{II.33})$$

and the rate at which energy leaves the cavity is given by

$$\partial_t E = -|t_1|^2 P_L - |t_2|^2 P_R \quad (\text{II.34})$$

such that the cavity energy decay rate is given by

$$\begin{aligned} \kappa(x) &= -\frac{\partial_t E}{E} = \frac{c(|t_1|^2 + |t_2|^2 P_R/P_L)}{2(L_1 + x) + 2(L_2 - x) P_R/P_L} \\ &= \frac{c|t_1|^2 (1 - |r_m|^2) + c|t_2|^2 (1 + |r_m|^2 + 2|r_m| \cos 2kx)}{2(L_1 + x)(1 - |r_m|^2) + 2(L_2 - x)(1 + |r_m|^2 + 2|r_m| \cos 2kx)}. \end{aligned} \quad (\text{II.35})$$

We can then derive the cavity finesse as

$$\mathcal{F}(x) = \frac{\pi c}{L\kappa(x)}. \quad (\text{II.36})$$

II.2.2 Quantum Langevin Equations

Using the same tools as in section II.2, we can derive the QLE of a membrane based optomechanical system. The membrane position now turns into an operator such that $\hat{x} \propto \hat{c} + \hat{c}^\dagger$ with \hat{c} the mechanical annihilation operator as in the previous section. As seen above, the membrane position modifies the resonance frequencies of the two subcavities, such that they both depend on the membrane position as $\omega_L(x)$ and $\omega_R(x)$ but with inverse trend: when one cavity shortens and its FSR increases, the other lengthens and its FSR decreases. To first order, we can linearize the resonance frequencies as

$$\omega_L(\hat{x}) \simeq \omega_L + G_L \hat{x}, \quad \omega_R(\hat{x}) \simeq \omega_R + G_R \hat{x}, \quad (\text{II.37})$$

with $\omega_{L,R}$ the unperturbed resonance frequencies of the subcavities and $G_L = \omega_L/L_1$ and $G_R = -\omega_R/L_2$ their respective optomechanical couplings. The whole system features a network of optical modes varying linearly with the membrane position, coupled by the membrane transmission.

In Vincent Dumont's PhD work, quadratic points (where $G^{(1)} = 0$ and $G^{(2)} \neq 0$) were the centerfold of the study, in the high membrane reflectivity regime [**dumont_cavity_2017**]. It was then sufficient to consider two optical modes coupled by photon tunneling through the membrane.

However, in our case, we focus on the sole dispersive coupling regime in the MATE configuration, and we additionally consider a low membrane reflectivity. The optimal point to do so is when the first long cavity is on resonance, and when the short one is anti-resonant. With a lowered reflectivity, the coupling between subcavity modes increases, leading to larger mode splittings at the avoided crossings, until the two subcavities are fully hybridized into new cavity modes spanning both subcavities [**thompson_strong_2008**, **thompson_coupling_2013**]. In this regime, we need to rescale the optomechanical couplings by the membrane reflectivity as

$$G_{L,R} \rightarrow \tilde{G}_{L,R} = |r_m| G_{L,R} \quad (\text{II.38})$$

to account for the reduced sensitivity of the cavity resonance frequencies to the membrane position [**thompson_strong_2008**]

The short cavity being precisely at an anti-node, it is equally probable for the tunneled photons from the long cavity to populate two short cavity modes on either side of the anti-

node. We then need to describe the system by a single long cavity mode coupled to two short cavity modes, as illustrated in figure ???. We introduce the annihilation operators \hat{a}_L for the long cavity mode, and \hat{a}_{R+} and \hat{a}_{R-} for the two short cavity modes on either side of the anti-node. The Hamiltonian of this system can then be written as

$$\begin{aligned}\hat{H} &= \hbar(\omega_L + \tilde{G}_L x) \hat{a}_L^\dagger \hat{a}_L + \hbar(\omega_{R-} - \tilde{G}_R x) \hat{a}_{R-}^\dagger \hat{a}_{R-} + \hbar(\omega_{R+} - \tilde{G}_R x) \hat{a}_{R+}^\dagger \hat{a}_{R+} & (= \hat{H}_\gamma) \\ &+ \hbar\Omega_m \hat{c}^\dagger \hat{c} & (= \hat{H}_m) \\ &+ \hbar\tilde{G}_L \hat{a}_L^\dagger \hat{a}_L \delta\hat{x} - \hbar\tilde{G}_R (\hat{a}_{R+}^\dagger \hat{a}_{R+} + \hat{a}_{R-}^\dagger \hat{a}_{R-}) \delta\hat{x} & (= \hat{H}_{\text{OM}}) \\ &- \hbar J [\hat{a}_L^\dagger (\hat{a}_{R+} + \hat{a}_{R-}) + (\hat{a}_{R+}^\dagger + \hat{a}_{R-}^\dagger) \hat{a}_L] & (= \hat{H}_{\text{tun}})\end{aligned}$$

where $J = c|t_m|/2\sqrt{L_1 L_2}$ is the photon tunneling rate through the membrane [thompson_strong_2008], and where we linearized the position as before as $\hat{x} = x + \delta\hat{x}$. The first line describes the free evolution of the subcavity modes, the second one the mechanical resonator, the third the optomechanical interaction between the membrane position and the subcavity modes, and the last the photon tunneling through the membrane. As before, the commutation relations are given by

$$[\hat{a}_L, \hat{a}_L^\dagger] = [\hat{a}_{R\pm}, \hat{a}_{R\pm}^\dagger] = [\hat{c}, \hat{c}^\dagger] = 1 \quad \text{and} \quad [\hat{a}_L, \hat{a}_{R\pm}] = [\hat{a}_L, \hat{a}_{R\pm}^\dagger] = 0$$

We will only consider the photonic part of the Hamiltonian, as to put it in matrix form such that we can diagonalize it and work in the basis of the new eigenmodes. Furthermore, we go the frame rotating at frequency $\omega_0 = \omega_{R-} = \omega_L$ i.e. when the long cavity mode is degenerate with the left short cavity mode, such that the photonic Hamiltonian becomes

$$\hat{H}_\gamma = \hbar\tilde{G}_L x \hat{a}_L^\dagger \hat{a}_L - \hbar\tilde{G}_R \left(x + \frac{\lambda}{4} \right) \hat{a}_{R-}^\dagger \hat{a}_{R-} + \hbar \left(\omega_{FSR} - \tilde{G}_R \left(x - \frac{\lambda}{4} \right) \right) \hat{a}_{R+}^\dagger \hat{a}_{R+} \quad (\text{II.39})$$

and we can rewrite both the photonic and tunneling hamiltonian i.e. the photonic manifold in matrix form as

$$\hat{H}_\gamma + \hat{H}_{\text{tun}} = \hbar \begin{pmatrix} \hat{a}_L^\dagger & \hat{a}_{R-}^\dagger & \hat{a}_{R+}^\dagger \end{pmatrix} \mathbf{M} \begin{pmatrix} \hat{a}_L \\ \hat{a}_{R-} \\ \hat{a}_{R+} \end{pmatrix} \quad (\text{II.40})$$

with

$$\mathbf{M} = \begin{pmatrix} \tilde{G}_L x & -J & -J \\ -J & -\tilde{G}_R(x + \lambda/4) & 0 \\ -J & 0 & \omega_{FSR} - \tilde{G}_R(x - \lambda/4) \end{pmatrix}.$$

One could then diagonalize this 3×3 matrix to get the new eigenmodes of the system, and rewrite the optomechanical interaction in this new basis. In the limit where the membrane transmittivity is high such that $|t_m| \sim 1$ and $|r_m| \ll 1$, the tunneling rate J becomes much larger than both optomechanical couplings $\tilde{G}_{L,R}x$ and the free spectral range ω_{FSR} . The cumberstone expression of the eigenmodes is not displayed here, but is equivalent to considering an system's eigenstate described by a annihilation operator \hat{a} with optomechanical coupling $G^{(1)}(x)$ and decay rate $\kappa(x)$ as derived in the previous section. The system's Hamiltonian can then be written as

$$\hat{H} = \hbar\omega_c(x = \lambda/4)\hat{a}^\dagger\hat{a} + \hbar\Omega_m\hat{c}^\dagger\hat{c} + \hbar G^{(1)}(x)\hat{a}^\dagger\hat{a}\hat{x} \quad (\text{II.41})$$

where we omitted the tilde on the optomechanical coupling for ease of notation.

Classical Description : Closed cavity model

We start by describing the classical behaviour of the cavity. Considering a high finesse cavity, with high reflectivity mirrors $r_1, r_2 \approx 1$, the cavity fields are written as

$$\alpha_1 = \alpha'_1 \quad (\text{II.42})$$

where E_{in} is the input field, E_1 the intracavity field before the membrane, E_2 the intracavity field after the membrane, E_3 the transmitted field and E_4 the reflected field. The cavity resonance frequencies are then obtained by solving these equations in the absence of input field $E_{\text{in}} = 0$, leading to the transcendental equation [5]

We describe the subcavity modes by annihilation operators \hat{a}_1 and \hat{a}_2 , with unperturbed resonance frequencies ω_1 and ω_2 . The membrane position operator is described by annihilation operator $\hat{x} \propto \hat{c} + \hat{c}^\dagger$ as in the previous section. Considering how the membrane position under the effect of radiation pressure modifies the resonance frequencies of the two subcavities, the subcavity length can be written as $L_1 = L_{1,0} + x$ and $L_2 = L_{2,0} - x$, with $L_{1,0}$ and $L_{2,0}$ the equilibrium lengths, and x the mean static displacement of the membrane. This mean displacement being small compared to the cavity length, we can linearize the resonance frequencies as

$$\omega_1(x) \simeq \omega_0 + G_1 x, \quad \omega_2(x) \simeq \omega_0 - G_2 x, \quad (\text{II.43})$$

with $G_1 = \omega_0/L_{1,0}$ and $G_2 = \omega_0/L_{2,0}$ the optomechanical couplings of the two subcavities, and where ω_0 is the common frequency of the two modes i.e. $\omega_{1,0} = \omega_{2,0} = \omega_0$. The system now features a network of optical modes varying linearly with the membrane position, coupled by the membrane transmission. The Hamiltonian of the system is then given by

[xu_cavity_2016]

$$\hat{H} = \hbar\omega_1(x)\hat{a}_1^\dagger\hat{a}_1 + \hbar\omega_2(x)\hat{a}_2^\dagger\hat{a}_2 + \hbar g(\hat{a}_1^\dagger\hat{a}_2 + \hat{a}_2^\dagger\hat{a}_1) + \frac{\hat{p}^2}{2m} + \frac{1}{2}m\omega_m^2\hat{x}^2 \quad (\text{II.44})$$

Two configurations are then possible: position the membrane at approximately half the total cavity length $L/2$, such that $L_{1,0} \simeq L_{2,0}$ and $G_1 \simeq G_2$; or position the membrane close to one of the mirrors, such that one subcavity is much shorter than the other, e.g. $L_{1,0} \gg L_{2,0}$ and $G_1 \ll G_2$. The first configuration is called the *membrane-in-the-middle* (MIM) configuration, while the second one is called the *membrane-at-the-edge* (MATE) configuration. The MIM configuration has been widely studied in the literature [thompson_strong_2008, xu_cavity_2016, 5, 6], and has been used to demonstrate various quantum effects such as ponderomotive squeezing [purdy_observation_2013], quantum non-demolition measurements of phonon number [6], or ground-state cooling of a mechanical resonator [peterson_laser_2016]. However, the MIM configuration suffers from a low optomechanical coupling rate due to the small value of $G_{1,2}$, which limits its use for quantum experiments. The MATE configuration has been less studied, but offers a much larger optomechanical coupling rate due to the large value of G_1 . This makes it a promising candidate for quantum experiments. In this work, we will focus on the MATE configuration.

Set-up and notation

We consider a three-mode optical model for a membrane-at-the-edge (MATE) cavity with a *highly transmissive* middle membrane. The long cavity mode is denoted by a ; the short cavity contributes two nearby modes, b_+ and b_- , centered $\pm\lambda/4$ away in displacement. In the mode basis $(a, b_+, b_-)^\top$ we take (with $\hbar = 1$)

$$\mathbf{H} = \begin{pmatrix} \delta_a & J & -J \\ J & \delta_+ & 0 \\ -J & 0 & \delta_- \end{pmatrix}, \quad \begin{aligned} \delta_a &= r_m G_1 \Delta x, \\ \delta_\pm &= r_m G_2 \left(\Delta x \mp \frac{\lambda}{4} \right), \end{aligned} \quad (\text{II.45})$$

with

$$J = \frac{c t_m}{2\sqrt{L_1 L_2}}, \quad t_m^2 + r_m^2 = 1, \quad G_1 = \frac{\omega_0}{L_1}, \quad G_2 = -\frac{\omega_0}{L_2}. \quad (\text{II.46})$$

Here Δx is the membrane displacement from the symmetry point, λ the optical wavelength, t_m (r_m) the middle-membrane amplitude transmission (reflection), and $L_{1,2}$ the long/short sub-cavity lengths. High transmissivity means $r_m \ll 1$ while $J = O(t_m)$ can be sizable.

The exact normal modes are eigenoperators $A_k = \alpha_k a + \beta_k b_+ + \gamma_k b_-$ obtained from

$(\mathbf{H} - \omega_k \mathbb{I})(\alpha_k, \beta_k, \gamma_k)^\top = 0$. From the lower rows one finds the exact amplitude ratios

$$\frac{\beta_k}{\alpha_k} = -\frac{J}{\delta_+ - \omega_k}, \quad \frac{\gamma_k}{\alpha_k} = +\frac{J}{\delta_- - \omega_k}. \quad (\text{II.47})$$

The “physical” orange branch in the figures is the one continuously connected to the long-cavity mode a .

Time-domain adiabatic elimination

Away from the two avoided crossings at $\Delta x \approx \pm \lambda/4$, the short-cavity detunings $|\delta_\pm - \omega|$ are large compared to the coupling:

$$\varepsilon_\pm \equiv \frac{J}{|\delta_\pm - \omega|} \ll 1. \quad (\text{II.48})$$

The Heisenberg equations generated by (??) read

$$\begin{aligned} i\dot{a} &= \delta_a a + Jb_+ - Jb_-, \\ i\dot{b}_+ &= \delta_+ b_+ + Ja, \\ i\dot{b}_- &= \delta_- b_- - Ja. \end{aligned} \quad (\text{II.49})$$

The fast spectators b_\pm can be slaved to the slow variable a by setting $\dot{b}_\pm \simeq 0$ to leading order:

$$b_+ \simeq -\frac{J}{\delta_+} a, \quad b_- \simeq -\frac{J}{\delta_-} a. \quad (\text{II.50})$$

Substituting (??) into the a equation in (??) gives an effective single-mode dynamics

$$i\dot{a} = \left[\delta_a - J^2 \left(\frac{1}{\delta_+} + \frac{1}{\delta_-} \right) \right] a. \quad (\text{II.51})$$

Equation (??) shows that, in the dispersive region, the spectators do not acquire population to leading order; they merely induce a frequency (phase) shift of the a mode of order J^2/δ_\pm .

If optical losses are included as κ_a, κ_\pm (phenomenologically via $\delta_a \rightarrow \delta_a - i\kappa_a/2$ etc.), the same elimination yields

$$i\dot{a} = \left[\delta_a - \frac{i\kappa_a}{2} - J^2 \left(\frac{1}{\delta_+ - i\kappa_+/2} + \frac{1}{\delta_- - i\kappa_-/2} \right) \right] a, \quad (\text{II.52})$$

and the validity condition strengthens to $J \ll \sqrt{\Delta_\pm^2 + \kappa_\pm^2/4}$ with $\Delta_\pm = \text{Re}(\delta_\pm - \omega)$.

Connection to eigenvectors. Using (??), for the branch connected to a one has $|\beta/\alpha|, |\gamma/\alpha| = O(\varepsilon_{\pm}) \ll 1$. Thus the b_{\pm} weights in the physical eigenoperator are $O(\varepsilon_{\pm}^2)$, fully consistent with the slaving picture (??).

Closed form for the physical eigenfrequency

The exact eigenvalue equation for the orange branch obtained from the first row of $(\mathbf{H} - \omega\mathbb{I})v = 0$ together with (??) is

$$\omega = \delta_a - J^2 \left(\frac{1}{\delta_+ - \omega} + \frac{1}{\delta_- - \omega} \right). \quad (\text{II.53})$$

In the dispersive regime $|\delta_{\pm}| \gg |\omega|$ one can set $\omega \rightarrow 0$ in the denominators at first order, giving the explicit approximation

$$\boxed{\omega_{\text{phys}}(\Delta x) \approx r_m G_1 \Delta x - J^2 \left[\frac{1}{r_m G_2 (\Delta x - \frac{\lambda}{4})} + \frac{1}{r_m G_2 (\Delta x + \frac{\lambda}{4})} \right].} \quad (\text{II.54})$$

Combining the two fractions yields a compact dispersive form

$$\boxed{\omega_{\text{phys}}(\Delta x) \approx r_m G_1 \Delta x - \frac{2J^2}{r_m G_2} \frac{\Delta x}{\Delta x^2 - (\lambda/4)^2}.} \quad (\text{II.55})$$

Close to the symmetry point $|\Delta x| \ll \lambda/4$, (??) becomes nearly linear:

$$\boxed{\omega_{\text{phys}}(\Delta x) \approx \underbrace{\left[r_m G_1 + \frac{32J^2}{r_m G_2 \lambda^2} \right]}_{\text{renormalized slope}} \Delta x.} \quad (\text{II.56})$$

In the usual MATE limit $L_1 \gg L_2$ (hence $|G_1| \ll |G_2|$), the second term typically dominates the slope; this analytic form explains the gentle “tilt” of the orange branch between the two avoided crossings.

Schrieffer–Wolff (block-diagonal) derivation

For completeness, write $H = H_0 + V$ with $H_0 = \text{diag}(\delta_a, \delta_+, \delta_-)$ and $V = \begin{pmatrix} 0 & J & -J \\ J & 0 & 0 \\ -J & 0 & 0 \end{pmatrix}$. Let S be anti-Hermitian satisfying $[H_0, S] = -V$. A suitable choice is

$$S = \begin{pmatrix} 0 & \frac{J}{\delta_a - \delta_+} & -\frac{J}{\delta_a - \delta_-} \\ -\frac{J}{\delta_a - \delta_+} & 0 & 0 \\ \frac{J}{\delta_a - \delta_-} & 0 & 0 \end{pmatrix}. \quad (\text{II.57})$$

The transformed Hamiltonian $\tilde{H} = e^S H e^{-S} = H_0 + \frac{1}{2}[S, V] + O(J^3/\Delta^2)$ is block-diagonal to second order, with the a block

$$H_{\text{eff}}^{(a)} = \delta_a - J^2 \left(\frac{1}{\delta_+ - \delta_a} + \frac{1}{\delta_- - \delta_a} \right), \quad (\text{II.58})$$

which reduces to (??) when $|\delta_{\pm}| \gg |\delta_a|$. Residual $a \leftrightarrow b_{\pm}$ couplings are suppressed to $O(J^3/\Delta^2)$.

Local avoided crossings (breakdown of elimination)

Near $\Delta x \simeq +\lambda/4$, only b_+ is near resonant; the relevant subspace is (a, b_+) with

$$H_{\text{loc}}^{(+)} = \begin{pmatrix} \delta_a & J \\ J & \delta_+ \end{pmatrix}, \quad \Rightarrow \quad \omega_{\pm}^{(+)} = \frac{\delta_a + \delta_+}{2} \pm \sqrt{\left(\frac{\delta_a - \delta_+}{2}\right)^2 + J^2}. \quad (\text{II.59})$$

The orange branch is the one connecting continuously to (??) away from the crossing. The same holds at $\Delta x \simeq -\lambda/4$ with b_- . Adiabatic elimination is invalid in windows where $\varepsilon_{\pm} \ll 1$.

Validity conditions and practical rule

The small parameter governing all steps is $\varepsilon_{\pm} = J/|\delta_{\pm} - \omega|$. With losses, $\varepsilon_{\pm} = J/\sqrt{\Delta_{\pm}^2 + \kappa_{\pm}^2/4}$. A conservative working criterion is

$\max\{\varepsilon_+, \varepsilon_-\} \lesssim 0.2 - 0.3 \quad \Rightarrow \quad \text{errors in } \omega_{\text{phys}} \text{ are } O(\varepsilon^2), \text{ and } |b_{\pm}|^2/|a|^2 = O(\varepsilon^2).$

(II.60)

Optional bright/dark re-basis

Defining $b_s = (b_+ - b_-)/\sqrt{2}$ and $b_d = (b_+ + b_-)/\sqrt{2}$, one finds that a couples only to the *bright* mode b_s with strength $\sqrt{2}J$, while b_d is dark to first order. In this basis the cubic spectrum becomes a quadratic (for a, b_s) plus a spectator b_d whose frequency lies near $r_m G_2 \Delta x$ and mixes weakly via $O(r_m G_2 \lambda/2)$. This re-basis is often convenient for fitting and for visualizing how the orange branch acquires its dispersive tilt.

Summary. In a high- T middle-membrane MATE system, the short-cavity modes are far detuned for most Δx . They can be adiabatically eliminated, yielding the explicit orange-branch dispersion (??) (or (??) near the center), with controlled accuracy quantified by ε_{\pm} . Only in narrow windows around $\Delta x = \pm\lambda/4$ is a 2×2 avoided-crossing description required.

II.2.3 Mechanical Resonators

Mechanical Resonators

II.2.4 Noise spectra

We will derive the Hamiltonian formalism of a three mirror cavity, and show how it can be used to describe the optomechanical coupling of a membrane in the cavity. We now have to consider two optical modes coupled to one another through the membrane transmittivities. The Hamiltonian of the system can be written as:

$$\hat{H} = \hbar\omega_1\hat{a}_1^\dagger\hat{a}_1 + \hbar\omega_2\hat{a}_2^\dagger\hat{a}_2 + \hbar g(\hat{a}_1^\dagger\hat{a}_2 + \hat{a}_2^\dagger\hat{a}_1) + \frac{\hat{p}^2}{2m} + \frac{1}{2}m\omega_m^2\hat{x}^2 \quad (\text{II.61})$$

where \hat{a}_1 and \hat{a}_2 are the annihilation operators of the two optical modes, ω_1 and ω_2 their respective frequencies, g the optomechanical coupling strength, \hat{p} and \hat{x} the momentum and position operators of the membrane, m its mass and ω_m its mechanical frequency. The optomechanical coupling strength g is defined as:

$$g = \frac{\omega_1}{L}\sqrt{\frac{\hbar}{2m\omega_m}}(T_1 + T_2) \quad (\text{II.62})$$

where T_1 and T_2 are the transmittivities of the two optical modes through the membrane. The Hamiltonian can be diagonalized by introducing the normal modes of the system, which are the eigenstates of the Hamiltonian. The normal modes can be expressed as:

$$\hat{b}_1 = \frac{1}{\sqrt{2}}(\hat{a}_1 + \hat{a}_2), \quad \hat{b}_2 = \frac{1}{\sqrt{2}}(\hat{a}_1 - \hat{a}_2) \quad (\text{II.63})$$

The normal modes \hat{b}_1 and \hat{b}_2 are the symmetric and antisymmetric modes of the system, respectively. The Hamiltonian can then be rewritten in terms of the normal modes as:

$$\hat{H} = \hbar\omega_1\hat{b}_1^\dagger\hat{b}_1 + \hbar\omega_2\hat{b}_2^\dagger\hat{b}_2 + \hbar g(\hat{b}_1^\dagger\hat{b}_2 + \hat{b}_2^\dagger\hat{b}_1) + \frac{\hat{p}^2}{2m} + \frac{1}{2}m\omega_m^2\hat{x}^2 \quad (\text{II.64})$$

Diagonalisation of two non-degenerate, tunnel-coupled optical cavities. Let a_1 and a_2 (with the usual bosonic commutation relations) annihilate photons in the first and second cavity, whose bare resonance frequencies are $\omega_1 \neq \omega_2$. Photon tunnelling at rate $J > 0$ through the semi-transparent middle mirror couples the two modes, giving the second-quantised Hamiltonian

$$H = \hbar \begin{pmatrix} a_1^\dagger & a_2^\dagger \end{pmatrix} \underbrace{\begin{pmatrix} \omega_1 & J \\ J & \omega_2 \end{pmatrix}}_{\mathbf{M}} \begin{pmatrix} a_1 \\ a_2 \end{pmatrix}.$$

Diagonalising the 2×2 Hermitian matrix \mathbf{M} one finds the normal-mode (super-mode) eigenfrequencies

$$\omega_{\pm} = \frac{\omega_1 + \omega_2}{2} \pm \sqrt{J^2 + \left(\frac{\omega_1 - \omega_2}{2}\right)^2}, \quad (\text{II.65})$$

and introduces a mixing angle θ via

$$\tan 2\theta = \frac{2J}{\omega_2 - \omega_1}, \quad 0 < \theta < \pi/2.$$

The corresponding canonical operators

$$A_+ = \cos \theta a_1 + \sin \theta a_2, \quad A_- = -\sin \theta a_1 + \cos \theta a_2,$$

obey $[A_\mu, A_\nu^\dagger] = \delta_{\mu\nu}$ and bring the Hamiltonian to the diagonal form

$$H = \hbar\omega_+ A_+^\dagger A_+ + \hbar\omega_- A_-^\dagger A_-,$$

revealing two independent harmonic oscillators whose frequency splitting $\omega_+ - \omega_- = 2\sqrt{J^2 + [(\omega_1 - \omega_2)/2]^2}$ interpolates smoothly between the strong-coupling limit ($\omega_1 \approx \omega_2$) and the large-detuning regime where each cavity mode retains its individuality and the admixture of its neighbour is suppressed by the small parameter $J/|\omega_2 - \omega_1| \ll 1$.

Chapter III

Experimental Methods

This chapter essentially covers feedback control techniques used in Chapter IV and V. It is thought as a practical guide to the implementation of various locking schemes using the LKB *home grown* control software PyRPL. The chapter begins with a general introduction to feedback control, PI controllers and error signal requirements. It then details specific locking techniques used in this work, with an emphasis on experimental aspects. For in depth technical description of the PyRPL working principle, we refer the reader to Chapter III or Leonard Neuhaus thesis [[Neuhauser_Thesis_2021](#)], as well as the PyRPL documentation [[PyRPL_Docs](#)] and original article [[PyRPL_Article](#)]. Some figures are adapted from this last reference (with authorization)

Contents

III.1 Feedback control	74
III.1.1 Overview	74
III.1.2 Proportion-Integral (PI) Controllers	75
III.1.3 PyRPL overview	77
III.1.4 IQ modules	78
III.2 Locking techniques	79
III.2.1 Temperature Locks	79
III.2.2 Optical paths Locks - Dither Locks	81
III.2.3 Side of Fringe Locks	81
III.2.4 Pound-Drever-Hall Locks	81
III.2.5 Offset frequency Locks	83

III.1 Feedback control

A central aspect of experimental quantum optics is the ability to stabilize various parameters of an optical setup against environmental fluctuations. These parameters include cavity lengths, laser frequencies, optical phases, and temperatures of nonlinear crystals, which all undergo unwanted drifts and noise due to thermal, acoustic, and mechanical perturbations. To achieve this stabilization, feedback control systems are employed, which rely on generating an error signal that quantifies the deviation from a desired setpoint. This error signal is then processed by a controller to compute a corrective feedback signal that drives an actuator to counteract the disturbance and maintain the parameter at its target value.

III.1.1 Overview

A feedback control loop then aims to stabilize the behaviour of a physical system that is continuously subject to disturbances. When the system may be linearized around its operating point, its response to a harmonic perturbation at angular frequency ω_0 is fully characterized by its complex transfer function $G(\omega)$. We denote by $V_{\text{exc}}(t)$ the real excitation applied to the system, taken to be sinusoidal,

$$V_{\text{exc}}(t) = A_{\text{exc}} \cos(\omega_0 t), \quad (\text{III.1})$$

with amplitude A_{exc} . In the frequency domain the system is described by its complex transfer function

$$G(\omega) = |G(\omega)| e^{i\phi(\omega)}, \quad (\text{III.2})$$

which specifies the amplitude response $|G(\omega)|$ and the phase shift $\phi(\omega)$ experienced by a sinusoid at frequency ω . The relation between input and output is expressed most naturally in complex notation. Writing the excitation as the real part of a complex exponential,

$$V_{\text{exc}}(t) = \text{Re}\left\{ A_{\text{exc}} e^{i\omega_0 t} \right\} \implies V_{\text{meas}}(t) = \text{Re}\left\{ G(\omega_0) A_{\text{exc}} e^{i\omega_0 t} \right\}$$

so that explicitly

$$V_{\text{meas}}(t) = |G(\omega_0)| A_{\text{exc}} \cos(\omega_0 t + \phi(\omega_0)). \quad (\text{III.3})$$

Thus the physical output remains real, while the complex transfer function $G(\omega_0)$ determines how the amplitude and phase of the input harmonic are modified.

In-phase and quadrature decomposition.

It is convenient to decompose the transfer function into its in-phase (I) and quadrature (Q) components such that Eq. (??) can be written as

$$V_{\text{meas}}(t) = I(\omega_0) \cos(\omega_0 t) + Q(\omega_0) \sin(\omega_0 t), \quad (\text{III.4})$$

which forms the basis of IQ demodulation. By multiplying $V_{\text{meas}}(t)$ by $\cos(\omega_0 t)$ and $\sin(\omega_0 t)$ and low-pass filtering the results with a filter $H_f(\omega)$ with a cutoff frequency $\omega_f \ll \omega_0$, one obtains the slowly varying quadratures $I(t)$ and $Q(t)$, from which the complex baseband signal

$$s_{\text{meas}}(t) = I(\omega_0) + i Q(\omega_0) \quad (\text{III.5})$$

is constructed.

Obviously, realistic excitation signals are never pure sinusoids, such that they can be decomposed into a superposition of harmonic components

$$V_{\text{exc}}(t) = \text{Re} \left\{ \int_0^\infty \frac{d\omega}{2\pi} A_{\text{exc}}(\omega) e^{i\omega t} \right\}.$$

where $A_{\text{exc}}(\omega)$ is the complex amplitude of the component at angular frequency ω . Demodulating the measured signal at a frequency ω_0 and low pass filtering it yields a measured signal given by

$$\begin{aligned} s_{\text{meas}}(t) &= \int_0^\infty \frac{d\omega}{2\pi} G(\omega - \omega_0) H_f(\omega) A_{\text{exc}}(\omega - \omega_0) e^{i\omega t} \\ &= I(t) + i Q(t) \end{aligned} \quad (\text{III.6})$$

such that the IQ demodulation produces time-dependent quadratures $I(t)$ and $Q(t)$, whose complex combination $s_{\text{meas}}(t)$ represents the slowly varying complex envelope.

In a feedback loop, a relevant observable derived from $s_{\text{meas}}(t)$ is fed into the controller and is denoted $s_{\text{in}}(t)$. Depending on the application, $s_{\text{in}}(t)$ may correspond to one of the quadratures, the reconstructed phase, or any real-valued function of (I, Q) .

III.1.2 Proportion-Integral (PI) Controllers

Now that both quadratures are accessible through the IQ demodulation, and that we obtained a signal $s_{\text{in}}(t)$ relevant for the control task at hand, we need to extract an error signal $\varepsilon(t)$ that quantifies the deviation from a desired setpoint at which we wish to *lock* the system.

It is typically expressed as the difference between a measured signal and its reference value:

$$\varepsilon(t) = s_{\text{in}}(t) - s_{\text{ref}}, \quad (\text{III.7})$$

where $s_{\text{in}}(t)$ is the physical quantity monitored in the experiment, and s_{ref} is the target value.

For effective feedback stabilization, this error signal must satisfy several essential criteria listed below.

High SNR: Near the setpoint, $\varepsilon(t)$ should exhibit a high SNR to ensure robust locking and minimize the influence of technical and electronic noise.

Linearity and antisymmetry: The error signal should be linear and antisymmetric in a neighborhood of the operating point. Small deviations from the setpoint should produce a proportional response in $\varepsilon(t)$, with opposite signs for deviations of opposite direction.

Monotonicity and uniqueness: The slope $\partial\varepsilon/\partial x$, where x denotes the control parameter (e.g., cavity length or laser frequency), should be monotonic and unambiguous near the lock point to avoid multiple equilibrium points and ensure stable locking behavior.

Steep slope near the setpoint: A steeper slope improves sensitivity to small deviations and enhances lock accuracy, although it must be balanced against potential noise amplification.

Bandwidth compatibility: The spectral content of $\varepsilon(t)$ must be compatible with the bandwidth of the actuator and the dynamics of the system. For example, in the case of a piezoelectric transducer, which acts as a low-pass mechanical element, the error signal high-frequency components won't be compensated by the actuator.

A standard way to achieve this stabilization is to use a Proportion-Integral (PI) controller. The PI controller computes the feedback signal $u(t)$ from the error signal $\varepsilon(t)$ according to:

$$s_{\text{out}}(t) = K_P \varepsilon(t) + K_I \int_0^t \varepsilon(\tau) d\tau \quad (\text{III.1})$$

where K_P and K_I are the proportional and integral gains, respectively. The proportional term $K_P \varepsilon(t)$ responds to the current error and primarily acts on mid-frequency deviations, enabling rapid corrections. The integral term $K_I \int \varepsilon(\tau) d\tau$ accumulates past errors and is most effective at low frequencies, helping to eliminate long-term drifts and steady-state offsets.

In classical control theory, PID (Proportional-Integral-Derivative) controllers are designed to stabilize dynamic systems by combining three terms: a proportional term for immediate response, an integral term to eliminate steady-state error, and a derivative term that anticipates future error based on the rate of change. However, in practical experimental setups—particularly in quantum optics—PI control (Proportional-Integral) is typically sufficient and even preferable to full PID control. The derivative term, which acts predominantly at high frequencies, is generally unnecessary and can be counterproductive. This is because the feedback actuator is often a piezoelectric transducer, which exhibits non-zero capacitance. Combined with the finite output impedance of the control electronics, this forms a natural low-pass filter that significantly attenuates high-frequency components of the feedback signal. As a result, any derivative term—which primarily targets high-frequency correction—would be both ineffective due to this filtering and potentially harmful by injecting high-frequency noise into the loop.

Therefore, PI control offers a balanced and robust approach: the integral term suppresses low-frequency drifts (typically below a few Hz to tens of Hz), the proportional term corrects intermediate-frequency deviations (up to a few kHz), and high-frequency components (above the mechanical resonance or actuation bandwidth) are naturally filtered out and deliberately left uncorrected. This allows for stable feedback while preserving high-frequency signals—such as thermal noise or mechanical sidebands—which carry essential physical information for analysis and measurement.

III.1.3 PyRPL overview

With the rise of digital signal processing, many feedback control systems have transitioned from analog electronics to software-based implementations. One such powerful and flexible platform is PyRPL (Python Red Pitaya Lockbox), an open-source software suite designed for real-time digital signal processing and feedback control using the Red Pitaya hardware and developed in our team. PyRPL provides a user-friendly interface for implementing various control algorithms, including PI controllers, and is now widely used in experimental physics laboratories across the world [[PyRPL Article](#), [PyRPL Docs](#)]. While we refer the reader to Leonhard Neuhaus' thesis [[Neuhauser Thesis 2021](#)] and the PyRPL documentation [[PyRPL Docs](#)] for an in-depth technical description of the PyRPL working principle, we will concisely summarize the main performance metrics and high abstraction blocks relevant for this work.

Red Pitaya is a compact FPGA-based platform that combines high-speed analog-to-

digital (ADC) and digital-to-analog (DAC) converters with a powerful FPGA for real-time signal processing. The onboard ADCs and DACs operate at a 125 MHz sampling rate with 14-bit nominal resolution, which enables the digitization and synthesis of signals up to about 60 MHz according to the Nyquist criterion. In practice, the effective resolution is about 12 bits for the ADC and 11 bits for the DAC, which remains more than sufficient for precision photodetection, modulation, and error-signal processing in quantum optics. A notable limitation is the digitization noise floor, as well as the noise added from the voltage shifter, bounding the output to $\pm 1V$. Sensible improvement of the order of 5 dBm/Hz can be achieved in the 100 Hz - 1 MHz frequency range by unsoldering the voltage shifter circuit, as well as taking of the regulator from the board and powering the Red Pitaya with a low noise external voltage source. Taking the voltage offset off actually makes the output range 0-2V, ideal as to not feed (high voltage amplified) negative voltages to our piezoelectric actuators (which would kill them). This modification was performed on all Red Pitayas used in this work, bringing the noise floor down to 140dBm/Hz at 1MHz. In the frequency range relevant to experimental quantum optics (from a few kHz to a few hundred kHz), the Red Pitaya noise floor is remarkably close—within 10–15 dB—to that of high-end laboratory lockboxes and diagnostic instruments. Above 1 MHz, however, professional RF analyzers remain significantly quieter and cleaner. 10dB for a fraction of the cost is a fair trade off in our opinion.

PyRPL leverages this hardware to implement various digital signal processing tasks. The modules available in PyRPL are a scope, a spectrum analyser, 2 Arbitrary Signal Generators (ASG), 3 PID controllers, 3 IQ modules and an Infinite Impulse Response (IIR) filter module. These modules can be interconnected in a flexible manner to create complex feedback loops tailored to specific experimental needs, by simply rerouting the signal flow either in a programmatic way using the PyRPL Python API, or graphically through the PyRPL GUI. This makes PyRPL a very versatile and cheap tool for monitoring and piloting a wide range of experimental setups.

III.1.4 IQ modules

We now turn more specifically to the PyRPL IQ modules, which can be used to filter inputs, generate error signals, and set as to be used as a network analyser. Using the Python API or the GUI, one can select which input channel (in1 or in2) is fed to the IQ module. The user can then set the various registers associated to gain, amplitude, phase etc... to set the IQ module as to perform the desired task.

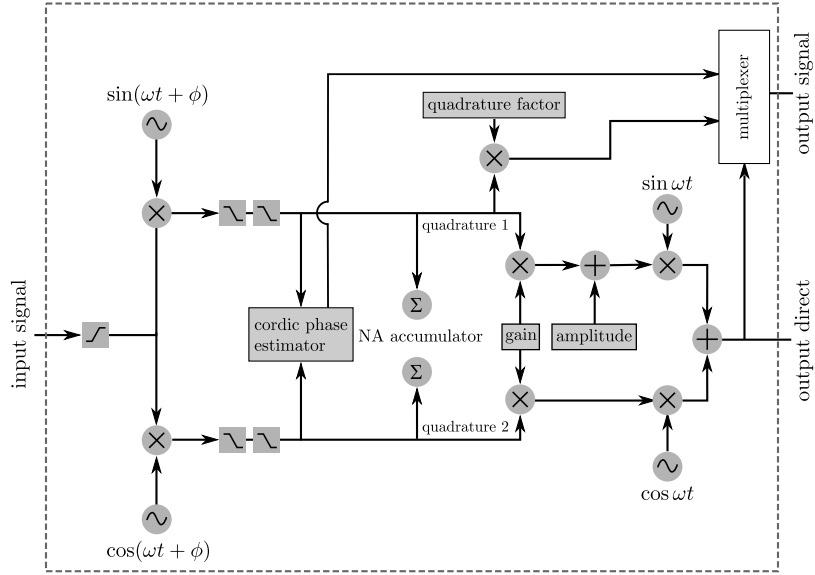


Fig. III.1 Basic working principle of the IQ module in PyRPL. One can set any register value using either the GUI or the Python API to manipulate the input signal as desired.

III.2 Locking techniques

III.2.1 Temperature Locks

A first example of a PI lock used in this work is the temperature lock, which is used to stabilize the temperature of non linear crystals embedded inside optical cavities. The error signal is derived from a temperature sensor, such as a thermistor, which measures the temperature of the crystal and simply written as:

$$\epsilon(\Delta T) \propto \Delta T \quad (\text{III.8})$$

where $\Delta T = T_{\text{meas}} - T_{\text{set}}$. The error signal is then fed into a PI controller, which adjusts the heating element, a peltier module in our case, to maintain the desired temperature setpoint.

The temperature lock is crucial for maintaining the phase matching conditions in nonlinear optical processes (developed in the next section), such as second-harmonic generation or optical parametric oscillation, where the efficiency of frequency conversion depends sensitively on the crystal temperature. By stabilizing the temperature, we ensure that the nonlinear interactions remain optimal, leading to consistent and reproducible results in experiments involving squeezed light generation or other nonlinear optical phenomena.

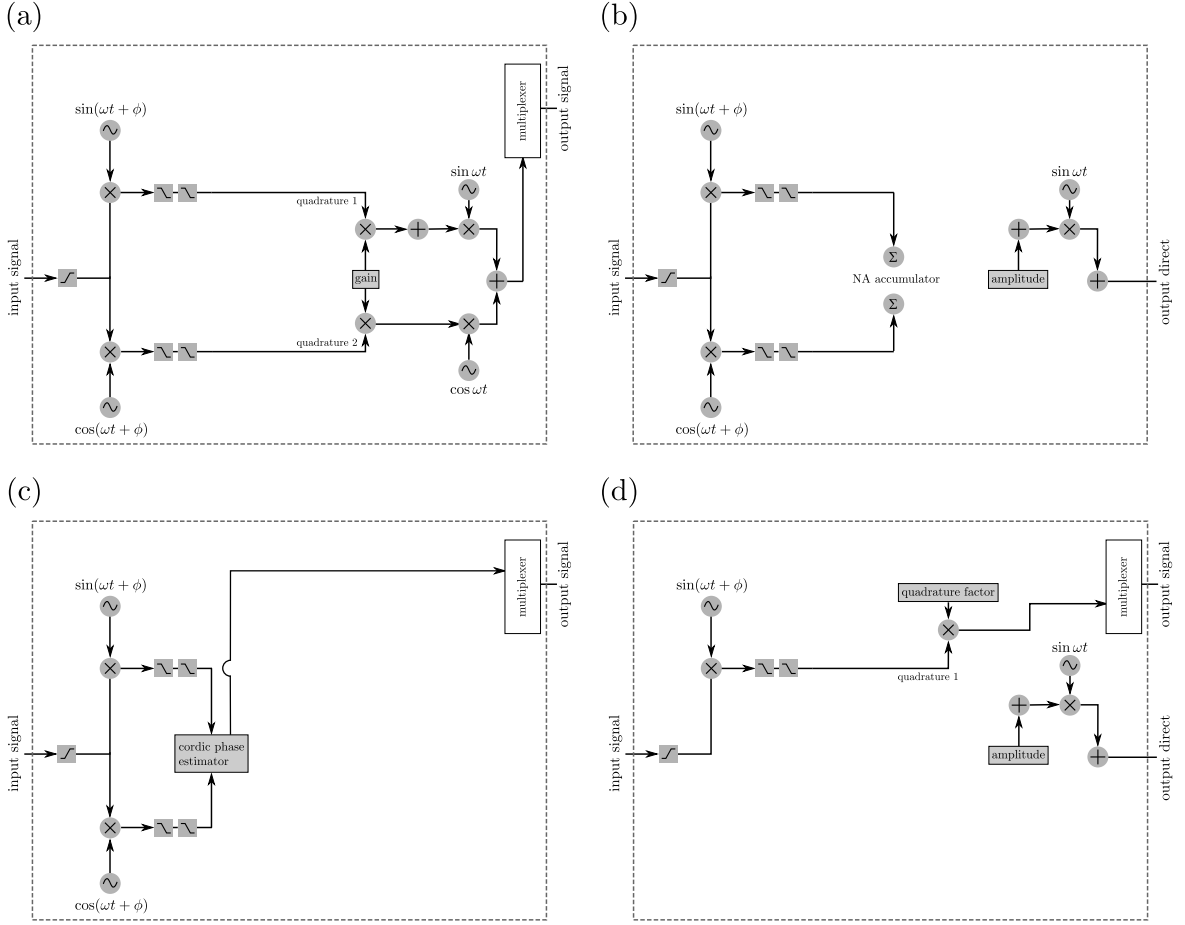


Fig. III.2 Basic operating modes of the IQ module in PyRPL, illustrating how different DSP functions can be implemented by appropriate choices of the module registers. (a) **Filter mode.** The input signal is demodulated using the internal $\cos(\omega t + \phi)$ and $\sin(\omega t + \phi)$ local oscillators, low-pass filtered, and subsequently remodulated. With amplitude set to zero and a finite gain and quadrature factor, the module acts as a tunable narrowband filter centered at the LO frequency. (b) **Network mode** zero value and routing the signal through output direct. The response of the device under test is demodulated and phase and quadrature components while sweeping the frequency register. (c) **Offset-frequency locking / timephase or frequency error mode** suitable for digital phase loop operation. (d) **PDH error-signal / dither-locking mode.** A small modulation tone is generated via a zero amplitude value and applied to the actuator using output direct. The incoming signal is demodulated at the pass filtered, and one of the demodulated quadratures is routed as the PDH error signal by selecting output s_1 quadrature. Together, these configurations highlight the versatility of the IQ module in implementing filter

III.2.2 Optical paths Locks - Dither Locks

Controlling the relative path length between two arms of an interferometer is a fundamental technique in quantum optics. The basic idea is to use the interference of light from two paths to lock the phase difference between them. Although not being the same experiential setups, Michelson interferometers, Mach-Zhender interferometers, and Local Oscillator stabilization error signals fall in the same category as they are derived from the same principle. Namely, the error signal is proportional to the sine of the phase difference between the two arms:

$$\epsilon(\Delta\phi) \propto \sin(\Delta\phi) \simeq \Delta\phi \quad (\text{III.9})$$

where $\Delta\phi = \phi_a - \phi_b$ is the phase difference between the two optical paths. Analogically, we would need to add an adjustable voltage offset, as to be able to tune the error signal to zero at the desired phase difference, before seeding this error signal to the PI block. Digitally, this is performed by adding a constant offset to the error signal, which can be adjusted to set the desired phase difference.

In practice, this is implemented by mounting a mirror on which one of the arms is reflected, and then using a piezoelectric transducer to control the position of the mirror, hence modulating the relative phase between the two optical paths. The piezo is then feedback controlled through a PI loop, which adjusts the voltage applied to the piezo to set the error signal to 0. FIGURE

III.2.3 Side of Fringe Locks

$$\epsilon(\Delta\omega) \propto \Delta\omega \quad (\text{III.10})$$

III.2.4 Pound-Drever-Hall Locks

Another key technique extensively used in this work is the *Pound-Drever-Hall* (PDH) method, a high-sensitivity scheme for stabilizing either the cavity length to a fluctuating laser frequency, or vice versa. The method relies on imposing phase modulation sidebands on the laser field, typically using an electro-optic modulator (EOM), and using these sidebands as phase-stable references. Because they lie far outside the cavity linewidth ($\Omega_{\text{mod}} \gg \kappa$), the sidebands are reflected nearly unchanged: $r(\omega_\ell \pm \Omega_{\text{mod}}) \approx 1$. In contrast, the carrier field near resonance acquires a frequency-dependent phase shift upon reflection, captured by the complex cavity reflection coefficient $r_c(\delta)$. The PDH error signal is obtained by detecting the reflected beam and demodulating the photocurrent at the modulation frequency, isolating the beat terms between carrier and sidebands. The resulting signal is proportional to the *imaginary part* of $r_c(\delta)$, which varies antisymmetrically with detuning and provides a

zero-crossing error signal ideal for linear feedback. The error signal near resonance is then given by

$$\epsilon(\Delta\omega) \propto \text{Im}\left(r_c(\Delta\omega)\right) \simeq \Delta\omega \quad (\text{III.11})$$

This imaginary component encodes the rapid phase dispersion near resonance that allows the system to discriminate the sign and magnitude of frequency deviations. In contrast, the real part of $r_c(\delta)$, being symmetric around resonance, does not yield a usable error signal.

The *demodulation phase* plays a critical role in selecting the appropriate quadrature of the signal for feedback. Since the beat signal between the carrier and sidebands has both in-phase (cosine) and quadrature (sine) components, choosing the correct demodulation phase ensures that the extracted error signal aligns with the imaginary part of the reflection coefficient. A misaligned demodulation phase can lead to mixing of the symmetric (real) part into the error signal, thereby reducing sensitivity and introducing offset or distortion near the lock point. In practice, the demodulation phase is optimized empirically—either via a variable phase shifter in the electronic demodulation path or by adjusting the physical delay in the reference oscillator—to maximize the slope of the error signal at zero-crossing, corresponding to pure detection of the dispersive component.

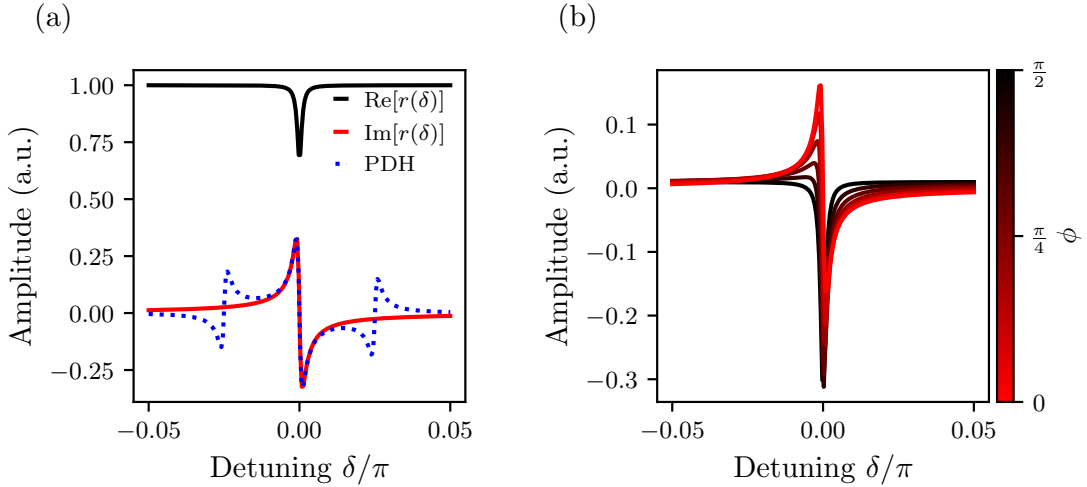


Fig. III.3 Schematic of the Pound-Drever-Hall (PDH) locking technique. The laser passes through an electro-optic modulator (EOM) generating phase modulation sidebands. The modulated beam is incident on the optical cavity, and the reflected light is detected by a photodiode (PD). The photocurrent is demodulated at the modulation frequency to produce the PDH error signal, which is fed to a PI controller driving the cavity actuator (e.g., piezo). Key components are labeled: EOM (electro-optic modulator), PD (photodiode), LO (local oscillator for demodulation), and PI (proportional-integral controller).

III.2.5 Offset frequency Locks

$$\epsilon(\Delta\omega_{\text{beat}}) \propto \Delta\omega_{\text{beat}} \quad (\text{III.12})$$

Appendix A: Two-photon derivations

Field Quantization

From discrete to continuous modes

We consider the quantised electromagnetic field in a volume V along a single polarization direction. We assume the field to be a gaussian beam such that the quantization volume is written as $\mathcal{V} = \mathcal{A}L$, with \mathcal{A} the effective mode cross-sectional area, normal to the propagation direction z . The electric field operator can be written as

$$\hat{\mathbf{E}}(\mathbf{r}, t) = i \sum_{\ell} \sqrt{\frac{\hbar\omega_{\ell}}{2\varepsilon_0\mathcal{V}}} \left[\hat{a}_{\omega_{\ell}} \mathbf{f}_{\ell}(\mathbf{r}) e^{-i\omega_{\ell}t} - \hat{a}_{\omega_{\ell}}^{\dagger} \mathbf{f}_{\ell}^*(\mathbf{r}) e^{+i\omega_{\ell}t} \right], \quad (\text{III.13})$$

The index ℓ then labels the different modes, discrete at this point. The bosonic operators satisfy the canonical commutation relations

$$[\hat{a}_{\omega_{\ell}}, \hat{a}_{\omega_{\ell'}}^{\dagger}] = \delta_{\ell\ell'}, \quad [\hat{a}_{\omega_{\ell}}, \hat{a}_{\omega_{\ell'}}] = [\hat{a}_{\omega_{\ell}}^{\dagger}, \hat{a}_{\omega_{\ell'}}^{\dagger}] = 0.$$

We consider a the polarization along the $\hat{\mathbf{x}}$ direction where the hat denotes the unit vector and not an operator. The mode function can then be written as $\mathbf{f}_{\ell}(\mathbf{r}) = f_{\ell}(\mathbf{r})\hat{\mathbf{x}}$. We consider 1D wavevectors along the $+z$ direction i.e. positive k_{ℓ} only, such that in the limit of quantization volumes tending to infinity i.e. $L \rightarrow \infty$, the discrete sum over k modes turns into an integral over frequencies

$$\sum_{\ell}(\dots) \rightarrow \frac{L}{2\pi} \int_0^{\infty} dk(\dots) = \frac{1}{\Delta f} \int_0^{\infty} \frac{d\omega}{2\pi}(\dots) \quad \text{with} \quad \Delta f = \frac{c}{L}$$

using the dispersion relation $\omega = c|k|$. We then simply relabel $\hat{a}_{\omega_\ell} \rightarrow \hat{a}_\omega$, $f_\ell(\mathbf{r}) \rightarrow f(\mathbf{r}, \omega)$ and plug back into the original expression to have

$$\hat{\mathbf{E}}(\mathbf{r}, t) = i \int_0^\infty \frac{d\omega}{2\pi} \sqrt{\frac{\hbar\omega}{2\varepsilon_0\mathcal{A}c}} \left[\lim_{L \rightarrow \infty} \frac{\hat{a}[\Omega]}{\sqrt{\Delta f}} f(\mathbf{r}, \omega) e^{-i\omega t} - \lim_{L \rightarrow \infty} \frac{\hat{a}^\dagger[\Omega]}{\sqrt{\Delta f}} f^*(\mathbf{r}, \omega) e^{+i\omega t} \right] \hat{\mathbf{x}},$$

and we can define the continuous bosonic operators as

$$\hat{a}[\omega] = \lim_{L \rightarrow \infty} \frac{\hat{a}_\omega}{\sqrt{\Delta f}} \quad \text{and} \quad \hat{a}^\dagger[\omega] = \lim_{L \rightarrow \infty} \frac{\hat{a}_\omega^\dagger}{\sqrt{\Delta f}}$$

such that the electric field operator reads

$$\hat{\mathbf{E}}(\mathbf{r}, t) = i \int_0^\infty \frac{d\omega}{2\pi} \mathcal{E} \left[\hat{a}[\omega] f(\mathbf{r}, \omega) e^{-i\omega t} - \hat{a}^\dagger[\omega] f^*(\mathbf{r}, \omega) e^{+i\omega t} \right] \hat{\mathbf{x}}, \quad \text{with} \quad \mathcal{E} = \sqrt{\frac{\hbar\omega}{2\varepsilon_0\mathcal{A}c}}.$$

Commutation relations

Using standard complex analysis techniques, the kronecker delta can be expressed as

$$\delta_{\ell\ell'} = \int_{-\pi}^{+\pi} dt \frac{e^{i(\ell-\ell')t}}{2\pi}.$$

Upon the aforementioned assumptions, we can introduce the frequency spacing $\Delta\omega = 2\pi\Delta f$ such that the discrete angular frequencies are written as $\omega_\ell = \ell\Delta\omega$. It then follows that $\ell - \ell' = (\omega_\ell - \omega_{\ell'})/\Delta\omega$. By changing the variable of integration from t to $t' = t/\Delta\omega$, we can rewrite the kronecker delta as

$$\delta_{\ell\ell'} = \int_{-L/2c}^{+L/2c} dt' \Delta f e^{i(\omega_\ell - \omega_{\ell'})t'}.$$

We can then see that in the limit of $L \rightarrow \infty$ i.e. $\Delta\omega \rightarrow 0$, the integral limits tend to infinity and the kronecker delta turns into a dirac delta such that

$$\lim_{L \rightarrow \infty} \frac{\delta_{\ell\ell'}}{\Delta f} = \int_{-\infty}^{+\infty} dt' e^{i(\omega - \omega')t'} = 2\pi\delta(\omega - \omega').$$

where we relabeled $\omega_\ell \rightarrow \omega$ and $\omega_{\ell'} \rightarrow \omega'$. The commutation relations for the continuous bosonic operators then read which satisfy the commutation relations

$$[\hat{a}[\omega], \hat{a}^\dagger[\omega']] = \lim_{L \rightarrow \infty} \frac{[\hat{a}_{\omega_\ell}, \hat{a}_{\omega_{\ell'}}^\dagger]}{\Delta f} = 2\pi\delta(\omega - \omega'), \quad [\hat{a}[\omega], \hat{a}[\omega']] = [\hat{a}^\dagger[\omega], \hat{a}^\dagger[\omega']] = 0.$$

Two photon formalism

Quadratures

We will now consider mode field frequencies $\omega = \omega_0 + \Omega$ around a carrier frequency ω_0 , such that the integral term becomes

$$\int_0^\infty \frac{d\omega}{2\pi}(\dots) \rightarrow \int_{-\omega_0}^\infty \frac{d\Omega}{2\pi}(\dots) \sim \int_{-B}^B \frac{d\Omega}{2\pi}(\dots) \sim \int_{-\infty}^\infty \frac{d\Omega}{2\pi}(\dots)$$

where B is the detection bandwidth, which is always much smaller than the optical frequency ω_0 . We can then safely extend the integral limits to infinity. Assuming that the mode function $f(\mathbf{r}, \omega)$ does not vary significantly over the bandwidth B , we can approximate it by its value at the carrier frequency $f(\mathbf{r}, \omega_0) \equiv f(\mathbf{r})$. Pulling out this term from the integral, one can then project the electric field operator onto both the proper polarization axis and this mode function such that the electric field operator becomes spatially independent and reads

$$\hat{E}(t) = i\mathcal{E}_0 \int_0^\infty \frac{d\Omega}{2\pi} \left[\hat{a}_+ e^{-i(\omega_0+\Omega)t} - \hat{a}_+^\dagger e^{+i(\omega_0+\Omega)t} + \hat{a}_- e^{-i(\omega_0-\Omega)t} - \hat{a}_-^\dagger e^{+i(\omega_0-\Omega)t} \right] \quad (\text{III.14})$$

with $\mathcal{E}_0 = \sqrt{\hbar\omega/2\varepsilon_0\mathcal{A}c}$, and where we additionally split the integral term in two, introducing negative and positive sideband frequencies whose annihilation and creation operators are written as

$$\hat{a}_\pm \equiv c_\pm \hat{a}[\omega_0 \pm \Omega] \quad \text{and} \quad \hat{a}_\pm^\dagger \equiv c_\pm \hat{a}^\dagger[\omega_0 \pm \Omega] \quad \text{with} \quad c_\pm = \sqrt{\frac{\omega_0 \pm \Omega}{\omega_0}}.$$

The commutators then read

$$[\hat{a}_\pm, \hat{a}_\pm^\dagger] = 2\pi c_\pm^2 \delta(\Omega - \Omega'), \quad [\hat{a}_\pm, \hat{a}_\mp] = [\hat{a}_\pm^\dagger, \hat{a}_\mp^\dagger] = 0$$

$$[\hat{a}_\pm, \hat{a}_\mp^\dagger] = 2\pi c_+ c_- \delta(\Omega + \Omega'), \quad [\hat{a}_\pm, \hat{a}_\mp] = [\hat{a}_\pm^\dagger, \hat{a}_\mp^\dagger] = 0$$

Computing expectation values for these operators in vacuum yields $\langle \hat{a}_\pm \rangle = \langle \hat{a}_\pm^\dagger \rangle = \langle 0 | \hat{a}_\pm^\dagger \hat{a}_\pm | 0 \rangle = 0$ and $\langle 0 | \hat{a}_\pm \hat{a}_\pm^\dagger | 0 \rangle = 2\pi c_\pm^2 \delta(0)$, which is consistent with the fact that no photons are present in these modes. We then regroup the terms along common quadratures $\cos \omega_0 t$ and $\sin \omega_0 t$ such that we get

$$\begin{aligned} \hat{E}(t) = i\mathcal{E}_0 & \left[\cos \omega_0 t \int_0^\infty \frac{d\Omega}{2\pi} \left[(\hat{a}_+ - \hat{a}_-^\dagger) e^{-i\Omega t} + (\hat{a}_- - \hat{a}_+^\dagger) e^{+i\Omega t} \right] \right. \\ & \left. - i \sin \omega_0 t \int_0^\infty \frac{d\Omega}{2\pi} \left[(\hat{a}_+ + \hat{a}_-^\dagger) e^{-i\Omega t} + (\hat{a}_- + \hat{a}_+^\dagger) e^{+i\Omega t} \right] \right] \end{aligned}$$

We now define the two-photon quadrature operators as

$$\hat{p}[\Omega] = \hat{a}_+ + \hat{a}_-^\dagger, \quad \hat{q}[\Omega] = i(\hat{a}_-^\dagger - \hat{a}_+)$$

such that the electric field operator reads

$$\begin{aligned} \hat{E}(t) = \mathcal{E}_0 & \left[\cos\left(\omega_0 t - \frac{\pi}{2}\right) \int_0^\infty \frac{d\Omega}{2\pi} [\hat{p}[\Omega] e^{-i\Omega t} + \hat{p}^\dagger[\Omega] e^{+i\Omega t}] \right. \\ & \left. + \sin\left(\omega_0 t - \frac{\pi}{2}\right) \int_0^\infty \frac{d\Omega}{2\pi} [\hat{q}[\Omega] e^{-i\Omega t} + \hat{q}^\dagger[\Omega] e^{+i\Omega t}] \right] \end{aligned} \quad (\text{III.15})$$

where we used the fact that $\hat{p}^\dagger[\Omega] = \hat{p}[-\Omega]$ and $\hat{q}^\dagger[\Omega] = \hat{q}[-\Omega]$. The $\pi/2$ phase shifts originate from the leading factor i in the electric-field operator. Had the field operator been written without that prefactor (and without the minus sign in the creation-term), the resulting cosine and sine components would contain no such phase offset. The commutation relations for these quadrature operators read

$$\begin{aligned} [\hat{p}[\Omega], \hat{q}^\dagger[\Omega']] &= [\hat{q}[\Omega], \hat{p}^\dagger[\Omega']] = 4\pi i \delta(\Omega - \Omega') \\ [\hat{p}[\Omega], \hat{p}^\dagger[\Omega']] &= [\hat{q}[\Omega], \hat{q}^\dagger[\Omega']] = 4\pi \frac{\Omega}{\omega_0} \delta(\Omega - \Omega') \sim 0 \quad \text{if } \Omega \ll \omega_0 \\ [\hat{p}[\Omega], \hat{q}[\Omega']] &= [\hat{p}^\dagger[\Omega], \hat{q}^\dagger[\Omega']] = 0. \end{aligned}$$

In the limit where the sideband frequencies are small compared to the carrier frequency i.e. $\Omega \ll \omega_0$, we can approximate these prefactors by $c_\pm \sim 1$.

Expectations values in vacuum

We now proceed to evaluate the first and second momenta of our field operators in the vacuum state $|0\rangle$. As expected, the annihilation and creation operators have zero mean in vacuum, such that

$$\langle 0 | \hat{a}_+ | 0 \rangle = \langle 0 | \hat{a}_-^\dagger | 0 \rangle = 0$$

so it follows that

$$\langle 0 | \hat{p}[\Omega] | 0 \rangle = \langle 0 | \hat{q}[\Omega] | 0 \rangle = 0.$$

Building the two-photon quadrature column vector as

$$\hat{\mathbf{u}}[\Omega] = \begin{pmatrix} \hat{p}[\Omega] \\ \hat{q}[\Omega] \end{pmatrix}, \quad \text{we have} \quad \langle \hat{\mathbf{u}}[\Omega] \rangle = \begin{pmatrix} 0 \\ 0 \end{pmatrix}$$

where we see that, for a vacuum state, the full operator $\hat{\mathbf{u}}[\Omega]$ actually equates the fluctuating part $\delta\hat{\mathbf{u}}[\Omega] = \hat{\mathbf{u}}[\Omega] - \langle \hat{\mathbf{u}}[\Omega] \rangle$ since the mean value is zero. In the following, we will assume

that expectation values are always computed in the vacuum state unless otherwise specified (we will omit the $|0\rangle$ notation for clarity). We only wrote the results for the \hat{a}_+ and \hat{a}_-^\dagger operators as there are the ones composing the \hat{p} and \hat{q} quadratures, but the same results hold for the other sideband operators as well. We can then compute the second momenta of the annihilation and creation operators, yielding

$$\langle 0 | \hat{a}_-^\dagger \hat{a}_- | 0 \rangle = \langle 0 | \hat{a}_+ \hat{a}_- | 0 \rangle = \langle 0 | \hat{a}_-^\dagger \hat{a}_+^\dagger | 0 \rangle = 0$$

$$\langle 0 | \hat{a}_\pm \hat{a}_\pm^\dagger | 0 \rangle = 2\pi\delta(\Omega - \Omega') .$$

Using these relations, we can compute the second momenta for the two-photon quadrature operators as

$$\begin{aligned} \langle 0 | \hat{p}[\Omega] \hat{p}^\dagger[\Omega'] | 0 \rangle &= \langle 0 | \hat{a}_+ \hat{a}_+^\dagger + \hat{a}_+ \hat{a}_- + \hat{a}_-^\dagger \hat{a}_+^\dagger + \hat{a}_-^\dagger \hat{a}_- | 0 \rangle \\ &= 2\pi\delta(\Omega - \Omega') , \\ \langle 0 | \hat{q}[\Omega] \hat{q}^\dagger[\Omega'] | 0 \rangle &= 2\pi\delta(\Omega - \Omega') . \end{aligned}$$

as well as

$$\langle 0 | \hat{p}[\Omega] \hat{q}^\dagger[\Omega'] | 0 \rangle = -\langle 0 | \hat{q}^\dagger[\Omega] \hat{p}[\Omega'] | 0 \rangle = i2\pi\delta(\Omega - \Omega') .$$

Using the expression for the symmetrized double sided covariance matrix given in the main text, we can compute the covariance matrix for the two-photon quadrature operators in vacuum as

$$\begin{aligned} \mathbf{S}[\Omega] &= \frac{1}{2} \int \frac{\delta\Omega'}{2\pi} \langle \{ \delta\hat{\mathbf{u}}[\Omega], \delta\hat{\mathbf{u}}^\dagger[\Omega'] \} \rangle \\ &= \frac{1}{2} \int \frac{\delta\Omega'}{2\pi} \begin{pmatrix} \langle \{\hat{p}[\Omega], \hat{p}^\dagger[\Omega']\} \rangle & \langle \{\hat{p}[\Omega], \hat{q}^\dagger[\Omega']\} \rangle \\ \langle \{\hat{q}[\Omega], \hat{p}^\dagger[\Omega']\} \rangle & \langle \{\hat{q}[\Omega], \hat{q}^\dagger[\Omega']\} \rangle \end{pmatrix} \\ &= \frac{1}{2} \int \frac{\delta\Omega'}{2\pi} \begin{pmatrix} 2 \cdot 2\pi\delta(\Omega - \Omega') & 0 \\ 0 & 2 \cdot 2\pi\delta(\Omega - \Omega') \end{pmatrix} \\ &= \begin{pmatrix} 1 & 0 \\ 0 & 1 \end{pmatrix} = \mathbf{1} . \end{aligned}$$

The vacuum state then features vacuum fluctuations of unity in both quadratures, across all sideband frequencies Ω , and no correlations between the quadratures.

States and Operators in the Two-Photon Formalism

In a similar fashion as in the single-mode case, we can define the displacement operator as

$$\hat{D}(\alpha) = \exp \left(\int_{-\infty}^{\infty} \frac{d\Omega}{2\pi} [\alpha(\Omega) \hat{a}_-^\dagger - \alpha^*(\Omega) \hat{a}_+] \right)$$

as well as a squeezing operator

$$\hat{S}(r, \theta) = \exp \left(r \int_{-\infty}^{\infty} \frac{d\Omega}{2\pi} [e^{-i2\theta(\Omega)} \hat{a}_+ \hat{a}_- - e^{i2\theta(\Omega)} \hat{a}_+^\dagger \hat{a}_-^\dagger] \right)$$

where r is the squeezing factor and $\theta(\Omega)$ the squeezing angle. Here we assumed the squeezing parameter to be frequency independent, but one can easily generalize to a frequency dependent squeezing parameter $r(\Omega)$. Using the sidebands annihilation operators defined previously, we can compute the action of the displacement and squeezing operators on the annihilation operator as

$$\begin{aligned} \hat{D}^\dagger(\alpha) \hat{a}_+ \hat{D}(\alpha) &= \hat{a}_+ + \alpha(\Omega), \\ \hat{S}^\dagger(r, \theta) \hat{a}_+ \hat{S}(r, \theta) &= \hat{a}_+ \cosh r - e^{i2\theta(\Omega)} \hat{a}_-^\dagger \sinh r. \end{aligned}$$

We consider a initial vacuum state $|0\rangle$, and we displace it by a coherent amplitude $\alpha(\Omega) = \alpha\delta(\Omega)$ i.e. a carrier, monochromatic field of complex amplitude α sitting at frequency 0 (we are in the frame rotating at ω_0 already since we factored out the $e^{-i\omega_0 t}$ term). The displacement operator then acts on the two photon quadrature operators as

$$\begin{aligned} \hat{D}^\dagger(\alpha) \hat{p}[\Omega] \hat{D}(\alpha) &= \hat{p}[\Omega] + 2 \operatorname{Re}\{\alpha\} \delta(\Omega), \\ \hat{D}^\dagger(\alpha) \hat{q}[\Omega] \hat{D}(\alpha) &= \hat{q}[\Omega] + 2 \operatorname{Im}\{\alpha\} \delta(\Omega). \end{aligned}$$

or in matrix form

$$\hat{D}^\dagger(\alpha) \hat{\mathbf{u}}[\Omega] \hat{D}(\alpha) = \hat{\mathbf{u}}[\Omega] + 2 \begin{pmatrix} \operatorname{Re}\{\alpha\} \\ \operatorname{Im}\{\alpha\} \end{pmatrix} \delta(\Omega).$$

In a similar fashion, the squeezing operator acts as

$$\begin{aligned} \hat{S}^\dagger(r, \theta) \hat{p}[\Omega] \hat{S}(r, \theta) &= \hat{p}[\Omega] (\cosh r - \sinh r \cos 2\theta) - \hat{q}[\Omega] \sin 2\theta \sinh r, \\ \hat{S}^\dagger(r, \theta) \hat{q}[\Omega] \hat{S}(r, \theta) &= \hat{q}[\Omega] (\cosh r + \sinh r \cos 2\theta) - \hat{p}[\Omega] \sin 2\theta \sinh r. \end{aligned}$$

and its matrix form reads

$$\hat{S}^\dagger(r, \theta) \hat{\mathbf{u}}[\Omega] \hat{S}(r, \theta) = \mathbf{S}(r, \theta) \hat{\mathbf{u}}[\Omega], \quad \text{with} \quad \mathbf{S}(r, \theta) = \begin{pmatrix} \cosh r - \sinh r \cos 2\theta & -\sin 2\theta \sinh r \\ -\sin 2\theta \sinh r & \cosh r + \sinh r \cos 2\theta \end{pmatrix}.$$

The state resulting from applying both operators onto the vacuum is written as

$$|\psi\rangle = \hat{S}(r, \theta) \hat{D}(\alpha) |0\rangle$$

and describes a squeezed coherent state, or bright squeezed state. One can then set the coherent amplitude to 0 as to get a vacuum squeezed state, or set the squeezing parameter to 0 to get a coherent state. This is one of the most generic gaussian state one can define in quantum optics. We write the operator product as $\hat{D}\hat{S}$ and we drop the Ω dependencies to lighten the notation, such that applying them to the field operators yields

$$\begin{aligned} \hat{D}^\dagger \hat{S}^\dagger \hat{a}_+ \hat{S} \hat{D} &= \hat{a}_+ \cosh r - e^{i2\theta} \hat{a}_-^\dagger \sinh r + \gamma \delta(\Omega) \\ \hat{D}^\dagger \hat{S}^\dagger \hat{a}_-^\dagger \hat{S} \hat{D} &= \hat{a}_-^\dagger \cosh r - e^{-i2\theta} \hat{a}_+ \sinh r + \gamma^* \delta(\Omega). \end{aligned}$$

as well as the quadratures

$$\begin{aligned} \hat{D}^\dagger \hat{S}^\dagger \hat{p} \hat{S} \hat{D} &= \hat{p}(\cosh r - \cos 2\theta \sinh r) - \hat{q} \sin 2\theta \sinh r + 2 \operatorname{Re}\{\gamma\} \delta(\Omega), \\ \hat{D}^\dagger \hat{S}^\dagger \hat{q} \hat{S} \hat{D} &= \hat{q}(\cosh r + \cos 2\theta \sinh r) - \hat{p} \sin 2\theta \sinh r + 2 \operatorname{Im}\{\gamma\} \delta(\Omega). \end{aligned}$$

where we introduced the scalar part of these transformed operators as

$$\begin{aligned} \gamma &= \alpha \cosh r - \alpha^* e^{i2\theta} \sinh r, \\ \gamma^* &= \alpha^* \cosh r - \alpha e^{-i2\theta} \sinh r. \end{aligned}$$

The matrix form then reads

$$\hat{D}^\dagger \hat{S}^\dagger \hat{\mathbf{u}} \hat{S} \hat{D} = \mathbf{S}(r, \theta) \hat{\mathbf{u}} + 2 \begin{pmatrix} \operatorname{Re}\{\gamma\} \\ \operatorname{Im}\{\gamma\} \end{pmatrix} \delta(\Omega).$$

The mean values is then straightforward to compute

$$\begin{aligned} \langle \hat{D}^\dagger \hat{S}^\dagger \hat{\mathbf{u}} \hat{S} \hat{D} \rangle &= \mathbf{S}(r, \theta) \langle \hat{\mathbf{u}} \rangle + 2 \begin{pmatrix} \operatorname{Re}\{\gamma\} \\ \operatorname{Im}\{\gamma\} \end{pmatrix} \delta(\Omega) \\ &= 2 \begin{pmatrix} \operatorname{Re}\{\gamma\} \\ \operatorname{Im}\{\gamma\} \end{pmatrix} \delta(\Omega). \end{aligned}$$

such that the fluctuating part reads

$$\delta \hat{\mathbf{u}} = \hat{D}^\dagger \hat{S}^\dagger \hat{\mathbf{u}} \hat{S} \hat{D} - \langle \hat{D}^\dagger \hat{S}^\dagger \hat{\mathbf{u}} \hat{S} \hat{D} \rangle = \mathbf{S}(r, \theta) \hat{\mathbf{u}} \quad \text{and} \quad \delta \hat{\mathbf{u}}^\dagger = \hat{\mathbf{u}}^\dagger \mathbf{S}(r, \theta).$$

where we used the fact that the squeezing matrix is symmetric, i.e. $\mathbf{S} = \mathbf{S}^T$. The covariance matrix for this squeezed coherent state then reads

$$\begin{aligned} \mathbf{S}[\Omega] &= \frac{1}{2} \int \frac{\delta\Omega'}{2\pi} \langle \{\delta \hat{\mathbf{u}}[\Omega], \delta \hat{\mathbf{u}}^\dagger[\Omega']\} \rangle \\ &= \frac{1}{2} \int \frac{\delta\Omega'}{2\pi} \langle \{\mathbf{S}(r, \theta) \hat{\mathbf{u}}[\Omega], \hat{\mathbf{u}}^\dagger[\Omega'] \mathbf{S}(r, \theta)\} \rangle \\ &= \mathbf{S}(r, \theta) \left(\frac{1}{2} \int \frac{\delta\Omega'}{2\pi} \langle \{\hat{\mathbf{u}}[\Omega], \hat{\mathbf{u}}^\dagger[\Omega']\} \rangle \right) \mathbf{S}(r, \theta) \\ &= \mathbf{S}(r, \theta) \cdot \mathbf{1} \cdot \mathbf{S}(r, \theta) = \mathbf{S}(r, \theta)^2 \\ &= \begin{pmatrix} \cosh 2r - \sinh 2r \cos 2\theta & -\sin 2\theta \sinh 2r \\ -\sin 2\theta \sinh 2r & \cosh 2r + \sinh 2r \cos 2\theta \end{pmatrix}. \end{aligned}$$

such that the expectation values are computed as

$$\begin{aligned} \langle \hat{a}_+ \rangle &= \gamma \delta(\Omega) \\ \langle \hat{a}_-^\dagger \rangle &= \gamma^* \delta(\Omega) \\ \langle \hat{p} \rangle &= 2 \operatorname{Re}\{\gamma\} \delta(\Omega) \\ \langle \hat{q} \rangle &= 2 \operatorname{Im}\{\gamma\} \delta(\Omega). \end{aligned}$$

and we compute the expectation value of our two-photon annihilation operator as

$$\langle \hat{a}_+ \rangle = \alpha \delta(\Omega) \quad \text{and} \quad \langle \hat{a}_-^\dagger \rangle = \alpha^* \delta(\Omega)$$

as well as their second momenta as

The electric field operator finally reads

$$\hat{\mathbf{E}}(\mathbf{r}, t) = i \sqrt{\frac{\hbar\omega_0}{\varepsilon_0 \mathcal{A}c}} \left[\int_{-\infty}^{\infty} \frac{d\Omega}{2\pi} \left[\hat{a}_\Omega e^{-i(\omega_0 + \Omega)t} - \hat{a}_\Omega^\dagger e^{+i(\omega_0 + \Omega)t} \right] \right] \quad (\text{III.16})$$

such that the classical part of the electric field reads

We start from the standard single-mode field quantization in terms of annihilation and

creation operators \hat{a} and \hat{a}^\dagger :

$$\hat{E}(t) = \sqrt{\frac{\hbar\omega_0}{2\varepsilon_0}} (\hat{a}e^{-i\omega_0 t} + \hat{a}^\dagger e^{i\omega_0 t}).$$

and we now make our bosonic operators time-dependent, $\hat{a} \rightarrow \hat{a}(t)$, to account for sidebands around the carrier frequency ω_0 . Using the Fourier transform convention

$$\hat{a}(t) = \int_{-\infty}^{+\infty} \frac{d\Omega}{2\pi} \hat{a}[\Omega] e^{-i\Omega t},$$

we rewrite the field operator as

$$\hat{E}(t) = \sqrt{\frac{\hbar\omega_0}{2\varepsilon_0}} \int_{-\infty}^{+\infty} \frac{d\Omega}{2\pi} (\hat{a}[\Omega] e^{-i(\omega_0+\Omega)t} + \hat{a}^\dagger[\Omega] e^{i(\omega_0+\Omega)t}).$$

$$\hat{p}[\Omega] = 2|\alpha|(\delta[\Omega] + \text{Re}\{\varepsilon[\Omega]\}) + \delta\hat{p}[\Omega], \quad (\text{III.17})$$

$$\hat{p}[\Omega] \hat{p}[\Omega'] = 4|\alpha|^2 (\delta[\Omega]S[\Omega'] + \delta[\Omega]\text{Re}\{\varepsilon[\Omega']\} + \delta[\Omega']\text{Re}\{\varepsilon[\Omega]\} + \text{Re}\{\varepsilon[\Omega]\}\text{Re}\{\varepsilon[\Omega']\}) + \delta\hat{p}[\Omega] \delta\hat{p}[\Omega'], \quad (\text{III.18})$$

$$\langle \dots \rangle = 4|\alpha|^2 (\delta(\Omega)\delta(\Omega') + \frac{\varepsilon}{2}\delta(\Omega)\delta(\Omega' - \Omega_m) + \frac{\varepsilon}{2}\delta(\Omega)\delta(\Omega' + \Omega_m)) \quad (\text{III.19})$$

$$+ \frac{\varepsilon}{2}\delta(\Omega')\delta(\Omega - \Omega_m) + \frac{\varepsilon}{2}\delta(\Omega')\delta(\Omega + \Omega_m) \quad (\text{III.20})$$

$$+ \frac{\varepsilon^2}{4} [\delta(\Omega - \Omega_m)\delta(\Omega' + \Omega_m) + \delta(\Omega - \Omega_m)\delta(\Omega' - \Omega_m) \quad (\text{III.21})$$

$$+ \delta(\Omega + \Omega_m)\delta(\Omega' + \Omega_m) + \delta(\Omega + \Omega_m)\delta(\Omega' - \Omega_m)] \big) + \langle \delta p[\Omega] \delta p[\Omega'] \rangle. \quad (\text{III.22})$$

Derivation of the optimal angle

Optimal fixed homodyne angle with complex \mathcal{K}

Assume the measured (reflected) quadrature is

$$\delta q_r = \delta q_{\text{in}} + \mathcal{K} \delta p_{\text{in}},$$

so that, for any input covariance matrix S^{in} ,

$$S_{qq}^r = S_{qq}^{\text{in}} + |\mathcal{K}|^2 S_{pp}^{\text{in}} + 2 \text{Re}\{\mathcal{K}\} S_{pq}^{\text{in}}.$$

For an input squeezed state of strength R and angle θ ,

$$S^{\text{in}}(r, \theta) = \begin{pmatrix} \cosh 2r + \sinh 2r \cos 2\theta & -\sinh 2r \sin 2\theta \\ -\sinh 2r \sin 2\theta & \cosh 2r - \sinh 2r \cos 2\theta \end{pmatrix}.$$

Hence

$$\begin{aligned} S_{qq}^r(\theta) &= \cosh 2r - \sinh 2r \cos 2\theta + |\mathcal{K}|^2(\cosh 2r + \sinh 2r \cos 2\theta) - 2 \operatorname{Re}\{\mathcal{K}\} \sinh 2r \sin 2\theta \\ &= (1 + |\mathcal{K}|^2) \cosh 2r - (1 - |\mathcal{K}|^2) \sinh 2r \cos 2\theta - 2 \operatorname{Re}\{\mathcal{K}\} \sinh 2r \sin 2\theta. \end{aligned} \quad (\text{III.23})$$

Optimal fixed angle. Differentiate (??) w.r.t. θ and set to zero:

$$\frac{\partial S_{qq}^r}{\partial \theta} = 2 \sinh 2r \left[(1 - |\mathcal{K}|^2) \sin 2\theta - 2 \operatorname{Re}\{\mathcal{K}\} \cos 2\theta \right] = 0,$$

which gives the optimal fixed readout angle

$$\tan(2\theta_{\text{opt}}) = \frac{2 \operatorname{Re}\{\mathcal{K}\}}{1 - |\mathcal{K}|^2} \quad (\text{III.24})$$

Writing $\mathcal{K} = |\mathcal{K}|e^{i\varphi_m}$ one may also use

$$\tan(2\theta_{\text{opt}}) = \frac{2|\mathcal{K}| \cos \varphi_m}{1 - |\mathcal{K}|^2}.$$

Minimum attained value. Plugging the optimal angle back into (??) then yields

$$S_{qq,\text{min}}^r = (1 + |\mathcal{K}|^2) \cosh 2r - \sqrt{(1 - |\mathcal{K}|^2)^2 + (2 \operatorname{Re}\{\mathcal{K}\})^2} \sinh 2r, \quad (\text{III.25})$$

Lower bound and the real- \mathcal{K} case. In the free mass limit, \mathcal{K} is purely real, so that $\varphi_m = 0$ and $\operatorname{Re}\{\mathcal{K}\} = |\mathcal{K}|$. In this case, the minimum variance (??) reduces to

$$S_{qq,\text{min}}^r = (1 + |\mathcal{K}|^2)e^{-2r}$$

Appendix B: Error Signals

In this appendix, we detail calculation details not mentionned in the main text regarding the detection of optical fields and error signals.

Direct detection error signals

We describe the completely generic photocurrent obtained from direct detection of two optical fields interfering on a photodetector. We consider two fields with field operators \hat{a} and \hat{a}' , with classical amplitudes $|\bar{\alpha}|$ and $|\bar{\alpha}'|e^{-i(\Delta\omega t+\phi)}$ as well as fluctuations $\delta\hat{a}$ and $\delta\hat{a}'e^{-i(\Delta\omega t+\phi)}$ i.e. $\bar{\alpha}$ is real. The photocurrent operator is then given by

$$\hat{I} = \left(|\bar{\alpha}| + \delta\hat{a}^\dagger + |\bar{\alpha}'|e^{i(\Delta\omega t+\phi)} + \delta\hat{a}'^\dagger e^{i(\Delta\omega t+\phi)} \right) \left(|\bar{\alpha}| + \delta\hat{a} + |\bar{\alpha}'|e^{-i(\Delta\omega t+\phi)} + \delta\hat{a}' e^{-i(\Delta\omega t+\phi)} \right)$$

We remind here the expression for the amplitude and phase quadratures for both fields

$$\delta\hat{p} = \delta\hat{a} + \delta\hat{a}^\dagger, \quad \delta\hat{q} = -i(\delta\hat{a} - \delta\hat{a}^\dagger),$$

and

$$\delta\hat{p}' = e^{-i(\Delta\omega t+\phi)}\delta\hat{a}' + e^{i(\Delta\omega t+\phi)}\delta\hat{a}'^\dagger, \quad \delta\hat{q}' = -i(e^{-i(\Delta\omega t+\phi)}\delta\hat{a}' - e^{i(\Delta\omega t+\phi)}\delta\hat{a}'^\dagger).$$

Expanding this expression and keeping only terms up to first order in the fluctuations, we find

$$\begin{aligned} \hat{I}(t) \approx & |\bar{\alpha}|^2 + |\bar{\alpha}'|^2 + 2|\bar{\alpha}||\bar{\alpha}'| \cos(\Delta\omega t + \phi) \\ & + |\bar{\alpha}|(\delta\hat{p} + \delta\hat{p}') \\ & + |\bar{\alpha}'| \cos(\Delta\omega t + \phi)(\delta\hat{p} + \delta\hat{p}') \\ & + |\bar{\alpha}'| \sin(\Delta\omega t + \phi)(\delta\hat{q} - \delta\hat{q}') \end{aligned}$$

The first line corresponds to the classical DC and beatnote terms, while the remaining lines correspond to the fluctuations. We will now explore the different detection regimes covered in the main text.

Single field detection

Let's first consider the single field case where we get rid of all terms related to \hat{a}' . The photocurrent operator then reduces to

$$\hat{I} \approx |\bar{\alpha}|^2 + |\bar{\alpha}|\delta\hat{p}.$$

The photocurrent fluctuations are then directly proportional to the amplitude quadrature fluctuations of the input field, scaled by the classical amplitude.

Two fields detection

Let's first consider two fields with the same frequency, i.e. $\Delta\omega = 0$. The photocurrent operator then reads

$$\begin{aligned}\hat{I} \approx & |\bar{\alpha}|^2 + |\bar{\alpha}'|^2 + 2|\bar{\alpha}||\bar{\alpha}'| \cos(\phi) \\ & + |\bar{\alpha}| (\delta\hat{p} + \delta\hat{p}') \\ & + |\bar{\alpha}'| \cos(\phi) (\delta\hat{p} + \delta\hat{p}') \\ & + |\bar{\alpha}'| \sin(\phi) (\delta\hat{q} - \delta\hat{q}')\end{aligned}$$

where the mean field is a simple interference between the two fields, while the fluctuations depend on both amplitude and phase quadratures of the two fields. By adjusting the relative phase ϕ , one can select which quadrature is measured. For example, setting $\phi = 0$ selects the amplitude quadratures, while setting $\phi = \pi/2$ selects the phase quadratures. The issue is that in this case, both fields contribute to the measured quadrature fluctuations, which is not desired when probing sub shotnoise fluctuations of a signal (the LO will add its own fluctuations).

Two fields detection with frequency offset

Now, we consider the case where the two fields have a frequency offset $\Delta\omega \neq 0$. The mean photocurrent then contains a beatnote at frequency $\Delta\omega$ and reads

$$\bar{I} = |\bar{\alpha}|^2 + |\bar{\alpha}'|^2 + 2|\bar{\alpha}||\bar{\alpha}'| \cos(\Delta\omega t + \phi).$$

such that demodulating the photocurrent at frequency $\Delta\omega' \sim \Delta\tilde{\omega}$ with phase $\tilde{\phi}$ and low-pass filtering yields

$$\bar{I}_{\text{demod}} \approx |\bar{\alpha}||\bar{\alpha}'| \cos((\Delta\omega - \Delta\tilde{\omega})t + \phi - \tilde{\phi}).$$

This very signal can then be used to lock the frequency of an auxiliary laser to the desired frequency offset $\Delta\tilde{\omega}$ from the main laser. However, this signal featuring many zero crossings, one needs to tune the auxiliary laser frequency close enough to the desired offset so that it

ensures the feedback loop locks to the correct zero crossing. This is generally done manually by scanning the auxiliary laser frequency until the right zero crossing is found, confirmed by monitoring the beatnote on a spectrum analyzer.

PDH error signal

the Pound-Drever-Hall (PDH) error signal starting from the real, quantum-normalized phase-modulated electric field expression. We aim to show how the demodulated signal is a linear combination of the real and imaginary parts of the cavity reflection coefficient, with the demodulation phase selecting the appropriate quadrature for locking.

Input Phase-Modulated Field

The electric field at the input of the cavity is assumed to be a coherent state that has been phase-modulated at frequency Ω , such that the classical (real) electric field takes the form:

$$E_{\text{cl}}^{(\text{PM})}(t) = i\sqrt{\frac{\hbar\omega_0}{2\varepsilon_0}} \alpha_0 \left[e^{-i\omega_0 t} - e^{i\omega_0 t} + \frac{i\epsilon_\phi}{2} (e^{-i(\omega_0-\Omega)t} + e^{i(\omega_0-\Omega)t}) + \frac{i\epsilon_\phi}{2} (e^{-i(\omega_0+\Omega)t} + e^{i(\omega_0+\Omega)t}) \right] \quad (\text{III.26})$$

where α_0 is the coherent amplitude of the carrier, $\epsilon_\phi \ll 1$ is a small modulation index (related to the phase modulation depth), and ω_0 is the optical carrier frequency. This field includes both the positive and negative frequency components, as expected for a physical (Hermitian) electric field operator.

Reflection from the Cavity

Each frequency component of the field is reflected with a complex frequency-dependent amplitude reflection coefficient $r(\omega)$, such that the reflected field is:

$$\begin{aligned} E_{\text{refl}}(t) = & i\sqrt{\frac{\hbar\omega_0}{2\varepsilon_0}} \alpha_0 \left[r(\omega_0)e^{-i\omega_0 t} - r^*(\omega_0)e^{i\omega_0 t} \right. \\ & + \frac{i\epsilon_\phi}{2} \left(r(\omega_0 - \Omega)e^{-i(\omega_0-\Omega)t} + r^*(\omega_0 - \Omega)e^{i(\omega_0-\Omega)t} \right) \\ & \left. + \frac{i\epsilon_\phi}{2} \left(r(\omega_0 + \Omega)e^{-i(\omega_0+\Omega)t} + r^*(\omega_0 + \Omega)e^{i(\omega_0+\Omega)t} \right) \right] \end{aligned} \quad (\text{III.27})$$

Photodetected Intensity

The photodetector measures the intensity:

$$I(t) \propto |E_{\text{refl}}(t)|^2$$

We isolate the terms oscillating at Ω , which arise from the interference between the carrier and sideband components. Keeping only the beat terms between the carrier and sidebands, we find:

$$I(t) \supset \epsilon_\phi \cdot \text{Re}[A_+ - A_-] \cos(\Omega t) + \epsilon_\phi \cdot \text{Im}[A_+ - A_-] \sin(\Omega t) \quad (\text{III.28})$$

where we define:

$$A_\pm = r(\omega_0)r^*(\omega_0 \pm \Omega)$$

Demodulation with Arbitrary Phase

The signal is demodulated using a local oscillator $\cos(\Omega t + \phi)$, where ϕ is the demodulation phase. Using trigonometric identities:

$$\cos(\Omega t + \phi) = \cos(\Omega t) \cos \phi - \sin(\Omega t) \sin \phi$$

we multiply Equation (??) and low-pass filter to obtain:

$$\epsilon_{\text{PDH}}(\phi) \propto \epsilon_\phi \{ \text{Re}[A_+ - A_-] \cos \phi + \text{Im}[A_+ - A_-] \sin \phi \} \quad (\text{III.29})$$

Sidebands Far Off-Resonance Approximation

In the standard PDH regime, the modulation frequency is much greater than the cavity linewidth:

$$\Omega \gg \kappa$$

so the sidebands are far off-resonance. This means:

$$r(\omega_0 \pm \Omega) \approx 1 \Rightarrow A_\pm \approx r(\omega_0)$$

and therefore:

$$A_+ - A_- \approx 0$$

However, if we retain the asymmetry between the sidebands (e.g., due to dispersion), or keep the finite detuning contribution, we approximate:

$$A_+ - A_- \approx r(\omega_0) [r^*(\omega_0 + \Omega) - r^*(\omega_0 - \Omega)] = r(\omega_0) \Delta r^*$$

Final Result

Substituting into Equation (??), we obtain:

$$\epsilon_{\text{PDH}}(\phi) \propto \epsilon_\phi \{ \text{Re}[r(\omega_0) \Delta r^*] \cos \phi + \text{Im}[r(\omega_0) \Delta r^*] \sin \phi \} \quad (\text{III.30})$$

In the limit where $\Delta r^* \rightarrow 1$ (normalized, symmetric sidebands), this simplifies to:

$$\epsilon_{\text{PDH}}(\omega_0, \phi) \propto \cos \phi \cdot \text{Re}[r(\omega_0)] + \sin \phi \cdot \text{Im}[r(\omega_0)] \quad (\text{III.31})$$

7. Interpretation

Equation (??) shows that the demodulated error signal is a linear superposition of the real and imaginary parts of the complex reflection coefficient. The demodulation phase ϕ selects the detected quadrature:

- $\phi = 0$: error signal is proportional to $\text{Re}[r]$ — symmetric around resonance, not suitable for locking.
- $\phi = \pi/2$: error signal is proportional to $\text{Im}[r]$ — antisymmetric, ideal dispersive error signal.
- $\phi \neq 0, \pi/2$: mixes quadratures, possibly introducing offset or distortion.

This derivation makes explicit how the PDH method uses phase-sensitive detection to extract the component of the reflection coefficient that varies linearly with detuning, enabling precise feedback locking of the laser to the cavity resonance.

Bibliography

- [1] O. Arcizet et al. “Radiation-pressure cooling and optomechanical instability of a micro-mirror”. In: *Nature* 444.7115 (Nov. 2006), pp. 71–74. ISSN: 0028-0836, 1476-4687. DOI: [10.1038/nature05244](https://doi.org/10.1038/nature05244). URL: <http://www.nature.com/articles/nature05244> (visited on 01/09/2023).
- [2] H. J. Kimble et al. “Conversion of conventional gravitational-wave interferometers into quantum nondemolition interferometers by modifying their input and/or output optics”. In: *Physical Review D* 65.2 (Dec. 2001), p. 022002. ISSN: 0556-2821. DOI: [10.1103/PhysRevD.65.022002](https://doi.org/10.1103/PhysRevD.65.022002). URL: <http://link.aps.org/doi/10.1103/PhysRevD.65.022002>.
- [3] A. A. Clerk et al. “Introduction to Quantum Noise, Measurement and Amplification”. In: *Reviews of Modern Physics* 82.2 (Apr. 15, 2010), pp. 1155–1208. ISSN: 0034-6861, 1539-0756. DOI: [10.1103/RevModPhys.82.1155](https://doi.org/10.1103/RevModPhys.82.1155). arXiv: [0810.4729\[cond-mat, physics:quant-ph\]](https://arxiv.org/abs/0810.4729). URL: <http://arxiv.org/abs/0810.4729> (visited on 05/27/2024).
- [4] H. J. Kimble et al. “Conversion of conventional gravitational-wave interferometers into quantum nondemolition interferometers by modifying their input and/or output optics”. In: *Physical Review D* 65.2 (Dec. 26, 2001), p. 022002. ISSN: 0556-2821, 1089-4918. DOI: [10.1103/PhysRevD.65.022002](https://doi.org/10.1103/PhysRevD.65.022002). URL: <https://link.aps.org/doi/10.1103/PhysRevD.65.022002> (visited on 05/22/2023).
- [5] A. M. Jayich et al. “Dispersive optomechanics: a membrane inside a cavity”. In: *New Journal of Physics* 10.9 (Sept. 2008), p. 095008. ISSN: 1367-2630. DOI: [10.1088/1367-2630/10/9/095008](https://doi.org/10.1088/1367-2630/10/9/095008). URL: <https://dx.doi.org/10.1088/1367-2630/10/9/095008> (visited on 08/27/2024).
- [6] J. C. Sankey et al. “Strong and tunable nonlinear optomechanical coupling in a low-loss system”. In: *Nature Physics* 6.9 (Sept. 2010). Publisher: Nature Publishing Group, pp. 707–712. ISSN: 1745-2481. DOI: [10.1038/nphys1707](https://doi.org/10.1038/nphys1707). URL: [https://www.nature.com/articles/nphys1707](http://www.nature.com/articles/nphys1707) (visited on 08/27/2024).

Sujet : Progress towards cryogenic squeezed light optomechanics

Résumé : .

Mots clés : Optomecanique, Lumière comprimée, Cavité de grande Finesse, Interferométrie, Bruit thermique, Bruit de grenaille quantique, Resonateur de grand facteur de Qualité, Interféromètres pour la detection d'ondes gravitationnelles, Bruit de pression de radiation quantique

Subject : Optomechanics and squeezed light

Abstract:

Keywords : Optomechanics, Squeezing, High-Finesse cavity, Interferometry, Thermal Noise, Quantum Shot Noise, High-Q Resonator, Gravitational wave Interferometer, Quantum Radiation Pressure Noise

